Received: 4 May 2022 | Revised: 22 June 2022 | Accepted: 24 June 2022

DOI: 10.1002/ar.25037

SPECIAL ISSUE ARTICLE

The Anatomical Record WILEY

A systematic compendium of turtle mandibular anatomy using digital dissections of soft tissue and osteology

Serjoscha W. Evers[1] | Jasper Ponstein[2,3] | Maren A. Jansen[2,3] | Jaimi A. Gray[4] | Jörg Fröbisch[2,3]

[1]Department of Geosciences, University of Fribourg, Fribourg, Switzerland

[2]Museum für Naturkunde, Leibniz-Institut für Evolutions- und Biodiversitätsforschung, Berlin, Germany

[3]Institut für Biologie, Humboldt-Universität zu Berlin, Berlin, Germany

[4]Division of Herpetology, Florida Museum of Natural History, University of Florida, Gainesville, Florida, USA

Correspondence
Serjoscha W. Evers, Department of Geosciences, University of Fribourg, Chemin du Musée 6, 1700 Fribourg, Switzerland.
Email: serjoscha.evers@googlemail.com

Funding information
Schweizerischer Nationalfonds zur Förderung der Wissenschaftlichen Forschung, Grant/Award Number: PZ00P2_202019/1; Elsa-Neumann scholarship; SNF Ambizione, Grant/Award Number: SNF PZ00P2_202019/1

Abstract

Turtles are a charismatic reptile group with a peculiar body plan, which most notably includes the shell. Anatomists have often focused descriptive efforts on the shell and other strongly derived body parts, such as the akinetic skull, or the cervical vertebrae. Other parts of turtle osteology, like the girdles, limbs, and mandibles, are documented with less rigor and detail. The mandible is the primary skeletal element involved in food acquisition and initial food processing of turtles, and its features are thus likely linked to feeding ecology. In addition, the mandible of turtles is composed of up to seven bones (sometimes fused to as little as three) and has thus anatomical complexity that may be insightful for systematic purposes and phylogenetic research. Despite apparent complexity and diversity to the mandible of turtles, this anatomical system has not been systematically studied, not even in search of characters that might improve phylogenetic resolution. Here, we describe the mandibular osteology for all major subclades of extant turtles with the help of digitally dissected 3D models derived from high-resolution computed tomography (μCT) scans of 70 extant species. We provide 31 fully segmented mandibles, as well as 3D models of the mandibular musculature, innervation, and arterial circulation of the cryptodire *Dermatemys mawii*. We synthesize observed variation into 51 morphological characters, which we optimize onto a molecular phylogeny. This analysis shows some mandibular characters to have high systematic value, whereas others are highly homoplastic and may underlie ecological influences or other factors invoking variation.

KEYWORDS

adductor muscles, character evolution, feeding ecology, lower jaw, mandible, mandibular artery, mandibular nerve, turtles

1 | INTRODUCTION

Turtles are a relatively species-poor clade of reptiles, with currently 352 recognized living species (TTWG, 2021), contrasting >10,000 species of squamates or birds, respectively (Gill et al., 2020; Uetz et al., 2020). Nevertheless, turtles evolved high ecological disparity, as they live today in a broad range of

terrestrial and aquatic habitats and employ a wide range of food processing strategies (e.g., Ernst & Barbour, 1989; Pritchard, 1984). Fully shelled turtles have a rich fossil record (e.g., Cleary et al., 2020), which dates back to the Late Triassic (Joyce, 2017). During their 230 Ma of evolution, turtles experienced several independent ecological transitions, such as the evolution of secondary marine lifestyles (Anquetin et al., 2015; Evers & Benson, 2019; Ferreira et al., 2015; Gaffney et al., 2006), the transition to terrestriality from an aquatic ancestral habitat (e.g., Claude et al., 2004), or the independent evolution of specialized feeding styles, including durophagy (Parham & Pyenson, 2010) and suction feeding (Bardet et al., 2013; Joyce, Rollot, et al., 2021).

Turtles provide a rich fossil record from which morphological phylogenetic characters are routinely gathered (e.g., Anquetin, 2012; Evers & Benson, 2019; Gaffney et al., 1991; Joyce, 2007; Sterli, 2010). Early morphological systematic work proposed many relationships among extant turtles (e.g., "Testudinoidea" content of Williams, 1950; "Trionychoidea + Testudinoidea" of Gaffney & Meylan, 1988) that were later overturned by results from analyses using or including molecular sequence data, thereby drastically changing the perception of the within-group relationships of turtles (Shaffer et al., 1997). Although later molecular studies again changed certain phylogenetic aspects (e.g., the position of *Platysternon megacephalum* as a chelydrid in Shaffer et al., 1997), the molecular consensus today is stabilizing regarding the major dichotomies of turtle subclades (e.g., Crawford et al., 2015; Pereira et al., 2017; Shaffer et al., 2017; Thomson et al., 2021). Molecular consensus topologies also find support from biogeographic and stratigraphic viewpoints (e.g., Crawford et al., 2015; Joyce et al., 2016; Pereira et al., 2017). These studies generally agree on a deep split of crown-group turtles into cryptodires and pleurodires (see also Joyce et al., 2013). Pleurodires include chelids and pelomedusoids, the latter of which can be distinguished into pelomedusids and podocnemidids. Within cryptodires, the split between Trionychia (Trionychidae + *Carettochelys insculpta*) and Durocryptodira forms the earliest branching event among extant clades. Durocryptodires include all other cryptodires and are formed of a sister group relationship of Testudinoidea and Americhelydia. The former can further be divided into Emysternia (*Platysternon megacephalum* + Emydidae) and Testuguria (Testudinidae + Geoemydidae). Americhelydia consists of Chelydroidea and Chelonioidea. Chelydroidea itself contains Chelydridae and their sister group, Kinosternoidea (Kinosternidae + *Dermatemys mawii*). Chelonioids can be decomposed into *Dermochelys coriacea* and Cheloniidae. Despite unclarities in the relationships of individual genera (e.g., *Rhinoclemmys* in Pereira et al., 2017 vs. Thomson et al., 2021), the above-mentioned relationships are well-supported (Crawford et al., 2015; Pereira et al., 2017; Shaffer et al., 2017, Thomson et al., 2021).

Morphological phylogenetic studies of turtles are usually performed on datasets containing fossil species, as paleontology is at present the primary driver of morphology-based phylogenetics. Paleontological phylogenies that focus on global turtle relationships mostly enforce a molecular backbone constraint, pre-defining a framework for living turtles as dictated by molecular studies (e.g., Brinkman et al., 2017; Cadena & Parham, 2015; Danilov & Parham, 2006, 2008; Evers, Barrett, & Benson, 2019; Evers & Benson, 2019; Joyce et al., 2016; Zhou & Rabi, 2015). Without the backbone constraint, even the most basal pleurodire-cryptodire dichotomy is often not supported (e.g., see Zhou and Rabi, 2015, in which topologies resulting from enforcing the backbone constraint and leaving it away are reported in conjunction).

Although the reasons for the differences between molecular and morphological phylogenetic results are currently unclear, it is safe to say that certain morphological partitions have been neglected more than others. For instance, of 136 osteological characters used in the seminal study of Joyce (2007), 57 pertain to the cranium (42%), 41 to the shell (30%), 19 to the vertebral column (14%), but only 12 to the girdles (8.8%); five to the limbs (3.7%), and two to the mandible (1.5%). Although this matrix has since been heavily used and expanded by other studies, the disproportions between the major and minor partitions of the matrix iterations have not changed in most global datasets. For instance, of 244 morphological characters in Joyce et al. (2016), 114 pertain to the cranium (47%), 73 to the shell (30%), 30 to the axial series (12%), 14 to the girdles (6%), 12 to the limbs (5%), and only one to the mandible (<1%). Morphological support for the molecular turtle tree, if there is any, may come from novel character sources. Those regions of the body that so far have been neglected, but which have high complexity (e.g., the mandible), provide a particularly accessible source and high potential for new characters. Some of the underrepresented anatomical partitions indeed seem to contain phylogenetically relevant variation. Mandibular synapomorphies have, for instance, been found for subclades of testudinoids by Vlachos and Rabi (2018), a study that includes an unusually high number of mandibular characters (18 out of 171 characters, or 10.5% of characters). Similarly, Evers and Benson (2019) described and figured eight new and six previously defined mandibular characters to a total of 14 of 345 characters (4%) and found mandibular

synapomorphies among their newly coded characters (e.g., a posterior notch in the coronoid) for their previously unrecognized clade of sandownids + thalassochelydians. These two examples reveal the potential of novel character observations for systematic studies of extant and extinct turtles.

A reason for the neglect the mandible of turtles has received may lie in the simple fact that there is no go-to comparative compendium for mandibles, analog to the great cranial anatomy compendium of Gaffney (1979). Although Gaffney's (1979) work has sections dedicated to generalized mandibular descriptions and established a working nomenclature for mandibular foramina (see also Gaffney, 1972), the paper lacks comprehensive mandibular figures for most clades.

The primary goal of this article is to provide a useful guide to turtle mandibular osteology. For this, we combine detailed osteological descriptions and figures with the deposition of publicly available 3D models of turtle mandibles. The data deposition is very important, in our opinion, not only for the reproducibility of the content of this article, but also to enable future research on turtle mandibles. Even a detailed osteological compendium cannot always figure or otherwise cover all anatomical details, and users of our content may consult the 3D models directly for additional views of the specimens other than the standard views provided in our figures. Our online repository of choice, MorphoSource (https://www.morphosource.org/), includes an online viewing panel for uploaded 3D data, so that 3D models can be viewed as long as the user has an internet connection. Alternatively, data can be downloaded and viewed in more specialized 3D viewing software. A secondary goal of our study is to summarize the observed osteological variation into newly coded mandibular character datasets. We test our character concept by optimizing scored characters onto a molecular turtle tree (Pereira et al., 2017) and briefly discuss the character evolution implied by this analysis. Finally, we provide summaries of osteological features, combinations of features, or synapomorphies that can be helpful in taxonomically and/or phylogenetically attributing mandibles, specifically fossils, to specific turtle clades.

2 | MATERIALS AND METHODS

2.1 | Sampling, digital dissections, and data deposition

For this study, we sampled 70 extant species of turtles by means of computed tomography (CT) scanning, or roughly one fifth of the species diversity of the group. Our sample covers turtle specimens for all major extant turtle subclades (see Joyce, Anquetin, et al., 2021), corresponding to the "subfamily" level in terms of classic nomenclature (Figure 1; Table 1). CT datasets were largely already uploaded to MorphoSource, either as part of previous turtle-specific collections (Evers, 2019; Evers & Benson, 2018; Hermanson, 2021; Werneburg & Joyce, 2021) or as part of larger museum digitization efforts, specifically "The oUTCT PEN: Outwardly Mobilizing the UTCT Vertebrate Archive for Research and Training" collection (MorphoSource Project ID 00000C887) and the Digitizing the Florida Museum of Natural History Herpetology collections collection (MorphoSource Project ID 00000C211). One CT scan (*Pelusios sinuatus* USNM 42144) is not available via MorphoSource, but was downloaded by us from the online repository Digimorph (http://www.Digimorph.org/). Eight specimens from the Zoological collection (ZMB) of the Museum für Naturkunde Berlin (MfN) were newly scanned with an YXLON FF35 µCT-scanner at different scanning settings, which are documented with the deposited scans (see below).

For each major turtle subclade, we selected one specimen (sometimes two) that was fully manually segmented (i.e., bone-by-bone), resulting in 31 fully segmented mandibles. As mandibles are bilaterally symmetric, we segmented only one (usually the left) mandibular ramus for each specimen. In species in which the right and left dentaries are fused, we produced a sagittal cut through the symphyseal area of the mandible, allowing us to produce unobscured views onto the medial mandibular side. For the remaining turtles in our sample (39 species), we segmented the mandible as single 3D models in which the individual bones are not separated. Throughout the text, we also refer to additional species and specimens for which we did not have digital anatomical data, if these provide additional context for understanding within-group variation.

Segmentation of CT slice data was performed by two of us (SWE, JP) with the software Mimics (versions 19.0–24.0; http://biomedical.materialise.com/mimics) or Volume Graphics Studio v3.2 (https://www.volumegraphics.com/), respectively. All mandibular models were uploaded to the digital repository MorphoSource (https://www.morphosource.org/), under a single project ID (Evers & Ponstein, 2022; Project ID 000408332; link: https://www.morphosource.org/projects/000408332). MorphoSource allows the linking of 3D models with their parent datasets, regardless of the CT datasets being part of the same digital collection or not. We linked our models to their parent CT datasets. We also uploaded the 3D models resulting from the segmentation of the *Pelusios sinuatus* (USNM 42144) scan to our MorphoSource project, that is, the only specimen

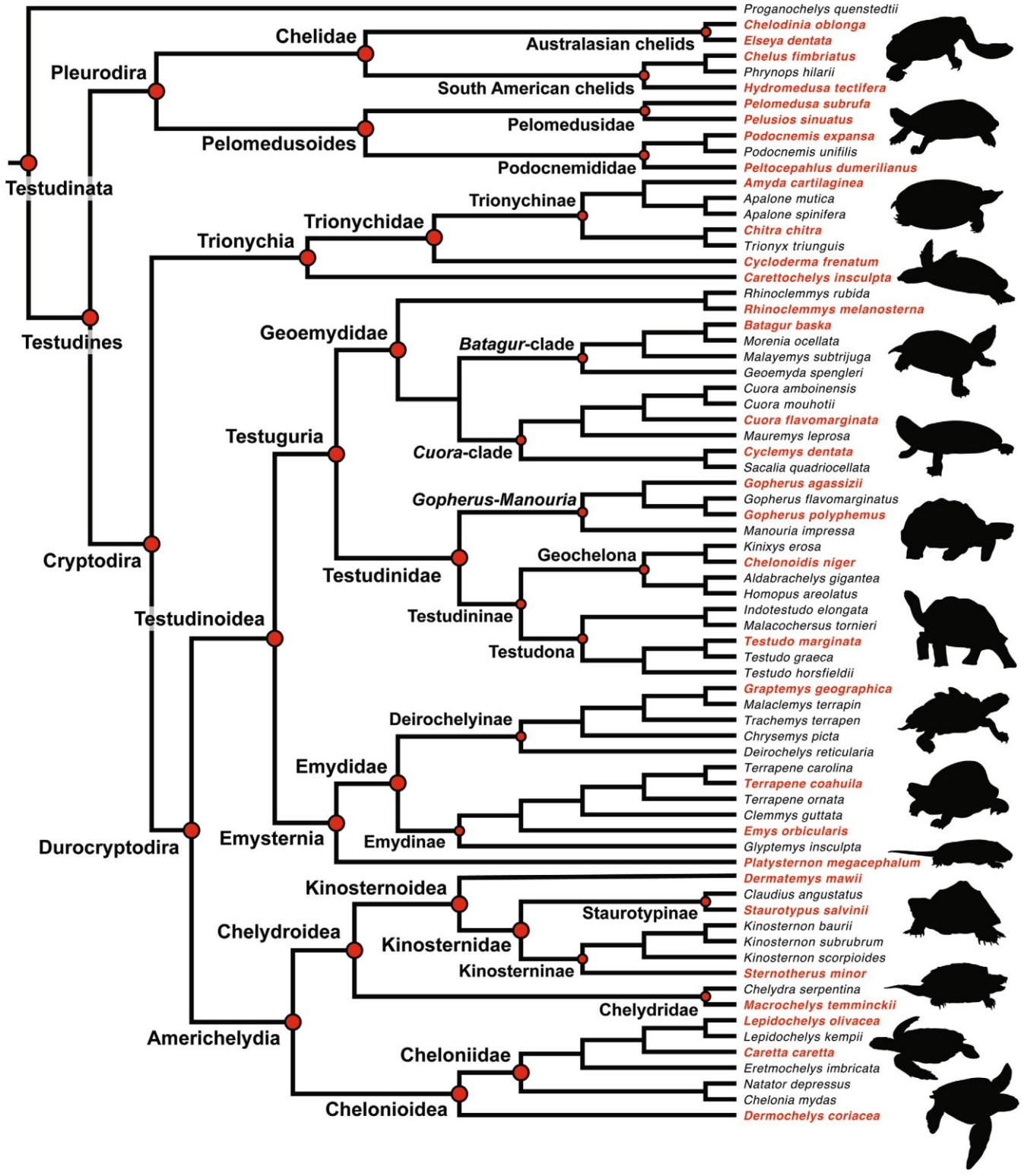

FIGURE 1 Phylogenetic representation of sampled turtle species. This tree shows the interrelationships of all turtle species sampled in this study. The topology follows the molecular tree of Pereira et al. (2017). Red terminal taxa are those for which we have completely segmented (i.e., bone-by-bone) mandibular 3D models, black terminals are taxa for which we provide single mandibular 3D models. Internal node labels indicate the most important turtle clades discussed in this work. Note that the tree includes the fossil species *Proganochelys quenstedtii*, for which we do not provide a 3D model

TABLE 1 Specimens used in this study, and weblinks to their CT scans and 3D models

Taxonomy	Identifier	Link to specimen (with CT scan and 3D models)
Aldabrachelys gigantea	ZMB 47494	https://www.morphosource.org/concern/biological_specimens/000414483
Amyda cartilaginea	FMNH 244117	https://www.morphosource.org/concern/biological_specimens/000S23086
Apalone mutica	FHSM 2746	https://www.morphosource.org/concern/biological_specimens/000S30480
Apalone spinifera emoryi	FMNH 22178	https://www.morphosource.org/concern/biological_specimens/000S10604
Batagur baska	NHMUK 67.9.28.7	https://www.morphosource.org/concern/biological_specimens/000S23062
Caretta caretta	ZMB 25470	https://www.morphosource.org/concern/biological specimens/000414058
Carettochelys insculpta	USNM 327960	https://www.morphosource.org/concern/biological_specimens/000412543
Chelodina oblonga	NHMUK 64.12.22	https://www.morphosource.org/concern/biological specimens/000S23060
Chelonia mydas	NHMUK 1969.776	https://www.morphosource.org/concern/biological_specimens/000S23057
Chelonoidis niger	ZMB 19103	https://www.morphosource.org/concern/biological_specimens/000414064
Chelus fimbriatus	UF 85199	https://www.morphosource.org/concern/biological_specimens/000S14807
Chelydra serpentina	UF 22159	https://www.morphosource.org/concern/biological_specimens/000S30711
Chitra chitra	NHMUK 1926.12.16.1	https://www.morphosource.org/concern/biological_specimens/000S23053
Chrysemys picta	NHMUK 76.1.31.19	https://www.morphosource.org/concern/biological specimens/000S23064
Claudius angustatus	SMNS 14380	https://www.morphosource.org/concern/biological_specimens/000S23096
Clemmys guttata	FMNH 22114	https://www.morphosource.org/concern/biological specimens/000S23080
Cuora amboinensis	NHMUK 9.42.145	https://www.morphosource.org/concern/biological_specimens/000S23063
Cuora flavomarginata	FMNH 21515	https://www.morphosource.org/concern/biological_specimens/000S23077
Cuora mouhotii	SMF 71599	https://www.morphosource.org/concern/biological_specimens/000353906
Cyclemys dentata	NHMUK97.11.22.3	https://www.morphosource.org/concern/biological_specimens/000S23071
Cycloderma frenatum	NHMUK 84.2.4.1	https://www.morphosource.org/concern/biological_specimens/000S23067
Deirochelys reticularia	FMNH 98754	https://www.morphosource.org/concern/biological_specimens/000S23093
Dermatemys mawii	CM 117802	https://www.morphosource.org/concern/biological_specimens/000S29387
Dermatemys mawii	UF 84770	https://www.morphosource.org/concern/biological specimens/000408252

TABLE 1 (Continued)

Taxonomy	Identifier	Link to specimen (with CT scan and 3D models)
Dermochelys coriacea	UMZC R3031	https://www.morphosource.org/concern/biological_specimens/000S10581
Elseya dentata	NHMUK 76.5.19.77	https://www.morphosource.org/concern/biological_specimens/000S10647
Emys orbicularis	ZMB 39445	https://www.morphosource.org/concern/biological_specimens/000414069
Eretmochelys imbricata	FMNH 22242	https://www.morphosource.org/concern/biological_specimens/000S23073
Geoemyda spengleri	FMNH 260381	https://www.morphosource.org/concern/biological_specimens/000S23087
Glyptemys insculpta	FMNH 22240	https://www.morphosource.org/concern/biological_specimens/000S23083
Gopherus agassizii	FMNH 216746	https://www.morphosource.org/concern/biological_specimens/000S23078
Gopherus flavomarginatus	FMNH 98916	https://www.morphosource.org/concern/biological_specimens/000S23094
Gopherus polyphemus	FMNH 211815	https://www.morphosource.org/concern/biological_specimens/000S10605
Graptemys geographica	NHMUK 55.12.6.11	https://www.morphosource.org/concern/biological_specimens/000S23058
Homopus areolatus	OUMNH 09403	https://www.morphosource.org/concern/biological_specimens/000354261
Hydromedusa tectifera	SMF 70500	https://www.morphosource.org/concern/biological_specimens/000354030
Indotestudo elongata	SMF 71585	https://www.morphosource.org/concern/biological_specimens/000354145
Kinixys erosa	SMF 40166	https://www.morphosource.org/concern/biological_specimens/000354049
Kinosternon baurii	FMNH 211705	https://www.morphosource.org/concern/biological_specimens/000S23075
Kinosternon scorpioides	SMF 71893	https://www.morphosource.org/concern/biological_specimens/000354117
Kinosternon subrubrum hippocrepis	FMNH 211711	https://www.morphosource.org/concern/biological_specimens/000S23076
Lepidochelys olivacea	SMNS 11070	https://www.morphosource.org/concern/biological_specimens/000S10580
Macrochelys temminckii	FMNH 22111	https://www.morphosource.org/concern/biological_specimens/000S23079
Malaclemys terrapin	SMF 36419	https://www.morphosource.org/concern/biological_specimens/000354078
Malaclemys terrapin	ZMB 16196	https://www.morphosource.org/concern/biological_specimens/000414518
Malacochersus tornieri	SMF 58702	https://www.morphosource.org/concern/biological_specimens/000354084
Malayemys subtrijuga	NHMUK 1920.1.20.2545	https://www.morphosource.org/concern/biological_specimens/000S23052
Manouria impressa	SMF 69777	https://www.morphosource.org/concern/biological_specimens/000354073

(Continues)

TABLE 1 (Continued)

Taxonomy	Identifier	Link to specimen (with CT scan and 3D models)
Mauremys leprosa	NHMUK unnumbered	https://www.morphosource.org/concern/biological_specimens/000S23072
Morenia ocellata	NHMUK 87.3.11.7	https://www.morphosource.org/concern/biological_specimens/000S23068
Pelomedusa subrufa	FMNH 17161	https://www.morphosource.org/concern/biological_specimens/0000S6913
Peltocephalus dumerilianus	MCT RR 354	https://www.morphosource.org/concern/biological_specimens/000405898
Pelusios sinuatus	USNM 42144	https://www.morphosource.org/concern/biological_specimens/000398467
Phrynops hilarii	NHMUK 91.3.16.1	https://www.morphosource.org/concern/biological_specimens/000S23070
Platysternon megacephalum	NCSM 76497	https://www.morphosource.org/concern/biological_specimens/000S10072
Podocnemis expansa	LIRP 0001	https://www.morphosource.org/concern/biological_specimens/000376383
Podocnemis expansa	ZMB 90084	https://www.morphosource.org/concern/biological_specimens/000414075
Podocnemis unifilis	FMNH 45657	https://www.morphosource.org/concern/biological_specimens/000S23090
Podocnemis sp.	NHMUK 60.4.16.9	https://www.morphosource.org/concern/biological_specimens/000S23059
Rhinoclemmys melanosterna	FMNH 44446	https://www.morphosource.org/concern/biological_specimens/000S23089
Sacalia quadriocellata	NCSM 13265	https://www.morphosource.org/concern/biological_specimens/000S10096
Staurotypus salvinii	NHMUK 1879.1.7.5	https://www.morphosource.org/concern/biological_specimens/000S23049
Sternotherus minor	FMNH 211696	https://www.morphosource.org/concern/biological_specimens/000S10648
Terrapene carolina	OUMNH 08795	https://www.morphosource.org/concern/biological_specimens/000354241
Terrapene coahuila	FMNH 47372	https://www.morphosource.org/concern/biological_specimens/000S23091
Terrapene ornata	FMNH 23014	https://www.morphosource.org/concern/biological_specimens/000S23085
Testudo graeca	ZMB 39442	https://www.morphosource.org/concern/biological_specimens/000414529
Testudo horsfieldii	OUMNH 10344	https://www.morphosource.org/concern/biological_specimens/000354232
Testudo marginata	FMNH 51672	https://www.morphosource.org/concern/biological_specimens/000S23095
Trachemys terrapen	ZMB 6572	https://www.morphosource.org/concern/biological_specimens/000414508
Trionyx triunguis	PCHP 4559	https://www.morphosource.org/concern/biological_specimens/000S30469

Note: Specimens in boldface in the taxonomy column were fully segmented for each bone of the left mandibular ramus.

for which the parent dataset is hosted outside of the MorphoSource repository (see above). In addition, we also added the eight new CT scans of mandibular specimens to our MorphoSource collection. In sum, all CT scans of specimens used herein are available on MorphoSource or Digimorph. We list all specimens and links to their specimen IDs in MorphoSource in Table 1. Users who wish to download our data can navigate through our MorphoSource project, or follow these specimen-specific links.

In addition to the osteological segmentations, we segmented the mandibular bones, mandibular musculature, mandibular arterial blood circulation, and mandibular innervation for a head-only specimen of *Dermatemys mawii* (UF herp 84770) that was subjected to diffusible iodine-based contrast-enhanced computed tomography (diceCT), performed by JAG. The specimen was CT scanned prior to staining to obtain a skeletal dataset, and then the storage ethanol concentration was stepped down from 70 to 50% (for 2 days), and then to 30% (for 2 days). It was then stained using a 1.25% Lugol's iodine solution for 97 days. Prior to scanning, the specimen was bathed in 30% ethanol for 1 hr, to wash away unbound iodine and bring down the contrast of any external features that may have become overstained. The specimen was then scanned with a General Electric v|tome| x m 240, at 170 kV with a 0.5 mm copper filter. After scanning, the specimen was de-stained by stepping the storage ethanol concentration back up from 30%, to 50%, and finally back to 70%. The 70% ethanol was refreshed regularly to sustain the de-staining process. Once the iodine had been completely removed from the specimen, it was returned to the herpetology collection at the Florida Museum of Natural History and remains there today. The data set was uploaded to MorphoSource, and the respective repository (Table 1) includes details about the staining and scanning procedure. We use the soft tissue segmentation performed by one of us (S.W.E.) as a guide to identifying canals and foramina formed in bone.

All figures were created by digitally rendering 3D models in Blender v. 2.71 (blender.org).

2.2 | Discrete osteological characters and phylogenetic optimization

Our segmentations and descriptions let to observations about mandibular variation that we encoded as discrete phylogenetic characters. We established primary hypotheses of homology (de Pinna, 1991) for character delimitation based on topographic correspondence and similarity of traits among taxa (de Pinna, 1991; Hawkins et al., 1997; Patterson, 1982; Rieppel, 1988). Character states, that is, the different transformations of variation a homologous character can take (de Pinna, 1991; Hawkins et al., 1997; Platnick, 1979), need to be independent from one another (Pimental & Riggins, 1987; Strong & Lipscomb, 1999; Wilkinson, 1995). We therefore carefully constructed character states to reflect independent variation on the character level. For some character traits, the variation of shape in that trait required the coding of multistate characters. For each multistate character, we carefully evaluated if it should be ordered in phylogenetic analysis or not. Ordering characters forces the character state transitions to occur with a predefined sequence (Wilkinson, 1992, 1995), and thus enforces a higher parsimony cost for certain character state transitions than for others. We only order multistate characters when character states form intermediate sequences. Our observations resulted in a total of 51 mandibular characters. These were scored for 70 extant turtle species for which we had digital anatomical data available, resulting in an in-group matrix block without unknown character states. In addition, we added the Late Triassic stem turtle *Proganochelys quenstedtii* to the matrix, based on published records (Gaffney, 1990) and personal observations by S.W.E. *Proganochelys* was added as an outgroup taxon for character polarization during the optimization process. The full matrix is available as a nexus file in the supplements, which also contains the phylogenetic tree used for character state optimizations (Data S1). We optimized all characters on a fixed tree topology that follows the molecular topology of Pereira et al. (2017), pruned to our taxon sample (Figure 1). Optimization was done in PAUP* for Macintosh (Swofford, 2002) according to two optimization criteria (accelerated transformations = ACCTRAN; delayed transformations = DELTRAN). Unambiguous synapomorphies are those character state changes that are optimized at the same nodal position using both the ACCTRAN and DELTRAN criteria. As our extant data partition lacks unobserved or unknown character states (i.e., no "?" scores), ambiguous optimizations result from character conflict among sister taxa (and not from unknown data). Character optimizations are reported in Data S2–S4 in full, but are discussed in the "remarks" section directly underneath each character description.

For each character, we traced back character definition origins to the papers that first encoded the underlying variation as a phylogenetic character. We limited our search to papers that explicitly use the cladistic method or those that list or tabulate characters; this includes all numerically solved cladistic analyses for turtles (the first of which is Dryden, 1988), and a few earlier studies (Gaffney, 1975a, 1975b, 1977), which provide modern character concepts although their cladistic analyses were done without formal numeric analyses. Whenever one of these early studies is the original character origin, we additionally cite the first study that included the

character in a formal, computer-aided analysis. We did not trace back the earliest mention of the variation underlying a character per se (i.e., we did not check who was the first person to record in writing that, for instance, the splenial is lost in most extant turtles), but our descriptive section cites previously reported mandibular anatomy when relevant. We declare characters as "new" when we did not find an earlier version of the respective character.

3 | RESULTS

Gaffney (1972, 1979) provided an anatomical nomenclatural system for the mandibular foramina and bony canals in turtles that is, by and large, still in use today. We generally follow this system, although we make some minor adjustments, which are justified in the description sections. Gaffney (1972, 1979) also referred to soft-tissue structures, particularly blood vessels (following Albrecht, 1967, 1976) and cranial nerves (following Soliman, 1964), and some structures were named after their respective soft-tissue content (e.g., foramen nervi auriculotemporalis). However, the soft-tissue structures were not known in all instances; for example, Gaffney (1972) reported the absence of literature reports for the content of the foramen dentofaciale majus. In order to examine the arterial blood supply and innervation of turtles, we segmented the major arteries, major relevant nerves, as well as the mandibular musculature of a diceCT scan of *Dermatemys mawii* (UF herp 04770), and describe these briefly in the following sections.

3.1 | Arterial blood supply of the mandible of *Dermatemys mawii*

In *Dermatemys mawii*, the internal carotid artery enters the cranium as described by Rollot et al. (2021): The foramen posterius canalis carotici interni lies within the cavum acustico-jugulare and is formed by the prootic and pterygoid. The internal carotid artery then extends anteriorly through the pterygoid and into the pterygoid-parabasisphenoid suture. At the level of the trigeminal foramen, the internal carotid artery branches into a medial, cerebral artery, and a thicker, anteriorly directed palatine artery (Figure 2a). The palatine artery continues anteriorly and exits the basicranium through a foramen formed by the pterygoid within the sulcus cavernosus. From there, it gives off a lateral branch, the mandibular artery, before continuing further anteriorly (Figure 2a,b). Thus, the mandible is supplied by the palatine artery in *Dermatemys mawii*, a consequence of the reduction of the stapedial artery in this turtle (see Rollot et al., 2021). The subsequent branching pattern of the mandibular artery has not been described in detail for any turtle (Albrecht, 1967, 1976; but see figures in Bojanus, 1819–1821: fig. 105 and Ogushi, 1913: p. 455). Thus, we herein use terms in the following for the individual subbranches that are largely new.

The mandibular artery of *Dermatemys mawii* curves posteromedially around the anterior end of the secondary braincase wall, and in a wide lateral arch around different muscle strands of the *m. adductor mandibulae internus* (Nos. 23–28; Figure 2a; Figure 3a,d). Along this arch, the mandibular artery gives off two major branches: first, the ventrally directed inframaxillary artery (Figure 2b; Figure 3d), which passes through the foramen palatinum posterius (Gaffney, 1972). The second branch, which we term internal adductor branch, ascends medial to the internal adductor musculature (Figure 2b; Figure 3a,d) and enters these muscles with several further branches (although at least one branch also supplies the external adductor musculature). The main mandibular artery continues posteroventrally and crosses path with the mandibular ramus of the trigeminal nerve (CN V_3; Figure 2). At this level, the mandibular artery branches into two subordinate arteries (Figure 2a). The first is a stronger, ventrally directed branch which we term internal mandibular branch, as it enters the mandible via the dorsal opening of the fossa Meckelii and alongside the CN V_3 (Figure 2b). The second branch extends posteromedially to the CN V_3, and then curves laterally between the *m. adductor mandibulae externus Pars medialis* (No. 17) and *Pars superficialis* (No. 21) (Figure 2a; Figure 3a). We term this second artery the external mandibular branch. At the lateral surface of the external adductor muscles, the external mandibular branch gives off an anterodorsal artery which we term the external adductor branch, as it curves around the *m. adductor mandibulae externus Pars superficialis* (No. 21) and reaches the *Pars profundus* (No. 19) at its insertion onto the coronar aponeurosis (Figure 2b; Figure 3a,d). From this branching point, the external mandibular artery continues ventrally along the external adductors and splits ventral to their insertion onto the surangular into an anterior and a posterior branch (Figure 2a; Figure 3a). We refer to the anterior branch as the dentofacial branch, as it enters the foramen dentofaciale majus, and also gives off numerus small vessels in the area of the foramen. We did not find any nerve strands entering the foramen dentofaciale majus, so that its function seems to be entirely circulatory in *Dermatemys mawii*. We call the posterior artery the glenoid branch. Besides reaching the posteriormost mandibular point at the ventral surface of the articular,

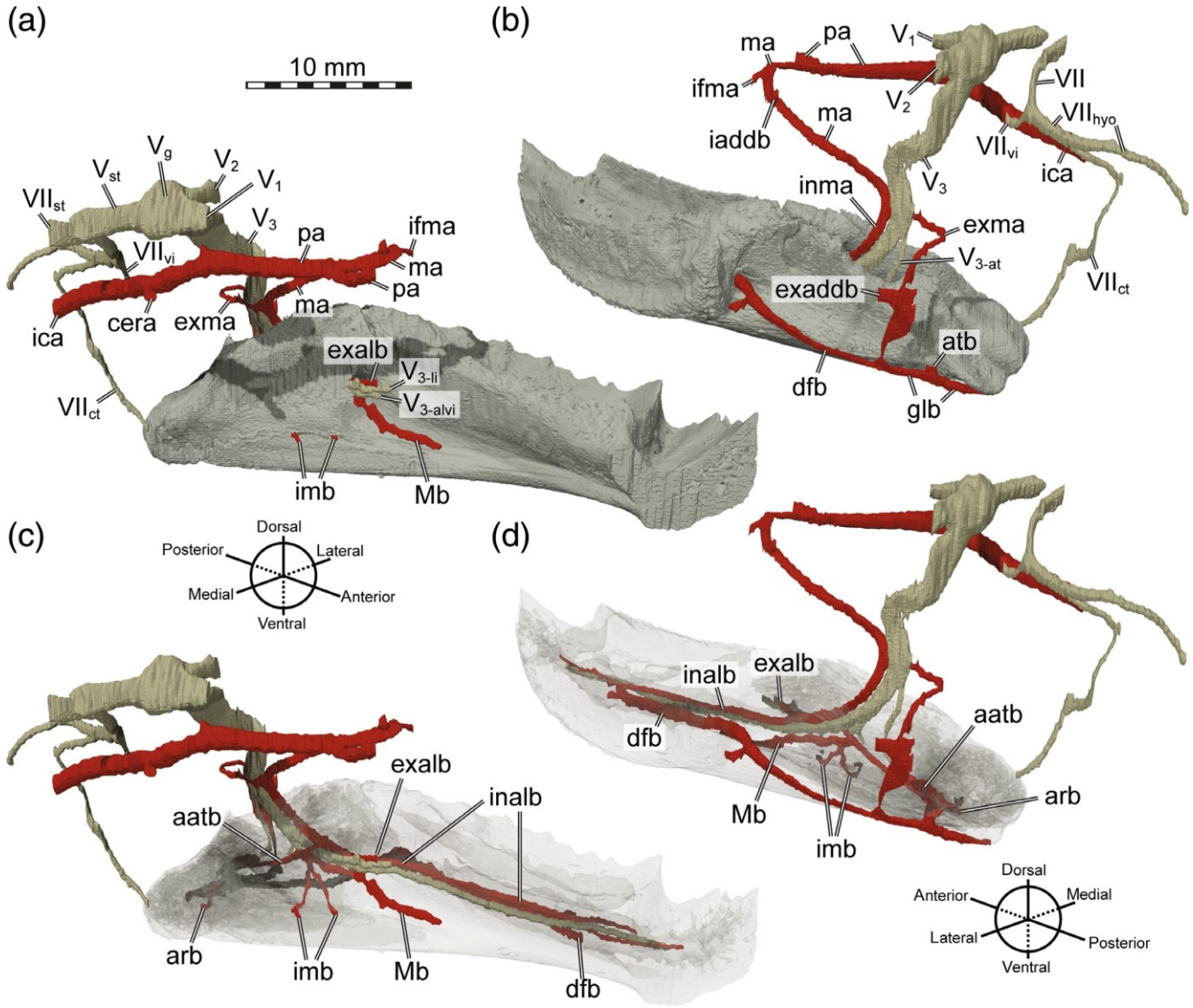

FIGURE 2 3D renderings of mandibular arterial circulation and innervation of *Dermatemys mawii* (UF herp 04770). (a and c) Anterodorsomedial view on left mandibular ramus. (b and d) Posterodorsolateral view on left mandibular ramus. (a and b) Bones rendered solid. (c and d) Bones rendered transparent. aatb, anterior auriculotemporal branch; atb, auriculotemporal branch; arb, articular branch; cera, cerebral artery; dfb, dentofacial branch; exaddb, external adductor branch; exalb, external alveolar branch; exma, external mandibular artery; glb, glenoid branch; iaddb, internal adductor branch; ica, internal carotid artery; ifma, inframaxillary artery; inalb, internal alveolar branch; inma, internal mandibular artery; imb, intermandibular branch; ma, mandibular artery; Mb, Meckelian branch; pa, palatine artery; V_1, ophthalmic ramus of trigeminal nerve; V_2, maxillary ramus of trigeminal nerve; V_3, mandibular branch of trigeminal nerve; $V_{3\text{-}alvi}$, nervus alveolare inferius (sensu Fuchs, 1931); $V_{3\text{-}at}$, nervus auriculotemporalis (sensu Fuchs, 1931); $V_{3\text{-}li}$, nervus lingualis (sensu Fuchs, 1931); V_g, trigeminal ganglion; V_{st}, trigeminal nerve stem; VII, facial nerve; VII_{ct}, chorda tympani ramus of facial nerve; VII_{hyo}, hyomandibular ramus of facial nerve; VII_{st}, facial nerve stem; VII_{vi}, vidian ramus of facial nerve

the glenoid branch gives off a medially directed auriculotemporal branch, which enters the respective auriculotemporal foramen in the surangular (Figure 2b). In Gaffney's (1972) nomenclature, following observations from Soliman (1964) and consistent also with descriptions by Fuchs (1931), the foramen is described as holding a branch of the mandibular nerve and was thus called the foramen nervi auriculotemporalis. In our segmentation, we found a minute nerve within the auriculotemporal foramen, whereas the artery passing through is prominent and fills nearly the full diameter of the foramen, which is usually quite large in turtles (although it can be separated into several distinct openings, see osteological descriptions below). Thus, within this contribution, we only use the term "auriculotemporal foramen/foramen auriculotemporalis," which

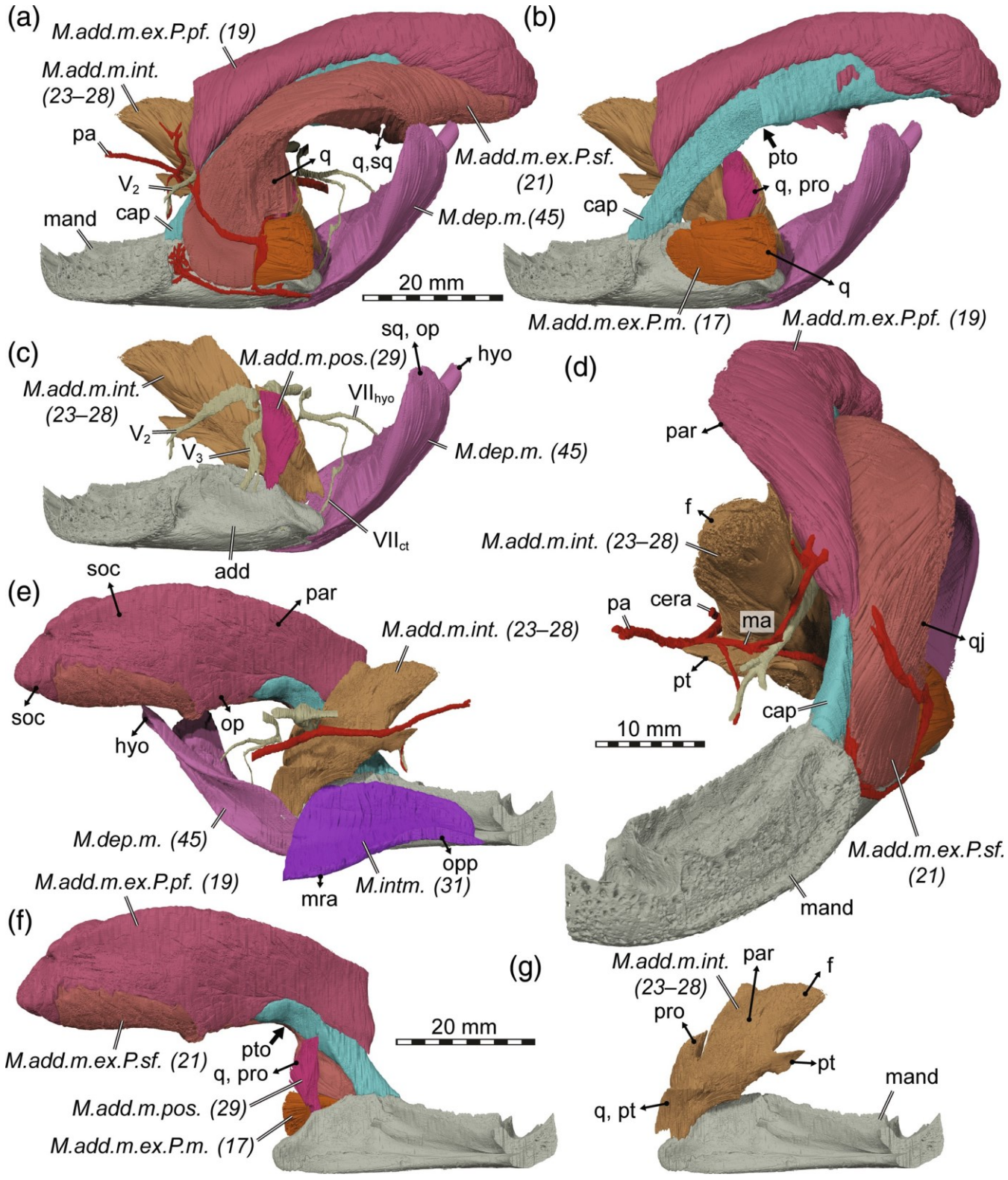

FIGURE 3 Legend on next page.

does not imply that its primary function is the passage of a nerve.

Within the surangular of *Dermatemys mawii*, the auriculotemporal branch of the mandibular artery complex splits into a short medial artery that we call articular branch (Figure 2d), as it enters and ends within the articular bone, and the anterior auriculotemporal branch (Figure 2c,d). This anterior branch enters the fossa Meckelii from posteriorly, where it gives off a large anteroventrally and medially directed Meckelian branch that supplies the Meckelian fossa, as well as two medioventrally directed branches that extend through the intermandibular foramina (Figure 2c,d). Contrary to the report of Gaffney (1972), we could not find any nerve stands extending through the intermandibular foramina. However, it is noteworthy that our arterial pattern within the fossa Meckelii closely resembles the nerve pattern depicted for *Podocnemis* by Fuchs (1931). Indeed, in many instances recorded by us here, mandibular nerve rami and mandibular artery branches are closely associated and follow near exact pathways. Thus, we consider it likely that those nerves that we could not detect in our diceCT scan may nonetheless be present as tiny structures, and may be closely associated with the arteries, which are easier to detect in this particular scan. We dismiss the possibility that we have accidentally segmented arteries for nerves within the fossa Meckelii, as the arterial branches are clearly connected to the main mandibular artery branch.

The anterior auriculotemporal branch of the mandibular artery complex of *Dermatemys mawii* merges anterodorsally with the internal mandibular artery (Figure 2c). This large branch of the mandibular artery enters the mandible through the dorsal foramen of the fossa Meckelii (Figure 2b). Within the fossa Meckelii, the artery splits into a lateral vessel that we term the internal alveolar branch, as it enters the dentary through the foramen alveolare inferius, alongside a branch of the CN V_3 (Figure 2d). The second, more medially extending branch is the external alveolar branch, which extends along the internal mandibular surfaces (Figure 2c), below the origination points of muscle fibers of the *m. intermandibularis* (No. 31).

3.2 | Innervation of the mandible of *Dermatemys mawii*

The trigeminal nerve (CN V) of *Dermatemys mawii* has a nerve stem that extends from the lateral brain surface anterolaterally toward the cavum epiptericum (Figure 2a, b). Here, the nerve forms a large, ovoid trigeminal ganglion, from which the three principal trigeminal divisions diverge. The ophthalmic nerve (CN V_1) extends anteriorly and intracranially, as reported for other turtles (Evers, Neenan, et al., 2019; Ogushi, 1913; Soliman, 1964). The maxillary (CN V_2) and mandibular (CN V_3) branches of the trigeminal nerve lie dorsoventrally adjacent to one another and extend laterally through the trigeminal foramen and then through two distinct muscle subdivisions of the internal adductor muscle, which attach to the prootic and parietal, respectively (Figure 2a,b; Figure 3c). The mandibular nerve (CN V_3) then extends ventrally and joins the course of the intramandibular artery into the fossa Meckelii (Figure 2b). Shortly before entering the fossa Meckelii, the mandibular nerve gives off a posteroventrally directed auriculotemporal nerve (sensu Fuchs, 1931), which enters the fossa Meckelii and extends posteriorly along the medial surangular surface to the auriculotemporal foramen (Figure 2b,d), as in *Podocnemis* (Fuchs, 1931). Poglayen-Neuwall (1953) identified the nerve for a range of different turtle species as well, but instead uses the term "Ramus cutaneus recurrens." We herein follow the nomenclature of Fuchs (1931: auriculotemporal nerve) instead, as the associated posterior foramina names are well established in the turtle literature (e.g., Gaffney, 1972, 1979). At the foramen into the fossa Meckelii, the small auriculotemporal nerve of *Dermatemys mawii* becomes surrounded by anastomosing vessels of the large auriculotemporal branch of the mandibular artery complex and exits laterally through the auriculotemporal foramen.

Upon entering the fossa Meckelii, the mandibular nerve course (CN V_3) and splitting pattern are closely associated to the arterial course and branching pattern:

FIGURE 3 3D renderings of mandibular musculature of *Dermatemys mawii* (UF herp 04770). (a–c) Lateral views of left mandibular ramus with various muscle models removed. (d) Anterolaterodorsal view of left mandibular ramus. (e-g) Medial views of left mandibular ramus with various muscle models removed. Muscle names are in italics. Double-sided arrows indicate muscle head origins, with round arrow head indicating the muscle head and pointed arrow head indicating origin site. Thick arrow points to the position of the processus trochlearis oticum. cap, coronar aponeurosis; cera, cerebral artery; f, frontal; ma, mandibular artery; *m.add.m.ex.P.m.*, *m. adductor mandibulae externus Pars medialis (No. 17)*; *m.add.m.ex.P.pf.*, *m. adductor mandibulae externus Pars profundus (No. 19)*; *m.add.m.ex.P.sf.*, *m. adductor mandibulae externus Pars superficialis (No. 21)*; *m.add.m.int.*, *m. adductor mandibulae internus (No. 23–28)*; *m.add.m.pos.*, *m. adductor mandibulae posterius (No. 29)*; *m.dep.m.*, *m. depressor mandibulae (No. 45)*; *m.intm.*, *m. intermandibularis (No. 31)*; mand, mandibular bones; mra, median raphe; op, opisthotic; opp, opposite sided muscular fibers; pa, palatine artery; par, parietal; pro, prootic; pt, pterygoid; pto, processus trochlearis oticum; q, quadrate; qj, quadratojugal; soc, supraoccipital; sq, squamosal; V_2, maxillary ramus of trigeminal nerve; V_3, mandibular branch of trigeminal nerve; VII_{ct}, chorda tympani ramus of facial nerve; VII_{hyo}, hyomandibular ramus of facial nerve

The mandibular nerve (CN V_3) splits into two major, anteriorly directed nerves that follow the intra- and extra-alveolar arterial branches (Figure 2a,c). The exterior nerve can be identified as the nervus lingualis of Fuchs (1931) (= Ramus intermandibularis medius of Poglayen-Neuwall, 1953), and the internal nerve as the nervus alveolaris inferior (Fuchs, 1931; = Ramus alveolaris of Poglayen-Neuwall, 1953). We also found a small posteriorly directed nerve, paralleling the course of the anterior auriculotemporal artery. In the CT scans, we could not trace this small nerve further posteriorly, but it may be a second auriculotemporal ramus. The nervus mylohyoideus of Fuchs (1931; ramus intermandibularis of V_3 of Soliman, 1964 and Gaffney, 1972; Ramus intermandibularis caudalis of Poglayen-Neuwall, 1953), which was observed to exit through the intermandibular foramina in turtles (Fuchs, 1931; Poglayen-Neuwall, 1953; Soliman, 1964), seems to be very small in *Dermatemys mawii*, and we could not consistently trace it through the CT scans.

The facial nerve (CN VII) is the second cranial nerve with relevance to mandibular innervation. In *Dermatemys mawii*, the facial nerve extends from the fossa acustico-facialis on the internal braincase surface through a canal in the prootic into the canalis cavernosus, where it forms the geniculate ganglion, as correctly inferred by Rollot et al. (2021) based on osteology. The anterior palatine branch of the facial nerve (CN VII) extends anteroventrally, entering the internal carotid artery canal (Figure 2b), the posterior hyomandibular branch extends through the canalis cavernosus and into the cavum acustico-jugulare. Here, the hyomandibular nerve sends off a ventral branch, the chorda tympani branch of the facial nerve (CN VII; Figure 2b). This branch enters the quadrate and extends ventrally through that bone, exits it again, and innervates the articular. In *Dermatemys mawii*, a large posterior chorda tympani foramen is absent in the articular, but the associated anterior canal in many turtles (see osteological descriptions) indicates that the chorda tympani nerve may further innervate more anterior mandibular structures in other taxa. The hyomandibular branch of *Dermatemys mawii* extends posteriorly to the *m. depressor mandibulae*, which it innervates (Werneburg, 2011; Figure 2b,d; Figure 3a,c,e).

3.3 | Mandibular musculature of *Dermatemys mawii*

We identified the mandibular musculature of *Dermatemys mawii* (UF herp 04770) based on the work of Werneburg (2011) and follow the nomenclature used in that study. We also include muscle numerical labels of Werneburg (2011) for easier readability. The *m. adductor mandibulae internus* (Nos. 23–28) is a large muscle with several distinct muscle heads that originate at different parts of the cranium (Figure 3c,g). One such muscle head originates dorsally above the eyeball, in a small fossa principally formed by the ventrolateral surface of the frontal (Figure 3d,g). Another muscle head originates on the dorsal surface of the pterygoid, anterolaterally to the secondary braincase wall (Figure 3g). The mandibular artery traverses between these two muscle heads (Figure 3a,d). The central part of the *m. adductor mandibulae internus* (Nos. 23–28) originates at the lateral surface of the descending process of the parietal, anterior to the position of the trigeminal foramen. At the trigeminal foramen, the muscle forms a posteromedial portion that is distinct from more anterior portions by a vertical gap through which the maxillary and mandibular rami of the trigeminal nerve pass (Figure 3c). This muscle portion originates at the anteroventral surface of the otic capsule, largely the prootic (Figure 3g), and is medially contacted by the *m. adductor mandibulae posterius* (No. 29; Figure 3c). A last distinct muscle head of the *m. adductor mandibulae internus* (Nos. 23–28) originates on ventromedially exposed skull surfaces of the quadrate and pterygoid (Figure 3g), thereby wrapping around the quadrate articular process. Although the *m. adductor mandibulae internus* (Nos. 23–28) can thus be separated into several distinct muscle portions near the origination sites, as also reported by Werneburg (2011), we segmented the muscle as a single 3D model. This is because the dorsally distinct muscle portions intertwine ventrally near the relatively small muscle insertion site, which is limited to the prearticular margin of the dorsal opening into the fossa Meckelii (Figure 3g).

The already mentioned *m. adductor mandibulae posterius* (No. 29) is a small muscle, which originates at the anterior surface of the otic capsule, primarily the quadrate and prootic (Figure 3b), and inserts to both sides (i.e., surangular and prearticular) of the posterior end of the opening into the fossa Meckelii (Figure 3c). The *m. adductor mandibulae posterius* (No. 29) becomes laterally completely covered by the different parts of the *m. adductor mandibulae externus* (Nos. 17, 19–21; Figure 3a,b), which could be well segmented into individual models. The *m. adductor mandibulae externus Pars medialis* (No. 17) is the smallest of the external adductors, and forms a short but broad muscle package that originates at the anterior surface of the quadrate and inserts within the adductor fossa onto the surangular and dentary (Figure 3b). The remaining two external adductor parts are much larger, and, together with the coronar aponeurosis (tendon), form the peculiar trochlear jaw mechanism of turtles.

As *Dermatemys mawii* is a cryptodire, the external jaw adductors are re-directed from their origination around an otic trochlear process (= processus trochlearis oticum; Gaffney, 1979), which is formed by the prootic and quadrate at the anterior margin of the otic capsule. In *Dermatemys mawii*, the processus trochlearis oticum is relatively inconspicuous, and formed a shallow transverse concave surface that only forms a mildly anteriorly projecting surface. The position of the otic trochlear is apparent from the coronar aponeurosis morphology by a clear kink (Figure 3b,f). The muscle fibers of the *Partes profundus* (No. 19) and *superficialis* (No. 21) of the *m. adductor mandibulae externus* (No. 17, 19–21) also show clear changes in orientation with regard to the trochlea: the fibers are predominantly vertically oriented at any position anterior to the trochlea, but have a strong horizontal component posterior to it (Figure 3a,d). The coronar aponeurosis originates posteriorly in the upper temporal fossa, between the *Partes profundus* (No. 19) and *superficialis* (No. 21) as a relatively thin band that lies in between the *Pars profundus* (No. 19) head dorsally, and the *Pars superficialis* (No. 21) head ventrally (Figure 3b). The head of the *m. adductor mandibulae externus Pars profundus* (No. 19) originates at the supraoccipital crest medially, whereas more anteriorly positioned muscle fibers originate on the lateral surfaces of the main supraoccipital portion and the parietal (Figure 3e). The posteriormost muscle fibers of the *Pars superficialis* (No. 21) have only a minor medial attachment to the supraoccipital, and are otherwise embedded in muscle (*Pars profundus* (No. 19), and cervicocranial musculature). Slightly more anteriorly, the muscle parts are reoriented to lie mediolaterally adjacent to another, whereby the *Pars superficialis* (No. 21) assumes the more lateral position (Figure 3a). The *Pars profundus* (No. 19) becomes dorsoventrally flatter but transversely broader and has a large ventrolateral surface along which muscle fibers originate from the lateral parietal surface within the temporal fossa (Figure 3e). The *m. adductor mandibulae externus Pars superficialis* (No. 21) has its primary contact to the bony cranium at this level. Along its ventral surface, muscle fibers originate on the dorsally exposed surfaces of the quadrate and squamosal (Figure 3a). The coronar aponeurosis becomes a vertically sheeted tendon at this level, which separates the *Partes profundus* (No. 19) and *superficialis* (Nos. 19, 21; Figure 3b). Our 3D models show nicely how individual muscle fibers of both muscle portions insert onto the tendon (Figure 3a,d). Hereby, the *Pars profundus* (No. 19) fibers cross the dorsal margin of the tendon and insert around the margin on the lateral surface of the coronar aponeurosis (Figure 3b). Fibers of the *Pars superficialis* (No. 21) pass anteromedially from their origin sites to insert onto the lateral surface of the coronar aponeurosis (Figure 3a,d). Immediately posterior to the otic trochlear process, the *Pars profundus* (No. 19) has a small sheeted muscle portion extending ventrally to the coronar aponeurosis. These fibers contact the opisthotic (Figure 3e). At the level of the otic trochlea, the coronar aponeurosis becomes ventrally broadened, and dorsoventrally thickened. It is likely that the thickened parts include the cartilage transiliens, as this is formed by the tendon (Werneburg, 2011). At the anterior trochlear margin, the coronar aponeurosis becomes anteroventrally deflected, still retaining its broad ventral surface (Figure 3b,f). The *m. adductor mandibulae externus Pars profundus* (No. 19) becomes smaller shortly anterior to the position of the otic trochlea. The anteriormost muscle fibers originate at the parietal, and insert at the dorsal surface of the coronar aponeurosis, but well above the insertion of the tendon onto the mandible (Figure 3D). The *Pars superficialis* (No. 21), on the other hand, becomes larger anterior to the otic trochlea position. A short but distinct additional muscle head originates on the anterior quadrate surface, above the level of the *Pars medialis* (No. 17) origin (Figure 3a). Laterally, the *Pars superficialis* (No. 21) also contacts the quadratojugal (Figure 3d). The anteroventral portion of the *Pars superficialis* (No. 21) has insertion sites along the coronar aponeurosis, but also along the margin of the mandibular adductor fossa, that is, at the dentary and surangular (Figure 3a,d). The coronar aponeurosis becomes less sheeted ventral to the last *Pars profundus* (No. 19) fiber insertions and forms a broad cap onto the coronoid process (Figure 3b,d,f), which, in *Dermatemys mawii*, is a low structure formed to equal parts by the dentary and coronoid bones.

The *m. depressor mandibulae* (No. 45) has two primary heads and muscle parts that can be distinguished for much of their course, but as the muscle portions are strongly intertwined along their central contact, we segmented them as a single model. The two muscle heads are mediolaterally adjacent. The lateral head originates at the lateral and ventral surface of the squamosal and extends to the posterior end of the paroccipital process of the opisthotic (Figure 3c). This lateral muscle parts extends ventrally around the mandibular articulation, and inserts on the angular, surangular, dentary, and articular. The medial muscle head is wrapped around the dorsal surface of the ceratobranchial I (Figure 3c), and ventrally the muscle inserts along the more medial surfaces around the cranial articulation area of the mandible, particularly the angular, prearticular, and articular.

The *m. intermandibularis* (No. 31) is a sheeted muscle that forms a dorsally concave muscle surface between the mandibular rami. Posteriorly, left and right

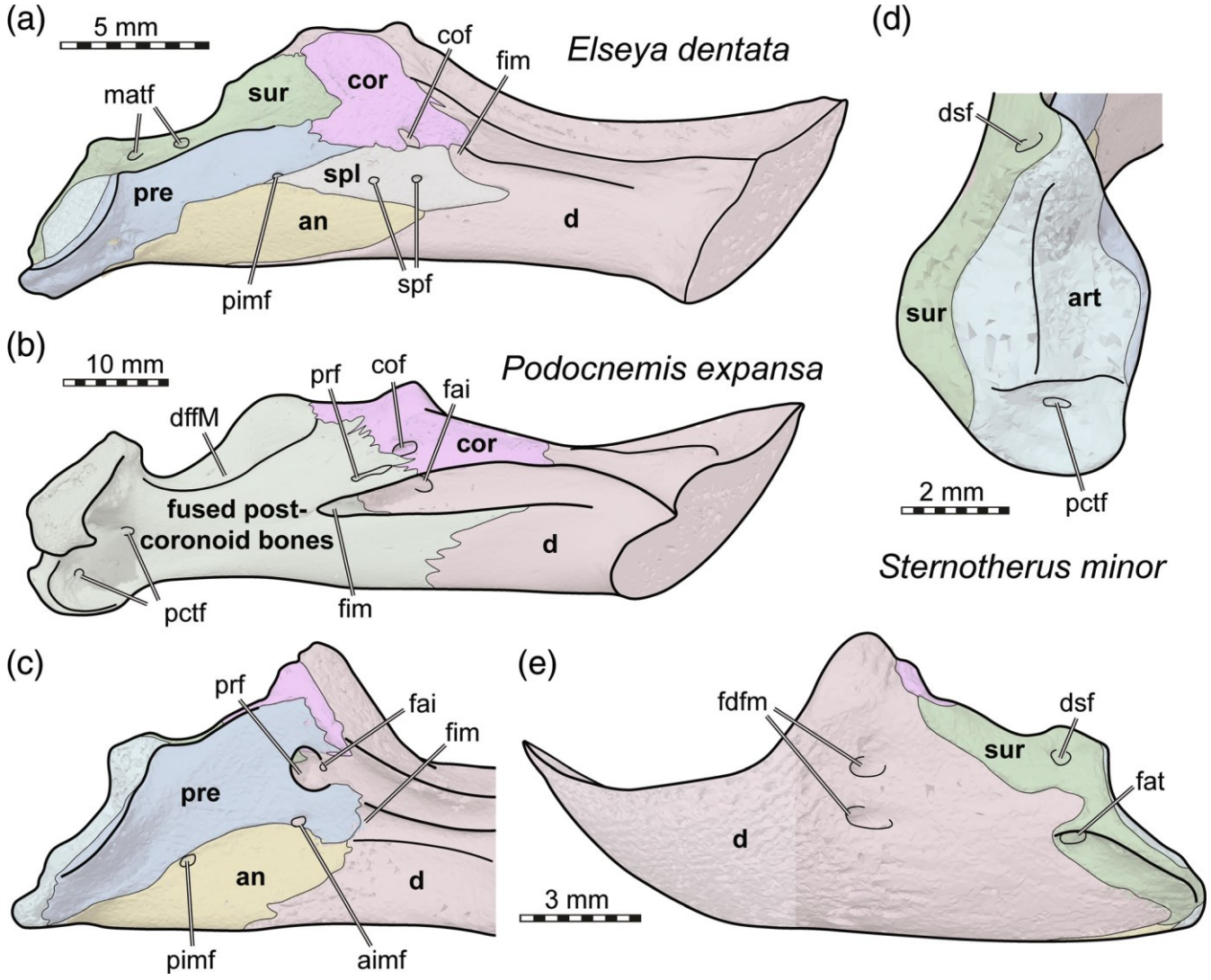

FIGURE 4 Overview of mandibular foramina of turtles. The panels show semitransparent 3D renderings of mandibles in different views with overlaid interpretative line drawings. Specimens and views are chosen so that all major foramina are illustrated. (a) Mandible of the chelid *Elseya dentata* in medial view. (b) Mandible of the podocnemidid *Podocnemis expansa* in medial view. (c) Posterior part of mandible of the kinosternid *Sternotherus minor* in medial view. (d), posterodorsal view onto the mandibular articulation area of *Sternotherus minor*. (e) Mandible of *Sternotherus minor* in lateral view. Note that bones are labeled in bold, and foramina in normal font. aimf, anterior intermandibular foramen; an, angular; art, articular; cof, coronoid foramen; cor, coronoid; d, dentary; dffM, dorsal foramen into the fossa Meckelii; dsf, dorsal surangular foramen; fai, foramen alveolare inferius; fat, foramen auriculotemporalis; fdfm, foramen dentofaciale majus; fim, foramen intermandibular medius; matf, medial auriculotemporal foramina; pctf, posterior chorda tympani foramen/foramina; pimf, posterior intermandibular foramen; pre, prearticular; prf, prearticular foramen; spf, splenial foramen; spl, splenial; sur, surangular

m. intermandibularis (No. 31) can be well distinguished, as their fibers attach to a median raphe (Werneburg, 2011). In *Dermatemys mawii*, however, more anterior portions of the right- and left-sided musculature are directly attached to one another, forming a singular muscle mass that we could not digitally separate, so that we simply performed a parasagittal cut in the skull midline across the muscle fibers (Figure 3e). Whereas Werneburg (2011) reported that the *m. intermandibularis* (No. 31) originates at the dentary, angular, and Meckelian cartilage for *Emydura subglobosa*, the muscle in *Dermatemys mawii* only originates dorsally to the level of the Meckelian cartilage along the prearticular, coronoid, and dentary (Figure 3e).

3.4 | Nomenclature of foramina

Anterior intermandibular foramen (= Foramen intermandibularis oralis of Gaffney, 1972). Small foramen that is not consistently present in turtles. The foramen is

positioned between the anterior ends of the prearticular and angular and can only be formed when an anteroventral process of the prearticular is ossified or when a splenial is present. It connects the anterior section of the fossa Meckelii with the intermandibular space and is traversed by both blood vessels and nerves. See Figure 4c.

Posterior chorda tympani foramen (= Foramen posterius chorda tympani of Gaffney, 1972). Small-to-mid-sized foramen for the chorda tympani nerve that is present in most, but not all turtles. The foramen is usually found in one of two positions: Either it lies within the articular notch or otherwise the posteroventral surface of the articular (Figure 4d), or it lies on the posteromedial part of the prearticular (Figure 4b). When present, the foramen leads into a canal that traverses the articular and/or prearticular and opens within the fossa Meckelii, either within its floor or within the medial surface of the prearticular.

Coronoid foramen. Small foramen that is present in some turtles within the anteroventral process of the coronoid. It connects the anterior part of the fossa Meckelii with the intermandibular space. See Figure 4a,b.

Dorsal surangular foramen. Relatively large foramen on the dorsal or lateral surface of the surangular, anterior to the mandibular articulation. The foramen is not consistently present in turtles, but common. It is connected via a ventrally directed, vertical surangular canal with the foramen auriculotemporalis. See Figure 4d,e.

Dorsal foramen into the fossa Meckelii. Large opening posterior to the coronoid process and anterior to the mandibular articulation, which is usually bound medially by the prearticular and laterally by the surangular. Anteriorly, the opening is usually formed by the coronoid, and sometimes the articular posteriorly. The opening leads into the fossa Meckelii, and the internal mandibular artery and the main branch of the mandibular nerve (CN V_3) pass through it. See Figure 4b.

Foramen alveolare inferius (as in Gaffney, 1972). Relatively large foramen on the medial surface of the dentary. The foramen is often concealed in medial view by the coronoid and/or prearticular (in which case it opens from within the fossa Meckelii), but remains exposed in many turtles (in which case it lies in the Meckelian groove). The foramen leads into an anteriorly directed alveolar canal, which houses the internal alveolar branch of the mandibular artery and the nervus alveolare inferius of the mandibular nerve (CN $V_{3\text{-}ai}$). See Figure 4b,c.

Foramen auriculotemporalis (= Foramen nervi auriculotemporalis of Gaffney, 1972). Usually, a large foramen at the posteroventral aspect of the lateral surface of the surangular. The foramen is usually positioned anteroventral to the ectocondyle flange of the surangular. The foramen can be a single large opening, two large openings, or a series of smaller openings. Sometimes, the foramen is positioned within a recessed fossa. The foramen leads to an anteromedial canal that projects through the surangular and opens into the fossa Meckelii. In turtles in which a dorsal surangular foramen is present, the foramen is additionally connected to the dorsal surangular foramen via a short vertical canal. Gaffney (1972) reported the foramen to hold the auriculotemporalis nerve (based on observations by Fuchs, 1931, Soliman, 1964). Besides this nerve, we found a large blood vessel (auriculotemporal branch of the mandibular artery) to pass through the foramen. In some turtles, the foramen internally communicates with the chorda tympani canal system on the medial jaw side. See Figure 4e.

Foramen dentofaciale majus (as in Gaffney, 1972). Usually, a large foramen at the lateral surface of the dentary, either in the anterior margin of the adductor fossa or slightly anterior to it. The foramen can be reduced in diameter, or formed as several smaller foramina. The respective canal(s) lead anteromedially into the dentary and meet the inferior alveolar canal. Gaffney (1972) did not report soft tissue structures that pass through the foramen, but our segmentations show that it houses a large arterial branch (dentofacial branch) of the mandibular artery. See Figure 4e.

Foramen intermandibulare medius (as in Gaffney, 1972). This foramen is simply the anterior opening of the fossa Meckelii into the intermandibular space and the Meckelian groove. Due to variation in the anterior development of the angular and prearticular, the position of the foramen varies. Both nerve and blood vessels pass through the opening. See Figure 4a–c.

Posterior intermandibular foramen (= Foramen intermandibularis caudalis of Gaffney, 1972). A foramen found in most turtles that can be quite large. It is usually positioned between the angular and prearticular but can be dorsally removed from the suture and thus lie entirely in the prearticular, or, less frequently, it can be ventrally positioned fully in the angular. It opens from the fossa Meckelii into the intermandibular space and houses both nerves and blood vessels. See Figure 4a,c.

Prearticular foramen. Foramen that is positioned in the anterodorsal area of the prearticular, either completely surrounded by it or between the prearticular-coronoid contact. It connects the fossa Meckelii with the intermandibular space. The prearticular foramen is distinct from the coronoid foramen, as both foramina are present in *Podocnemis* spp. (Figure 4b). The foramen is present in only few turtle species, and its correspondent soft-tissue structures are unclear. See Figure 4b,c.

Splenial foramen. Foramen that passes mediolaterally through the splenial, and thus connects the fossa Meckelii with the intermandibular space. See Figure 4a.

3.5 | Osteological descriptions of turtle mandibles

For the descriptions below, we list the digitally prepared specimens at the beginning of each taxonomic section, but we do not recite the specimen numbers for following mentions of the specimens. Sometimes, we refer to additional specimens for which we do not have CT scans and 3D models; in these instances, the specimen numbers are given at each mention.

3.5.1 | Trionychidae

Trionychids can be distinguished into two major subclades, the Cyclanorbinae and Trionychinae. The following descriptions are based on 3D models of the cyclanorbine *Cycloderma frenatum* (NHMUK 84.2.4.1) and the trionychines *Amyda cartilaginea* (FMNH 244117), *Apalone mutica* (FHSM herp 2746), *Apalone spinifera* (FMNH 22178), *Chitra chitra* (NHMUK 1936.12.16.1), and *Trionyx triunguis* (PCHP 4559). The mandibles of trionychids are generally very similar among the group, with some omnipresent characteristic features, such as dorsally tall coronoid processes, the presence of retroarticular processes, and the constriction of the fossa Meckelii to a narrow, slit-like opening.

The dentaries are well fused in trionychids. The symphyseal area is variously elongated with respect to the width of the triturating surface along each mandibular ramus, without a clear systematic trend: Within trionychines, extended symphyses are present in *Apalone spinifera* and *Amyda cartilaginea*, but not in *Chitra chitra*. In cyclanorbines this character is variable; *Lissemys punctata* (USNM 293690) has an extended symphyseal area, but this is not the case in *Cycloderma frenatum*. Extreme symphyseal elongation is known from some fossil species, such as the plastomenid *Plastomenus thomasii* (Hay, 1908), but this is not observed in extant trionychids. Symphyseal ridges are generally absent in trionychids, although *Amyda cartilaginea* has a weakly developed ridge (Figure 5a; Meylan & Gaffney, 1989). In taxa with expanded symphyseal areas, the triturating surfaces are medially expanded and form dorsally oriented surfaces that occlude with respective cranial surfaces (e.g., *Apalone spinifera*, *Amyda cartilaginea*, *Lissemys punctata*; Figure 5a). In taxa without this expansion (e.g., *Chitra chitra*, *Cycloderma frenatum*), the triturating surfaces are sloping ventromedially from a relative sharp-edged labial ridge (Figure 5e; Figure 6a). The labial ridges in trionychids are generally lined with a densely spaced single row of neurovascular foramina. Such foramina are otherwise not abundant on trionychid dentaries, but usually a second row of larger foramina is found toward the ventral edge of the keratinous rhamphotheca (Figure 5b,f; Figure 6b). Lingual ridges are generally absent or at least extremely reduced in trionychids; among our studied specimens, only *Chitra chitra* has a lingual ridge, but it is not continuous along the entire dentary ramus, as it fades anteriorly (Figure 5e). The foramen dentofaciale majus is strongly reduced in trionychids, and entirely absent in cyclanorbines (*Lissemys punctata*, *Cycloderma frenatum*; Figure 6b) as well as some trionychines (e.g., *Chitra chitra*; Figure 5f). When present, the foramen is positioned far anteriorly to the coronoid process. Laterally, the dentaries of trionychids bear only extremely shallow adductor fossae (Figure 5b,f; Figure 6b), which are ventrally defined by a slightly laterally protruding edge of the ventral dentary margin. Posteriorly, the dentary overlaps most of the surangular, and it also forms the ventral margin of the mandible, so that the angular is much better visible in medial view than ventral view. In all trionychids, the dentary forms a dorsal process that ascends in the anterior margin of the coronoid process (Figure 5b,f; Figure 6b). On its medial surface, the dentary forms the Meckelian groove, with extends anteriorly deeply into the symphyseal area in taxa in which this region is expanded. The foramen alveolare inferius opens dorsally to the level of the Meckelian groove and ventrally below the articulation with the coronoid, and is well visible in medial view of trionychid mandibles (Figure 5d,h; Figure 6d).

The surangular of trionychids has moderate exposure due to the overlap of the dentary. In all trionychids, the surangular forms a rounded lateral ectocondyle flange, which expands the articulation area for the quadrate and forms the lateral half of the articulation surface (Figure 5c,g; Figure 6c; Meylan, 1987). The dorsal surface of this surangular ectocondyle flange is gently concave, whereas the sutural area to the articular bone forms an anteroposterior, raised ridge that separates the articular surface into two concave subfacets. On the lateral surface of the mandible, the surangular of trionychids bears several small foramina nervi auriculotemporalis (Gaffney, 1972), which in trionychids are usually formed as two anteroposterior foramina which are relatively widely spaced (e.g., *Cycloderma frenatum*; *Amyda cartilaginea*; see also Meylan, 1987; Meylan & Gaffney, 1989), but which can vary in number (Figure 5b,f; Figure 6b). These are positioned just ventrally to the ectocondyle flange. Posterior to the articulation area, the surangular is expanded to form the lateral half of the retroarticular process (Figure 5c,g; Figure 6c). The anterior part of the surangular is laminar and forms a bony sheet parallel to the prearticular. Both bones are only narrowly spaced, thereby constricting the opening to the fossa Meckelii to a narrow slit-like opening, which is anterodorsally

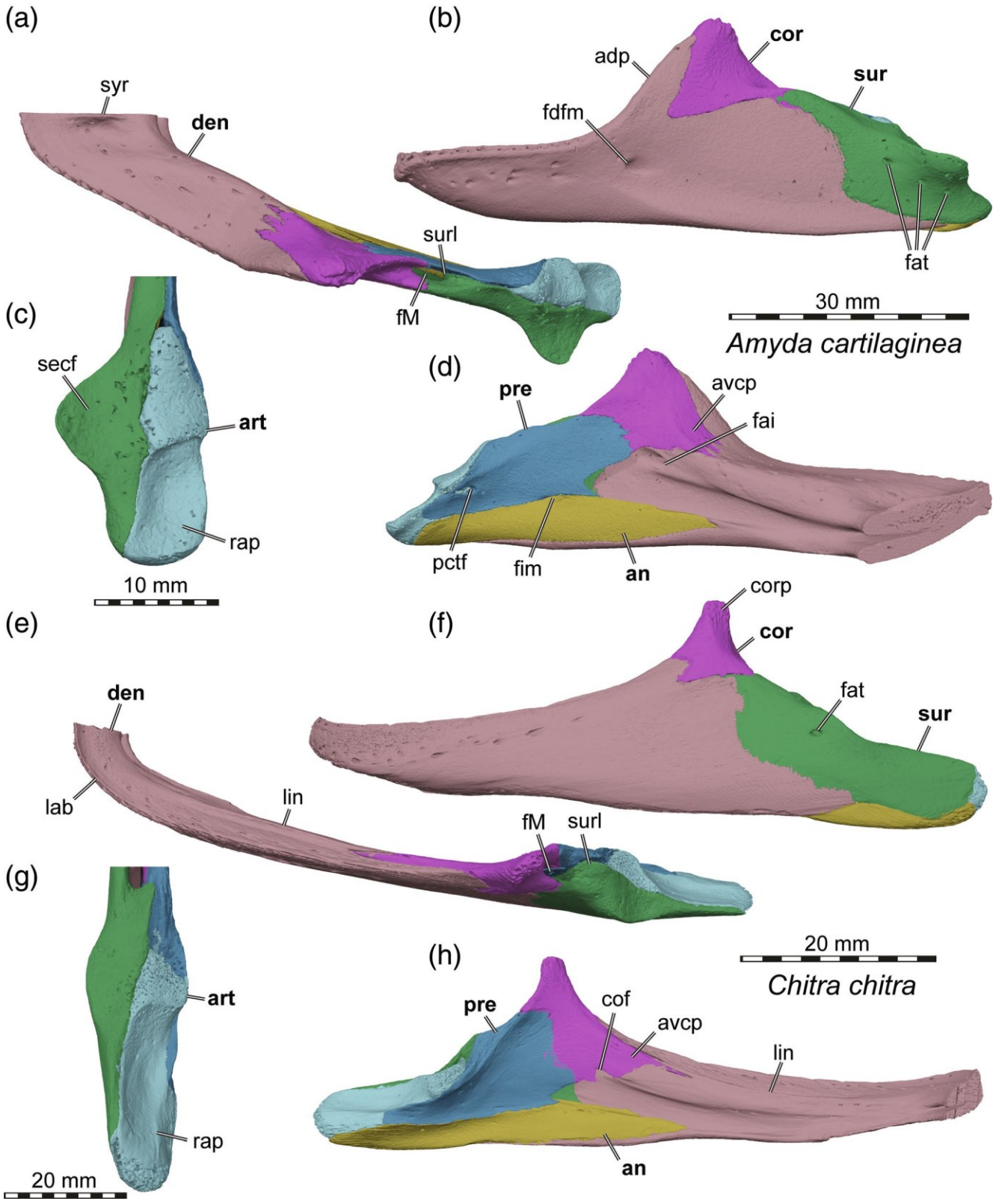

FIGURE 5 Legend on next page.

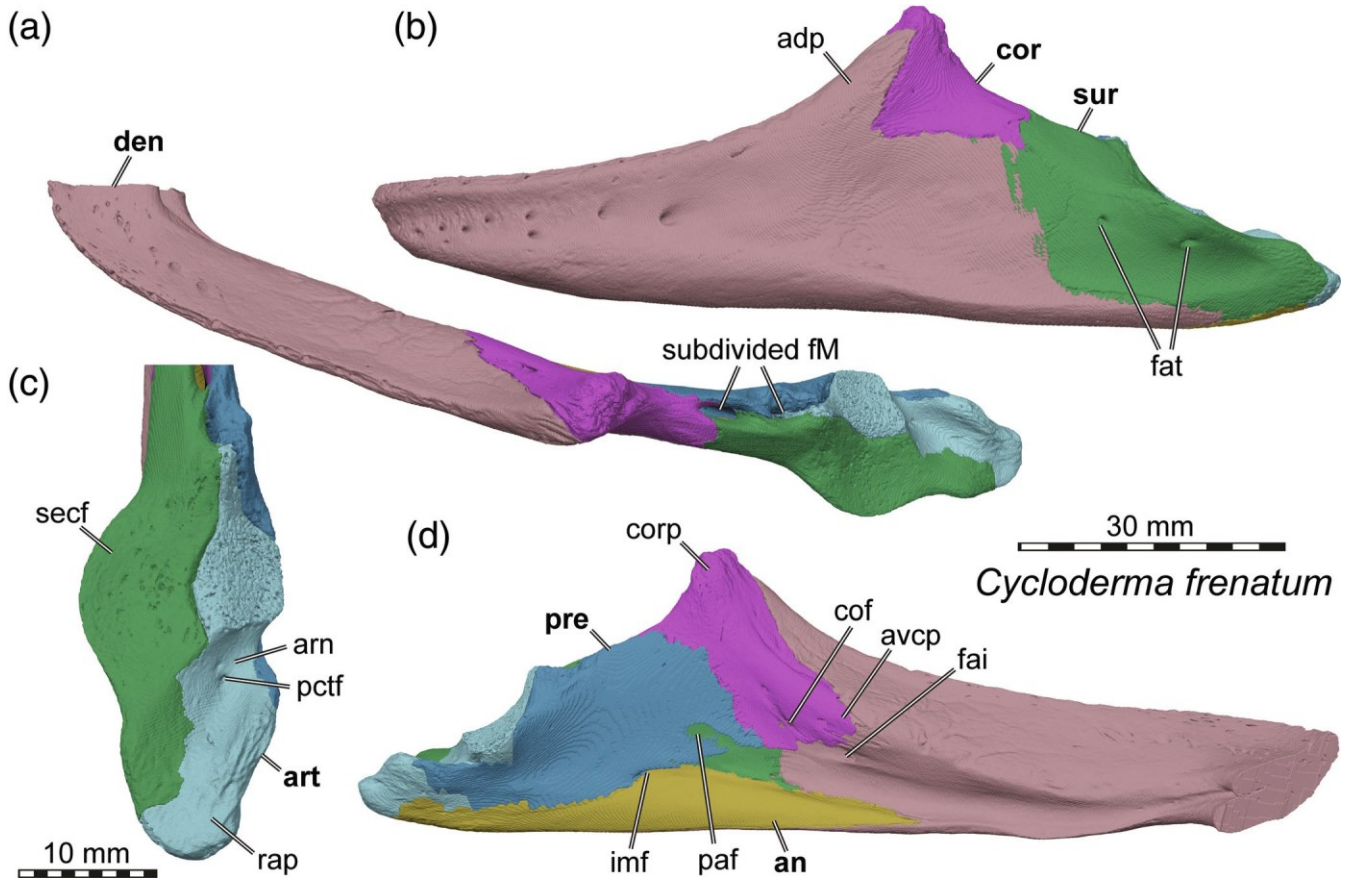

FIGURE 6 3D renderings of mandible of the cyclanorbine trionychid *Cycloderma frenatum* (NHMUK 84.2.4.1). (a) Dorsal view. (b) Left lateral view. (c) Close-up of articular surface. (d) Medial view onto left mandibular ramus. Note that bones are labeled in bold, and other features in normal font. adp, ascending dentary process; an, angular; arn, articular notch; art, articular; avcp, anteroventral process of the coronoid; cof, coronoid foramen; cor, coronoid; corp, coronoid process; den, dentary; fai, foramen alveolare inferius; fat, foramen auriculotemporalis; fM, fossa Meckelii; imf, intermandibular foramen; paf, prearticular foramen; pctf, chorda tympani foramen; pre, prearticular; rap, retroarticular process; secf, ectocondylar flange of surangular; sur, surangular

closed by the coronoid. A recurved and prominent surangular lamina within the fossa Meckelii is not developed (Evers & Benson, 2019). In *Cycloderma frenatum*, the opening into the fossa Meckelii is subdivided by a bony contact between the surangular and prearticular (Gaffney, 1979; Meylan, 1987; Figure 6a).

The coronoid of trionychids is well developed and forms a triangular, tall coronoid process (Figure 5b,d,f,h; Figure 6b,d). In most species, the process is almost spike-like and projects dorsally (e.g., *Chitra chitra*), but the tip of the process may be gently posteriorly recurved, as in *Apalone spinifera*. Anteroventrally, the coronoid forms a medial process that usually is weakly involved in the posterior part of the triturating surface (Figure 5a,e; Figure 6a; Siebenrock, 1897). A coronoid foramen is variably present in this anteromedial process and sometimes remains only party ossified (e.g., Figure 5h).

The prearticular in trionychids is a sheet-like bone, which posteriorly bulges somewhat medially to make room for the articular. Intermandibular foramina are

FIGURE 5 3D renderings of mandibles of selected trionychine trionychids. (a–d) *Amyda cartilaginea* (FMNH 244117). (e–h) *Chitra chitra* (NHMUK 1936.12.16.1). (a and e) Dorsal view. (b and f) Left lateral view. (c and g) Close-up of articular surface. (d and h) Medial view onto left mandibular ramus. Note that bones are labeled in bold, and other features in normal font. adp, ascending dentary process; an, angular; art, articular; avcp, anteroventral process of the coronoid; cof, coronoid foramen; cor, coronoid; corp, coronoid process; den, dentary; fat, foramen auriculotemporalis; fdfm, foramen dentofaciale majus; fM, fossa Meckelii; imf, intermandibular foramen; lab, labial ridge; lin, lingual ridge; pctf, posterior chorda tympani foramen; pre, prearticular; rap, retroarticular process; secf, ectocondylar flange of surangular; sur, surangular; surl, surangular lamina; syr, symphyseal ridge

generally absent (e.g., *Apalone mutica*, *Apalone spinifera*, *Chitra chitra*, *Trionyx triunguis*; Siebenrock, 1897, Meylan, 1987), but a single posterior intermandibular foramen in the suture with the ventrally adjacent angular is present in *Amyda cartilaginea* (Figure 5d), and the foramen is anteriorly not fully ossified but present in *Cycloderma frenatum* (Figure 6d).

The angular of trionychids is mostly restricted to the medial surface of the mandibular ramus (Figure 5; Figure 6) and forms an anteriorly tapering wedge between the prearticular dorsally and dentary ventrally. Posterior to the dentary extent, the posteriormost part of the angular is mediolaterally broadened, and twisted so that it forms a cup-like ventral buttress to the articular.

The splenial is absent in trionychids.

The articular of trionychids is anteroposteriorly elongated, as it forms the medial half of the articulation surface anteriorly, and most of the retroarticular process posteriorly (Figure 5c,g; Figure 6c). The articular is not well co-ossified with the surrounding bones (surangular laterally, angular ventrally, prearticular medially) and is often lost in osteological specimens. In all trionychids, the margin of the articular that faces the surangular in the articulation surface is slightly bulged, creating an anteroposteriorly trending ridge that separates the ecto- and entocondyle subfacets. The dorsal surface of the articular is usually slightly medially inclined, but only very weakly concave. The beginning of the retroarticular process is usually marked by a step-like ridge in the posterior margin of the articular surface. The retroarticular process is dominated by a strongly concave groove that we call articular notch, and this concavity may be hypertrophied by lateral and medial ridges, such as in *Chitra chitra* or *Cycloderma frenatum*. Overall, the retroarticular process is extremely elongate in trionychids (Meylan, 1987).

3.5.2 | Carettochelyidae

Carettochelyidae today is represented by a single species, *Carettochelys insculpta*. The mandible of this species was described in some detail by Walther (1922), but the original text is in German and the anatomical description uses old termini (e.g., interchangeably "operculare" or "spleniale" for what today is called the "prearticular"). Our description below is based on the full segmentation of an adult individual (USNM 327960).

The dentaries of *Carettochelys insculpta* are fused along a slightly expanded symphysis. The tip of the beak forms a gently upcurved symphyseal hook. The labial ridges are present and sharp-edged, but low (Figure 7a,b,d). A lingual ridge is absent, as is a symphyseal ridge. The triturating surfaces are medially gently inclined, and somewhat broader at the symphysis than near the coronoid process. There is a single line of relatively large neurovascular foramina that lines the center of the triturating surface, which curves along both dentary rami and along the symphysis (Figure 7a). On the lateral dentary surface, there is a relatively dense network of small neurovascular foramina, which are concentrated near the labial ridge (Figure 7b). A dorsally ascending dentary process is present although much shorter than in trionychids. It slots deeply into a respective groove on the coronoid. Posteriorly to this dentary-coronoid contact, the dentary is deeply excavated by a strongly developed adductor fossa, which is anteriorly and ventrally lined by a clearly defined edge, which we term lateral dentary ridge (Figure 7b). The foramen dentofaciale majus is a large opening within the anterior edge of the adductor fossa (Figure 7b), but becomes internally divided by a lamina of bone to form several canals. Ventrally below the adductor fossa, the lateral surface of the dentary is lined by anteroposteriorly extending striations (Figure 7b). Overall, the posterior extent of the dentary is relatively short in *Carettochelys insculpta*, revealing much of the surangular in lateral view (Figure 7b). As in trionychids, the foramen alveolare inferius on the medial surface of the dentary is well exposed (Figure 7d). In *Carettochelys insculpta*, the foramen is extremely large.

The surangular of *Carettochelys insculpta* is a relatively prominent bone of the mandible, and much of its extent is exposed in lateral view, where it contacts the dentary and the coronoid (Figure 7b). With its anterodorsal process, it forms the lateral wall of a narrow but elongate opening into the fossa Meckelii (Figure 7a). On the medial surface, the surangular bears a small recurved surangular lamina (Figure 7a). In the posterior half, the surangular forms a laterally well expanded and rounded ectocondyle flange, which forms the lateral half of the mandibular articular surface (Figure 7c). As such, the surangular is the main bone forming most of this surface in *Carettochelys insculpta*. The surangular part of the articulation surface is flat or very gently concave. Posterior to the articulation area, the surangular narrows mediolaterally and forms parts of the retroarticular process, which is largely formed by the articular (Figure 7c). Ventrally below the ectocondyle flange, the lateral surface of the surangular is excavated by an unusual fossa, which is roughly bean-shaped and which bears the foramen auriculotemporalis within its anterior perimeter (Figure 7b).

The coronoid is a tall bone in *Carettochelys insculpta* and forms a dorsally pointed and slightly posteriorly recurved coronoid process (Walther, 1922), so that a weak coronoid notch is present (Figure 7b). Anteromedially, the coronoid forms a short but distinct process that extends into the triturating surface (Figure 7a,d), and which is sutured to the dentary via two large, spike-like

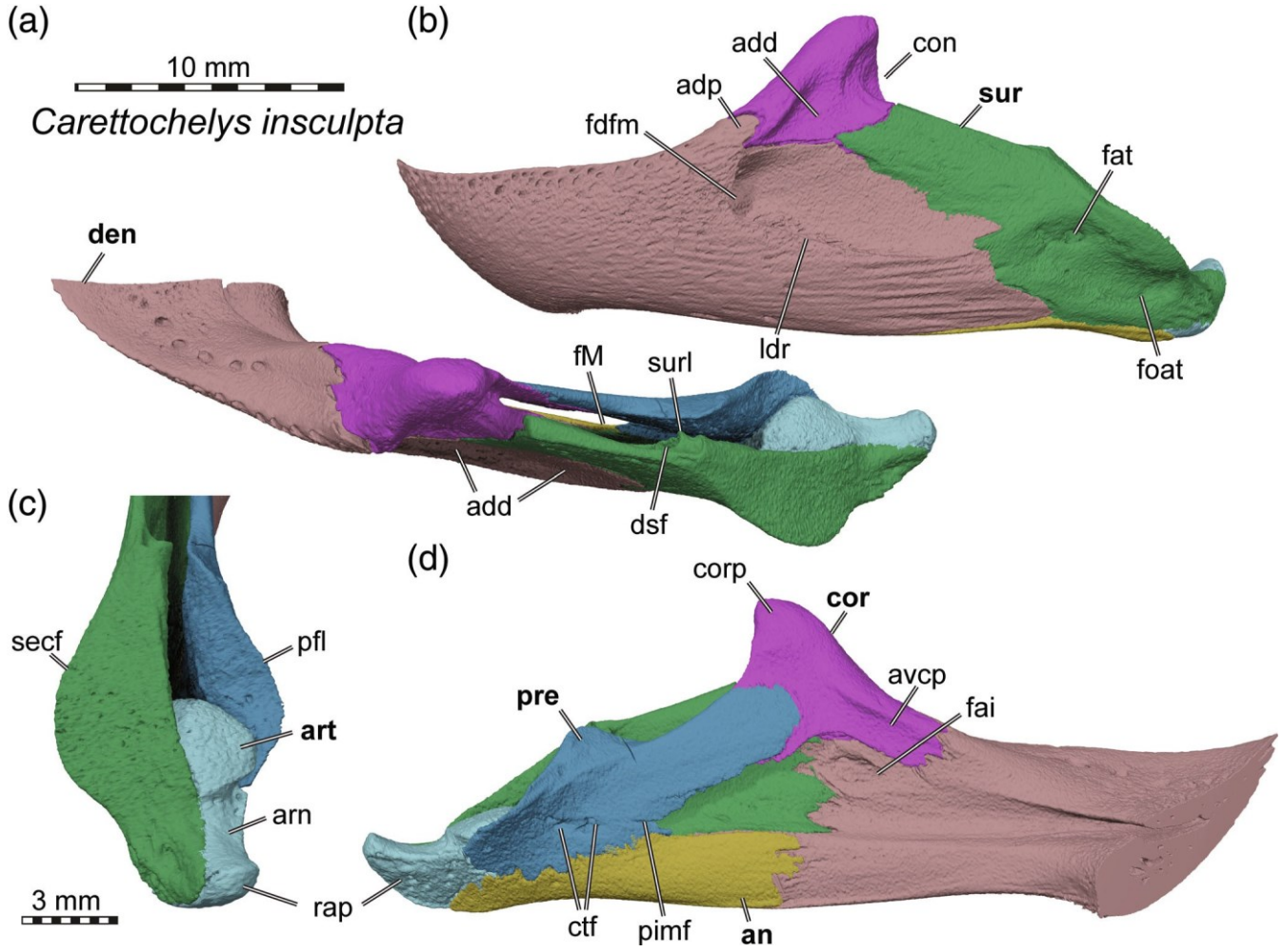

FIGURE 7 3D renderings of mandibles of the carettochelyid *Carettochelys insculpta* (USNM 327960). (a) Dorsal view. (b) Left lateral view. (c) Close-up of articular surface. (d) Medial view onto left mandibular ramus. Note that bones are labeled in bold, and other features in normal font. add, adductor fossa; adp, ascending dentary process; an, angular; arn, articular notch; art, articular; avcp, anteroventral process of the coronoid; con, coronoid notch; cor, coronoid; corp, coronoid process; ctf, chorda tympani foramen; den, dentary; dsf, dorsal surangular foramen; fai, foramen alveolare inferius; fat, foramen auriculotemporalis; fdfm, foramen dentofaciale majus; foat, fossa auriculotemporalis; fM, fossa Meckelii; ldr, lateral dentary ridge; pimf, posterior intermandibular foramen; pfl, prearticular flange; pre, prearticular; rap, retroarticular process; secf, ectocondylar flange of surangular; sur, surangular; surl, surangular lamina

interdigitations. A coronoid foramen is absent on the medial surface. Laterally, the coronoid is recessed as part of the adductor fossa (Figure 7b). This is unusual for turtles, in which the adductor fossa, if present, is usually limited to the dentary.

The prearticular of *Carettochelys insculpta* forms a well-developed anterodorsal process, which forms the lateral wall to the fossa Meckelii and which reaches the coronoid (Figure 7a,d). Due to its steep dorsal orientation, the prearticular is strongly angled away from the anterior part of the angular, forming a V-shaped medial opening into the fossa Meckelii (Figure 7d). The posterior part of the prearticular contacts the angular and articular. The posterior intermandibular foramen is small and completely within the prearticular, and the anterior intermandibular foramen seems unossified (Figure 7d). The posterior part of the dorsal margin of the prearticular is medially bulged around the articular, forming a prearticular flange analogous to the ectocondyle flange on the surangular (Figure 7c). This bulged part has a small lateral surface that contributes to the articulation surface.

The angular of *Carettochelys insculpta* consists of a vertical plate anteriorly, and a more horizontally twisted posterior part that underlies the posterior bones of the mandible (Figure 7d). Unlike in trionychids, the anterior part of the angular is not only limited to the medial surface of the mandible, but contacts its ventral margin (Figure 7d). The posterior parts of the angular are even visible in lateral view (Figure 7b).

The splenial is absent in *Carettochelys insculpta*.

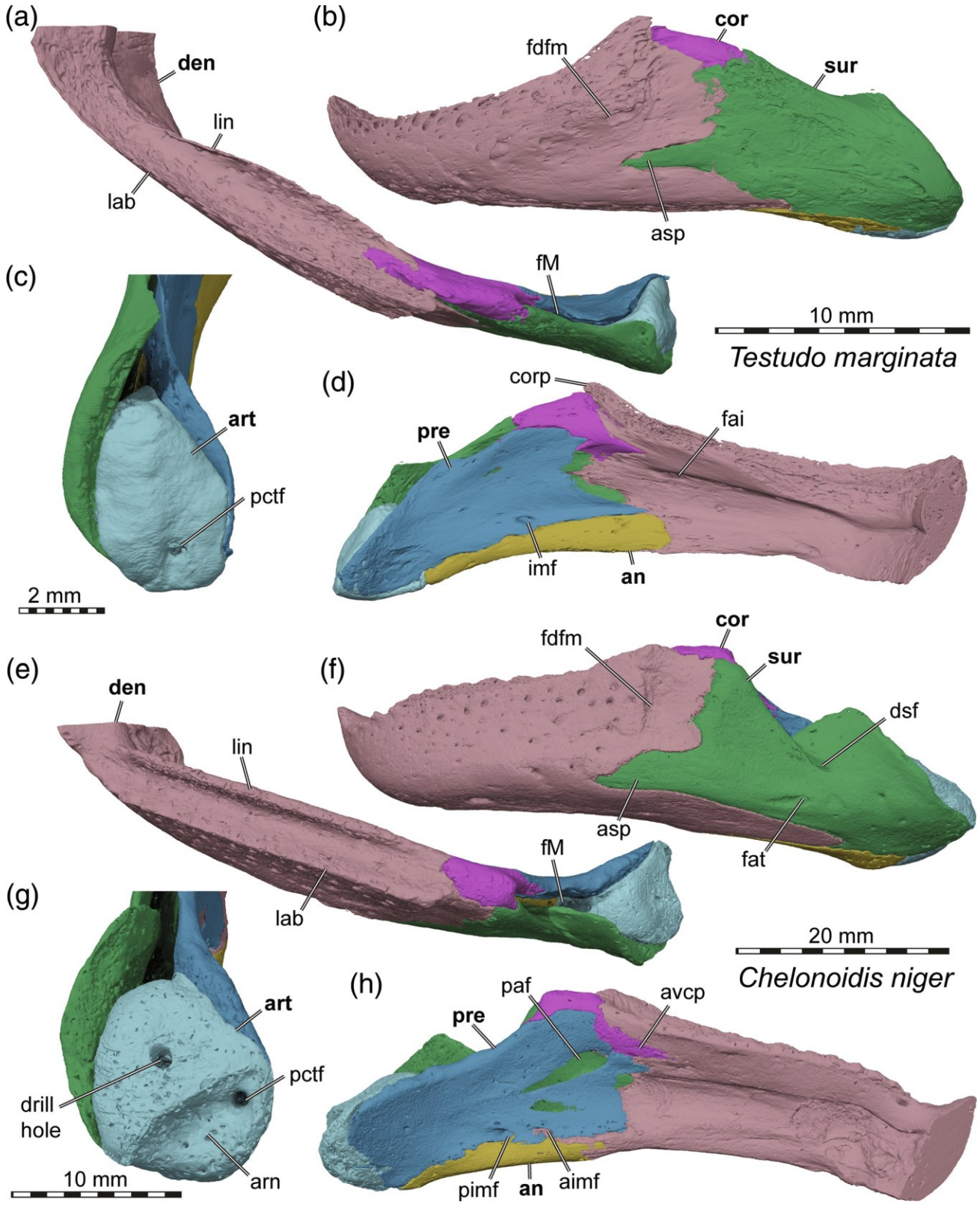

FIGURE 8 Legend on next page.

The articular of *Carettochelys insculpta* is relatively small, but anteroposteriorly elongated (Figure 7c). The anterior part of the bone forms a convex surface which is integrated into the surface for the jaw articulation. Posterior to the hemispherical convexity, the articular narrows mediolaterally and forms a posterodorsally recurved, hooked retroarticular process, which is laterally supported by the surangular and separated from the articular surface by a transverse articular notch (Figure 7c).

3.5.3 | Testudinidae

Testudinids are a speciose clade of turtles. For this description, we distinguish between the *Manouria-Gopherus* clade, and Testudona and Geochelona, which form Testudininae (Joyce, Anquetin, et al., 2021). For the *Gopherus-Manouria* clade, we have 3D models of *Gopherus agassizii* (FMNH 216746), *Gopherus flavomarginatus* (FMNH 98916), *Gopherus polyphemus* (FMNH 211815), and *Manouria impressa* (SMF 69777). Testudona is represented by *Indotestudo elongata* (SMF 71585), *Malacochersus tornieri* (SMF 58702), *Testudo graeca* (ZMB 39442), *Testudo horsfieldii* (OUMNH 10344), and *Testudo marginata* (FMNH 51672). For Geochelona, we have 3D data of *Aldabrachelys gigantea* (ZMB 47494), *Chelonoidis niger* (ZMB 19103), *Homopus areolatus* (OUMNH 9403), and *Kinixys erosa* (SMF 40166).

In testudinids, the dentary is relatively short, and extends posteriorly only to about the anterior end of the mandibular articular surfaces. The depth of the mandible is relatively high and remains so for the entire anteroposterior length (Figure 8b,f, Figure 9b,f). The foramen dentofaciale majus is relatively small (Joyce & Bell, 2004), and usually positioned in a low depression on the lateral surface of the dentary, and sometimes anteriorly bound by a short vertical ridge. Adductor fossae on the lateral surface of the mandible are virtually absent in testudinids (Figure 8b,f, Figure 9b,f). Each mandibular ramus is relatively straight, and most of the curvature is achieved near the symphysis, where the anterior end of the dentary forms a sharp medial turn (Figure 8a,e, Figure 9a,e). The dorsal margin of the dentary forms a serrated labial ridge in many testudinids (Figure 8b,f, Figure 9b,f). Together with a well-developed, equally serrated lingual ridge that is nearly as deep as its labial counterparts, the ridges define a transversely narrow and deeply excavated, trough-like triturating surface (Figure 8a,e, Figure 9a,e). In Testudona, the lingual side of the triturating surface is medially expanded, and the lingual ridge becomes anteriorly weaker, leaving a symphyseal gap in the ridge (e.g., *Indotestudo elongata*; *Malacochersus tornieri*; *Testudo marginata*; Figure 8a,d). Posteriorly, the triturating surface of testudinids ends just anterior to the low coronoid, and anteriorly the triturating surfaces are confined to each mandibular ramus. The symphyseal area varies somewhat among testudinid species, but the lingual ridge vanishes in this area, so that the ridge is not continuous between the right and left rami of the mandible. True symphyseal hooks are absent in testudinids, but some species have a low, tooth-like symphyseal edge that is separated from the labial ridge by a notch on each side of the symphysis (e.g., *Aldabrachelys gigantea*). The medial surface of the dentary of testudinids is dominated by a large Meckelian groove (= sulcus cartilaginis meckelii of Gaffney, 1979). Below and above the groove, the dentary is thickened. The foramen alveolare inferius is often positioned relatively far anteriorly along the medial surface of the dentary (Figure 8d, Figure 9d). Vlachos and Rabi (2018) code a new character (ch. 65) that differentiates between testudinids that supposedly have the coronoid included or excluded from the foramen alveolare inferius. However, this foramen is universally a structure limited to the dentary. Vlachos and Rabi included a second character that is affected (ch. 64), which encodes proposed variation about whether the foramen alveolare inferius is fused with the foramen intermandibular medius or not. However, the foramen intermandibular medius is the opening from the fossa Meckelii into the open intermandibular space (Gaffney, 1972, 1979), whereas the foramen alveolare inferius is an opening from within the fossa Meckelii that leads to a canal within the dentary (Gaffney, 1972, 1979). Future studies of testudinids using the matrix of Vlachos and Rabi (2018) should thus be weary of using these two characters, which seem to be based on an

FIGURE 8 3D renderings of mandibles of selected testudinine testudinids. (a–d) *Testudo marginata* (FMNH 51672). (e–h) *Chelonoidis niger* (ZMB 19103). (a and e) Dorsal view. (b and f) left lateral view. (c and g) close-up of articular surface. (d and h) medial view onto left mandibular ramus. Note that bones are labeled in bold, and other features in normal font. aimf, anterior intermandibular foramen; an, angular; arn, articular notch; art, articular; asp, anterior surangular process; avcp, anteroventral process of the coronoid; cor, coronoid; corp, coronoid process; den, dentary; fai, foramen alveolare inferius; fat, foramen auriculotemporalis; fdfm, foramen dentofaciale majus; fM, fossa Meckelii; imf, intermandibular foramen; lab, labial ridge; paf, prearticular foramen; pctf, posterior chorda tympani foramen; pimf, posterior intermandibular foramen; pre, prearticular; sur, surangular

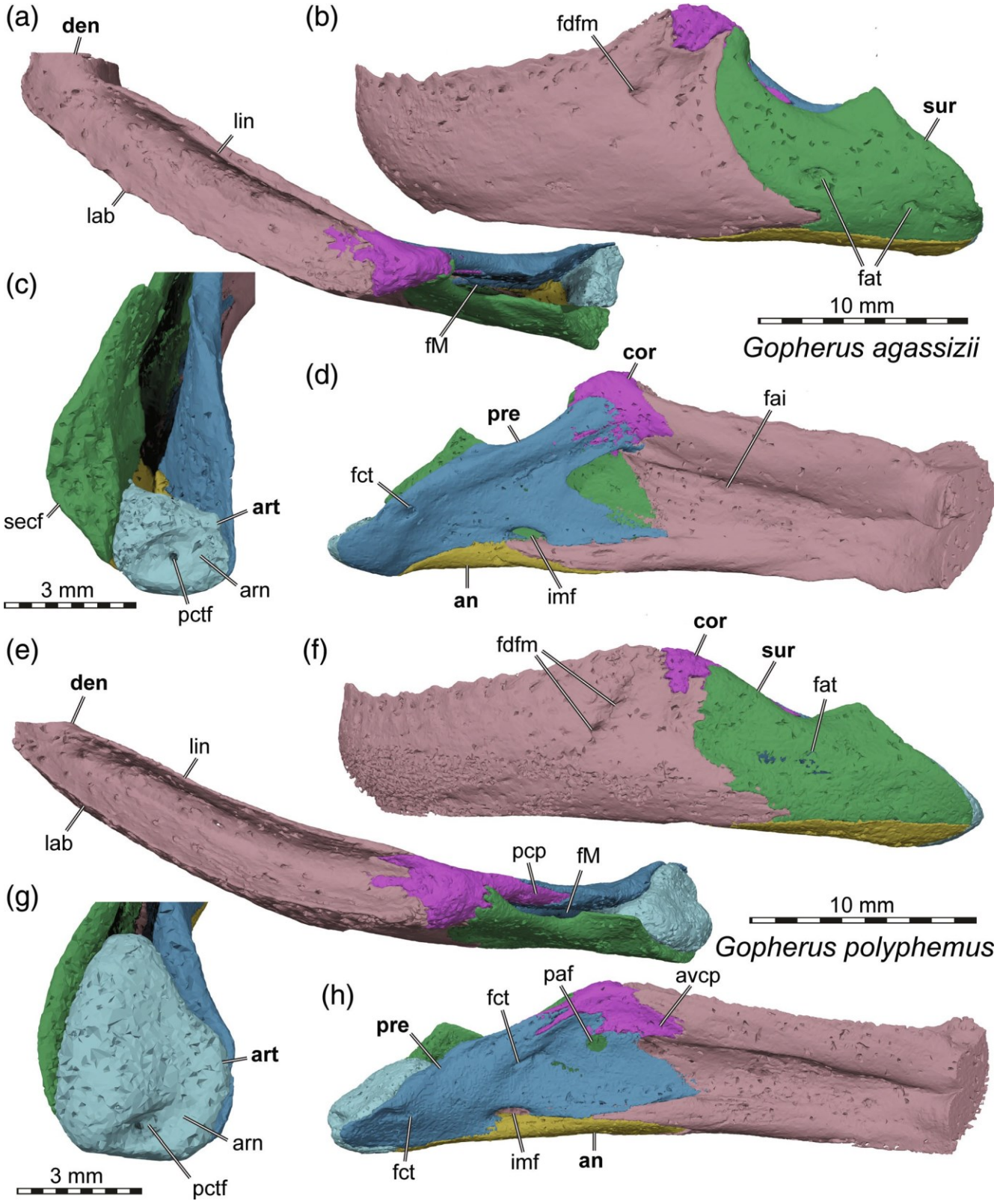

FIGURE 9 3D renderings of mandibles of selected *Gopherus* species. (a–d) *Gopherus agassizii* (FMNH 216746). (e–h) *Gopherus polyphemus* (FMNH 211815). (a and e) Dorsal view. (b and f) Left lateral view. (c and g) Close-up of articular surface. (d and h) Medial view onto left mandibular ramus. Note that bones are labeled in bold, and other features in normal font. an, angular; arn, articular notch; art, articular; avcp, anteroventral process of the coronoid; cor, coronoid; den, dentary; fat, foramen auriculotemporalis; fdfm, foramen dentofaciale majus; fM, fossa Meckelii; imf, intermandibular foramen; lab, labial ridge; paf, prearticular foramen; pcp, posteroventral process of the coronoid; pctf, chorda tympani foramen; pre, prearticular; secf, ectocondyle flange of the surangular; Sur, surangular

anatomical misconception about the identity of the foramen alveolare inferius.

The surangular of testudinids has a short dorsal process that contacts the coronoid and forms the medial wall of the fossa Meckelii, which opens as a mediolaterally narrow slit. A surangular lamina (sensu Evers & Benson, 2019) is absent in testudinids. Posteriorly, the surangular frames the lateral margin of the articular in the jaw articulation region, but a laterally expanded surangular flange is mostly absent, except in some species like *Gopherus agassizii* (Figure 9c). The lateral surface of the surangular bears a foramen auriculotemporalis, situated usually in the constricted part between coronoid process and articular surface for the quadrate. The foramen is smaller than in many other groups, and further anteriorly positioned. Most testudinines have an anterior surangular process that slots into a posteriorly bifurcated dentary (Figure 8b,f; Crumly, 1982; Joyce & Bell, 2004). The process is relatively short in *Homopus areolatus* and *Malacochersus tornieri*. In the *Gopherus-Manouria* clade, the dentary instead completely overlies the surangular laterally, and the contact of these bones forms a posteriorly concave sutural line (Joyce & Bell, 2004).

The coronoid of testudinids is small and forms a low, mount-like coronoid process (Figure 8b,f, Figure 9b,f). The element contacts the dentary anteriorly, and is usually ventrally bifurcated into two small processes, one contacting the surangular laterally, and the other the prearticular medially. These ventral processes form the dorsal margin to the fossa Meckelii. The coronoid expression on the medial surface of the jaw is small in testudinids, and an anteroventral process is short or absent.

The prearticular of testudinids is a thin, sheeted bone that forms the medial wall to the fossa Meckelii. Posteriorly, it frames the articular medially but is not included in the formation of the articulation surface for the mandible (Figure 8c,g, Figure 9c,g). The prearticular is deepest anteriorly at its contact with the coronoid. Ventrally, it has a long suture with the angular but also contacts the dentary anterior to that contact in most species (Figure 8d,h, Figure 9d,h). The prearticular forms several foramina. Along its contact with the angular, two mid-sized foramina are formed (e.g., in *Chelonoidis niger*: Figure 8h), the anterior and posterior intermandibular foramina (foramen intermandibulare oralis and caudalis of Gaffney, 1979). The foramina are closely spaced in testudinids, and may form a single, larger, anteroposteriorly elongated foramen which we then simply call the intermandibular foramen, as in gopher tortoises but also many testudinines. Along the anterodorsal contact of the prearticular with the coronoid, the prearticular splits into two rami that enclose a large, often circular foramen, which in some specimens is sometimes not preserved at all when the anterior end of the prearticular is poorly ossified. This foramen has no name in the nomenclature of Gaffney (1972, 1979), and which we herein name "prearticular foramen" (Figure 8h, Figure 9h). The prearticular foramen can easily be confused with the foramen intermandibulare medius, which, according to Gaffney (1972, 1979), is simply the anterior opening of the fossa Meckelii toward the Meckelian groove, which is bound by the prearticular medially, and the dentary laterally.

The angular is a small component of the testudinid jaw and forms a ventral cap between the prearticular and surangular. Posteriorly, it wraps laterally around the articular, and anteriorly its extent is shorter to or level with the anterior extend of the prearticular.

The splenial is absent in testudinids.

The articular of testudinids is a small block of bone forming nearly the entire surface for the articulation with the quadrate. The dorsal surface of the articular is largely convex, except for a small grooved articular notch at the posterior end, which extends obliquely across the element (Figure 8c,g, Figure 9c,g). Testudinines have a relatively prominent chorda tympani foramen within the articular notch (Figure 8c,g). Our fully segmented mandibles allow to see that the foramen leads through the articular (and even into the prearticular in *Chelonoidis niger*), before it enters the floor of the fossa Meckelii. Although similar foramina are present in gopher tortoises, we could not trace the foramen into a true canal anteriorly in any of our gopher tortoise scans. A median longitudinal articular ridge that would separate two facets of the condyle is absent in testudinids, contrary to the general statements of Gaffney (1979) according to which these features are generally present in cryptodiran jaws. Anteriorly, the articular of testudinids forms the posterior wall of the fossa Meckelii between the prearticular and surangular, and it is lateroventrally buttressed by the angular. Although retroarticular processes are generally absent in testudinids, *Manouria impressa* has a well-developed and posterodorsally recurved retroarticular process. Despite being largely formed by the articular, the prearticular also contributes to the retroarticular process in this species.

3.5.4 | Geoemydidae

Geoemydids have extremely variable mandibular anatomy, which may be expected given their relatively high species richness and ecological disparity. Despite being a speciose group, the subclades of geoemydids do not have commonly used subclade definitions (e.g., Joyce, Anquetin, et al., 2021). For the purpose of this description, we break geoemydids informally into three large

subclades retrieved in the Pereira et al. (2017) phylogeny, the *Rhinoclemmys*-group, the *Batagur*-group, and the *Cuora*-group. The *Rhinoclemmys* group contains only species of the genus *Rhinoclemmys*. This clade may form the sister lineage to all other geoemydids (Pereira et al., 2017), but it may also be more deeply nested among other geoemydids (Thomson et al., 2021). Molecular divergence times estimates in Pereira et al. (2017) place the next order branching between the *Batagur*-group and the *Cuora*-group into the Paleocene, with all subsequent branching events having Eocene or younger ages. Our sample for the *Rhinoclemmys*-group is composed of two species, whereby we fully (i.e., bone-by-bone) segmented *Rhinoclemmys melanosterna* (FMNH 44446) and have an additional mandibular model of *Rhinoclemmys rubida* (MVZ-herps-78373). For the *Batagur*-group, we consider *Geoemyda spengleri* (FMNH 260381), *Malayemys subtrijuga* (NHMUK 1920.1.20.2545), *Batagur baska* (NHMUK 67.9.28.7), and *Morenia ocellata* (NHMUK 87.3.11.7), which form successively closer-related sister-group relationships. Note that while this classification follows the topology of Pereira et al. (2017), Thomson et al. (2021) found alternative placements for *Geoemyda* (i.e., among the *Cuora*-group). For the *Cuora*-group, our sample includes three *Cuora* species; *Cuora mouhotii* (SMF 71599), *Cuora amboinensis* (NHMUK 69.42.145), and *Cuora flavomarginata* (FMNH 21515). The genus *Cuora* forms a sister group with the genus *Mauremys* (Pereira et al., 2017; Thomson et al., 2021), of which we sampled *Mauremys leprosa* (NHMUK unnumbered). We also sampled *Sacalia quadriocellata* (NCSM 13265) and *Cyclemys dentata* (NHMUK 97.11.22.3), which are more closely related to one another than either is to *Cuora* spp. or *Mauremys* spp.

Due to the high variation in mandibular anatomy, there are few features that are omnipresent among all our sampled geoemydids. However, geoemydids generally seem to have relatively reduced sizes of the articular, which leaves a dorsal gap between the prearticular and surangular walls to the fossa Meckelii, the dorsal opening of which therefore becomes open posteriorly. For some other turtles, we provide evidence that this gap closes ontogenetically (see *Platysternon megacephalum*, below; the emydid *Pseudemys texana*: Bever, 2008). In geoemydids, this does not seem to be the case. For instance, although all our examined species of the genus *Rhinoclemmys* have small articular sizes and large gaps toward the fossa Meckelii, their head and carapace sizes indicate adult sizes based on literature reports (TTWG 2021). Another feature that is generally present in geoemydids is the surangular foramen, which is connected ventrally with the foramen nervi auriculotemporalis via a vertical canal, as in many emydids and kinosternids. The surangular lacks a prominent ectocondyle flange, but is still integrated into the lateral margin of the articular facet. Geoemydids furthermore all have relatively prominent coronoid bones that clearly form the coronoid process, although the height and shape of the process varies strongly among species.

Rhinoclemmys melanosterna has a dentary shape that is reminiscent of emydids; the dentary is relatively gracile, and the triturating surface is narrow (Figure 10a). The labial ridge is low, and a lingual ridge or symphyseal ridge is absent. The foramen dentofaciale majus is small and located at the anterior end of an extremely weakly developed adductor fossa (Figure 10b).

Within the *Batagur*-group, *Batagur baska* and *Morenia ocellata* can be distinguished from other sampled taxa by complex dentary shapes that include extremely pronounced and serrated cutting ridges along expanded triturating surfaces (Figure 11e–h). Both taxa have well-developed labial ridges and a single accessory ridge that parallels the labial ridge in the central aspect of each triturating surface. Labial and accessory ridges are serrated in both taxa. The accessory ridges converge anteriorly in the centrum of the posteriorly expanded symphyseal area. In *Batagur baska*, both ridges encase a narrow anteroposterior symphyseal groove (Figure 11e), whereas the ridges merge into a symphyseal ridge in *Morenia ocellata*. The tips of the symphysis form a pointed albeit low hook in both species. In *Morenia ocellata*, the tip is hypertrophied by lateral notches in the labial ridge. *Batagur baska* has a well-developed and serrated lingual ridge (Figure 11e), which is absent in *Morenia ocellata*. The lateral surface of the dentary is bulged below the labial ridge in both taxa. This dentary rhamphotheca ridge separates a dorsolateral surface that is strongly vascularized, and which seems to be the attachment area for the rhamphotheca, from the smooth ventrolateral surface of the dentary (Figure 11f). The lateral surface of the dentary posterior to the triturating surfaces is dominated by a deep adductor fossa, which is ventrally shelfed by a strong lateral dentary ridge (Figure 11f). The ridge is dorsally upcurved along its margin, thus forming a grooved shelf that leads anteriorly to an extremely large foramen dentofaciale majus (Figure 11f). A large foramen dentofaciale majus is also seen in the closely related *Malayemys subtrijuga*, but this taxon lacks the lateral dentary shelf ridge and the adductor fossa thus remains relatively less conspicuous. *Malayemys subtrijuga* also shares an expanded triturating surface with the *Batagur* + *Morenia* clade, but all triturating ridges are absent and instead the surface is flat. Unlike in *Batagur* and *Morenia*, the coronoid is integrated into the triturating surface of *Malayemys*. The lateral dentary surface of *Malayemys* lacks a rhamphotheca ridge, and is relatively poorly vascularized

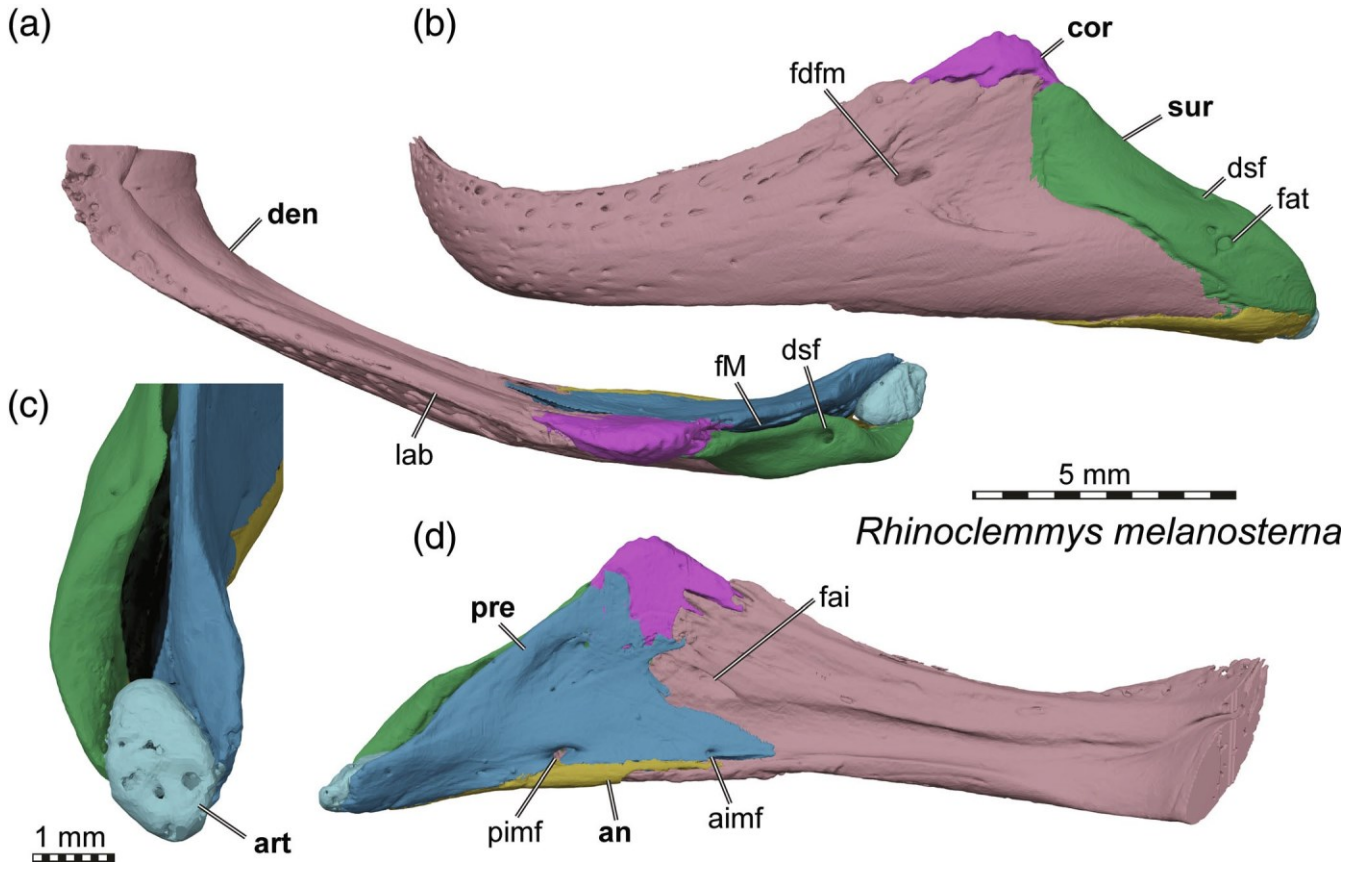

FIGURE 10 3D renderings of mandibles of the geoemydid *Rhinoclemmys melanosterna* (FMNH 44446). (a) Dorsal view. (b) Left lateral view. (c) Close-up of articular surface. (d) Medial view onto left mandibular ramus. Note that bones are labeled in bold, and other features in normal font. aimf, anterior intermandibular foramen; an, angular; art, articular; cor, coronoid; den, dentary; dsf, dorsal su rangular foramen; fai, foramen alveolare inferius; fat, foramen auriculotemporalis; fdfm, foramen dentofaciale majus; fM, fossa Meckelii; lab, labial ridge; pimf, posterior intermandibular foramen; pre, prearticular; Sur, surangular

in comparison with *Batagur* and *Morenia*. The dentary of *Geoemyda spengleri* is completely different from other taxa examined within the *Batagur*-group, possibly supporting alternative placements among the *Cuora*-group (see Thomson et al., 2021). The triturating surfaces of *Geoemyda spengleri* are extremely narrow, and a single, sharp-edged labial ridge defines the surface. The foramen dentofaciale majus is extremely small, and the adductor fossa is weakly developed. The dentaries of our sampled *Cuora* species are all relatively similar, although *Cuora flavomarginata* (Figure 11a–d) has a notably more elongated and gracile mandibular shape compared to *Cuora mouhotii* and *Cuora amboinensis*. The triturating surfaces in all *Cuora* species are narrow, and the labial ridge is low, but forms a sharp-edged margin. The lingual side of the triturating surface is formed as sharp edge, but there is no dorsally protruding lingual ridge. The triturating surface is flat and horizontally oriented (Figure 11a,d), or slopes gently ventromedially as in *Cuora amboinensis*. In *Mauremys leprosa*, the triturating surface is medially broadened along the central part of the dentary ramus: In this region, the labial margin forms a medially convex shelf-like lamina. Weak symphyseal hooks are common in the *Cuora*-group, and we observed a very subtle symphyseal ridge in *Cuora mouhotii*. The lateral dentary surfaces have weakly (*Cuora amboinensis*, *Cuora flavomarginata*; Figure 11b) to moderately (*Cuora mouhotii*, *Mauremys leprosa*) developed adductor fossae with clearly visible foramina dentofaciale majus. A lateral dentary ridge defines the adductor fossa in *Mauremys leprosa*, but is otherwise absent in the *Cuora*-group.

The surangular of all geoemydids is only minorly expanded laterally around the small articular and lacks a prominent ectocondyle flange. The surangular of *Rhinoclemmys melanosterna* is relatively broadly exposed behind the dentary. The foramen auriculotemporalis is relatively far dorsally positioned on the surangular, and leads dorsally into a small surangular canal that opens in a respectively small foramen anterior to the jaw articulation region, which we herein name the dorsal surangular foramen (Figure 10b). An anterior canal leading into the fossa Meckelii additionally branches internally from the foramen

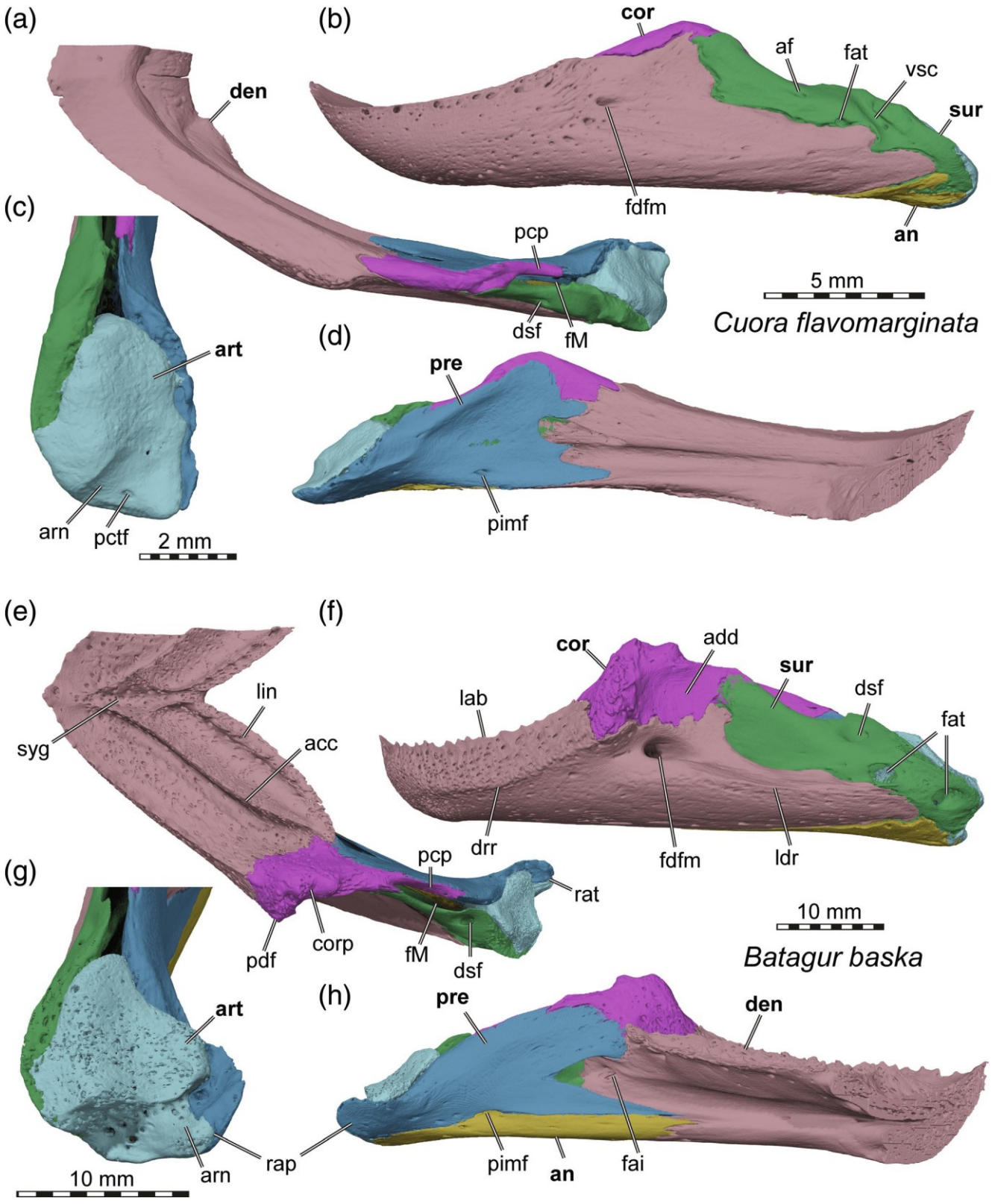

FIGURE 11 Legend on next page.

auriculotemporalis. Surangular and prearticular form the lateral and medial walls to the fossa Meckelii, respectively, but they do not contact one another posteriorly. Consequentially, the dorsal opening to the fossa Meckelii remains posteriorly open toward the articulation surface (Figure 10c), which is common in geoemydids and only seems to have been secondarily reduced in some species (see below). The presence of a dorsal surangular foramen and associated vertical surangular canal is variable among species of the *Batagur*-group; while both features are absent in *Geoemyda spengleri* and *Morenia ocellata*, they are present in *Malayemys subtrijuga* and *Batagur baska*. The vertical surangular canal has a large internal diameter in *Batagur baska*. The dorsal surangular foramen and canal are present in all species of the *Cuora*-group. The foramen auriculotemporalis has two openings in most geoemydids (e.g., *Batagur baska*: Figure 11f).

The coronoid of *Rhinoclemmys melanosterna* forms a moderately well-developed coronoid process. As in all geoemydids (Figure 11d,h), the bone lacks an anteroventromedial process (Figure 10d), so that a dorsal contact between the prearticular and dentary is often realized below the ventral coronoid margin. A posteroventromedial process along the opening of the fossa Meckelii that is characteristic for other geoemydids is absent in *Rhinoclemmys melanosterna* (Figure 10a). Coronoid shape varies greatly among geoemydids of the *Batagur*-group. The bone always forms the coronoid process, but the process can be low and well rounded (e.g., *Morenia ocellata*), relatively tall and well rounded (e.g., *Geoemyda spengleri*), tall and irregular along its dorsal margin (e.g., *Batagur baska*; Figure 11f), or extremely hypertrophied, rod-like, and posteriorly projecting (e.g., *Malayemys subtrijuga*; Joyce & Bell, 2004). In *Malayemys subtrijuga*, the coronoid contributes to the triturating surface, but this is not the case in other examined taxa. Taxa of the *Batagur*-group and *Cuora*-group share the presence of a posteroventromedial process of the coronoid, which forms parts of the medial wall of the fossa Meckelii, hereby partially excluding the prearticular from forming this wall. The length of the process is variable and extends only halfway along the dorsal opening of the fossa Meckelii in some taxa (e.g., *Malayemys subtrijuga*, *Mauremys leprosa*), whereas it fully excludes the prearticular from the dorsal fossa Meckelii opening in others (e.g., *Batagur baska*, *Cuora flavomarginata*; Figure 11a,e). The process is notably short in *Cuora mouhotii*, and entirely absent in *Cyclemys dentata*.

In all geoemydids including *Rhinoclemmys melanosterna*, the fossa Meckelii remains posteriorly open due to a relatively small articular and absence of a contact of the prearticular with the surangular in this region (Figure 10c; Figure 11c,g). The prearticular-angular suture surrounds two intermandibular foramina in *Rhinoclemmys melanosterna*: a larger posterior one and a small anterior one (Figure 10d). The same is seen in *Rhinoclemmys rubida*, although the posterior intermandibular foramen lies completely within the prearticular in this species. Non-*Rhinoclemmys* geoemydids examined only have one intermandibular foramen (Figure 11d,h; with the exception of *Cuora mouhotii*). As the size and relative position of this opening matches the posterior intermandibular foramen of *Rhinoclemmys melanosterna*, *Rhinoclemmys rubida*, and *Cuora mouhotii*, we suggest that the single intermandibular foramen of most geoemydids is homologous to the posterior intermandibular foramen. Given that all geoemydids have elongate anterior prearticular processes (Figure 11d,h), it seems likely that the absence of an anterior intermandibular foramen in most species (but *Rhinoclemmys melanosterna* and *Cuora mouhotii*) is the result of a reduction of this foramen, rather than the incomplete anterior ossification of the prearticular. Within the *Batagur*-group, the posterior intermandibular foramen always lies within the suture of prearticular and angular (Figure 11h). In contrast, the foramen always lies entirely within the prearticular in species of the *Cuora*-group, (e.g., *Cuora* spp., *Cyclemys dentata*, *Mauremys leprosa*, *Sacalia quadriocellata*; Figure 11d). The prearticular of all geoemydids but *Rhinoclemmys melanosterna* forms a prominent lip at the posteromedial jaw end, which curves around the articular as a short retroarticular process posterior to the jaw articulation surface. Although the development of the retroarticular process varies (see Figure 11c,g), it is generally present.

The angular is generally reduced in size and prominence in the geoemydid mandible, although to somewhat varying degrees. In *Rhinoclemmys melanosterna*, the

FIGURE 11 3D renderings of mandibles of selected geoemydids. (a–d) *Cuora flavomarginata* (FMNH 21515). (e–h) *Batagur baska* (NHMUK 67.9.28.7). (a and e) Dorsal view. (b and f) Left lateral view. (c and g) Close-up of articular surface. (d and h) Medial view onto left mandibular ramus. Note that bones are labeled in bold, and other features in normal font. Also note that the vertical surangular canal in *Cuora* is laterally open in (b), but closed on the right side of the same mandible. acc, accessory ridge; add, adductor fossa; af, accessory foramen; an, angular; arn, articular notch; art, articular; cor, coronoid; corp, coronoid process; den, dentary; drr, dentary rhamphotheca ridge; dsf, dorsal surangular foramen; fai, foramen alveolare inferius; fat, foramen auriculotemporalis; fdfm, foramen dentofaciale majus; fM, fossa Meckelii; lab, labial ridge; ldr, lateral dentary ridge; lin, lingual ridge; pcp, posteroventral process of the coronoid; pctf, posterior chorda tympani foramen; pdf, processus dentofacialis; pimf, posterior intermandibular foramen; pre, prearticular; rap, retroarticular process; sur, surangular; syg, symphyseal groove; vsc, vertical surangular canal

angular remains mediolaterally relatively broad at its posterior end, but becomes anteriorly reduced to a thin, rod-like projection between the dentary and surangular (Figure 10b,d). This anterior angular process does not fully separate surangular and dentary, which form an expanded contact along the anterior prearticular process. The angular is comparatively large and prominent posteriorly in species of the *Batagur*-group (Figure 11f,h), but it can still be short anteriorly, as *in Malayemys subtrijuga*, in which there is an extensive prearticular-dentary contact anterior to the termination of the short angular. Among species of the *Cuora*-group, the angular is strongly reduced in size, and often only forms a thin rod that is marginally broadened posteriorly, as in *Cuora flavomarginata* (Figure 11b,d).

The splenial is absent in geoemydids.

The articular of *Rhinoclemmys melanosterna* is extremely reduced in size and forms an ovoid, potato-reminiscent block wedged between the posteriormost end of the surangular, prearticular and angular. The dorsal surface of the articular is convex unlike in most cryptodires, and there is a very gently mediolaterally trending notch across the posterior part of the articular. The articulars of species within the *Batagur*-group are relatively large for geoemydids, although several species retain the posterodorsally open fossa Meckelii. Articular surface orientations vary significantly among taxa, with *Batagur baska* and *Morenia ocellata* having more dorsally facing jaw articulation surfaces, whereas these are more posteriorly facing in *Geoemyda spengleri* and *Malayemys subtrijuga*. A low anteroposteriorly trending ridge separating ecto- and entocondyle subfacets is present in all species (Figure 11g). A posterior articular notch is sometimes present (e.g., *Batagur baska*, *Morenia ocellata*; Figure 11g), but can also be clearly absent (e.g., *Malayemys subtrijuga*). Within the *Cuora*-group, the jaw articulation surface is gently concave in most species, so that lateral and medial subfacects of the articulation area are largely absent. An articular notch is generally present, and this groove separates the articulation surface from the retroarticular process (Figure 11c).

3.5.5 | Platysternidae

Only a single species of platysternid is alive today, *Platysternon megacephalum*, of which we completely segmented a juvenile specimen (NCSM herps 76,497; Figure 12). Because the CT scan we had available was of a juvenile, we additionally refer to a photographed specimen of an adult individual (FMNH 51627).

The dentary of *Platysternon megacephalum* is very prominent on the lateral mandibular side, and covers nearly all of the coronoid and surangular (Figure 12b). Right and left dentaries are fully fused across the midline, and are anteriorly raised to a distinct symphyseal hook (Figure 12b,d; Gaffney, 1975b). A symphyseal ridge is absent. The triturating surface is extremely narrow, and laterally bound by a sharp-edged labial ridge (Figure 12a). The triturating surface slopes gently medioventrally. Although a raised lingual ridge is absent, the lingual margin of the triturating surface is marked by an edge that is trending along the entire triturating surface length. The lateral surface of the dentary has very few neurovascular foramina, which are concentrated in a single band around the periphery of the labial margin (Figure 12b). The foramen dentofaciale majus is small, and enters the dentary at the level of the coronoid process, and just shortly below the dorsal mandibular margin (Figure 12b). Any impression of an adductor fossa is absent in our juvenile specimen (Figure 12b), but FMNH 51627 shows a moderately developed adductor fossa, which is ventrally bound by a stout lateral dentary ridge. Anteriorly, this ridge terminates in a little mount-like dentofacial process. The differences in adductor fossa morphology between NCSM herps 76497 and FMNH 51627 highlight ontogenetic changes of mandibular morphology that should be kept in mind when scoring anatomical characters from mandibles. Posteriorly, the dentary of *Platysternon megacephalum* nearly reaches the jaw articulation surface. It forms two posterior prongs dorsally and ventrally around the foramen auriculotemporalis of the surangular (Figure 12b).

Most of the surangular of *Platysternon megacephalum* is concealed by the dentary in lateral view. A narrow band of the bone is dorsally exposed, forming the lateral margin of the dorsal opening of the fossa Meckelii (Figure 12a,b). Medially, the surangular has an anteriorly recurved surangular lamina (Figure 12b). In our segmented juvenile specimen, this lamina does not contact the prearticular, but the adult specimen FMNH 51627 shows that this contact is achieved during ontogeny. The foramen auriculotemporalis is extremely small in *Platysternon megacephalum* (Figure 12b), although the internal foramen connecting to the fossa Meckelii is large, as is usually the case in turtles. A dorsal surangular foramen and associated vertical surangular canal from the foramen auriculotemporalis are absent. The surangular is laterally expanded to an ectocondyle flange that forms at least one third of the articulation surface (Figure 12c).

The coronoid of *Platysternon megacephalum* is a relatively small bone. The coronoid process, although principally formed by the coronoid, is a low structure with a dorsally broad, textured surface in our juvenile specimen (NCSM herps 76497; Figure 12a,b,d), but becomes dorsally more prominent and gently posteriorly recurved in

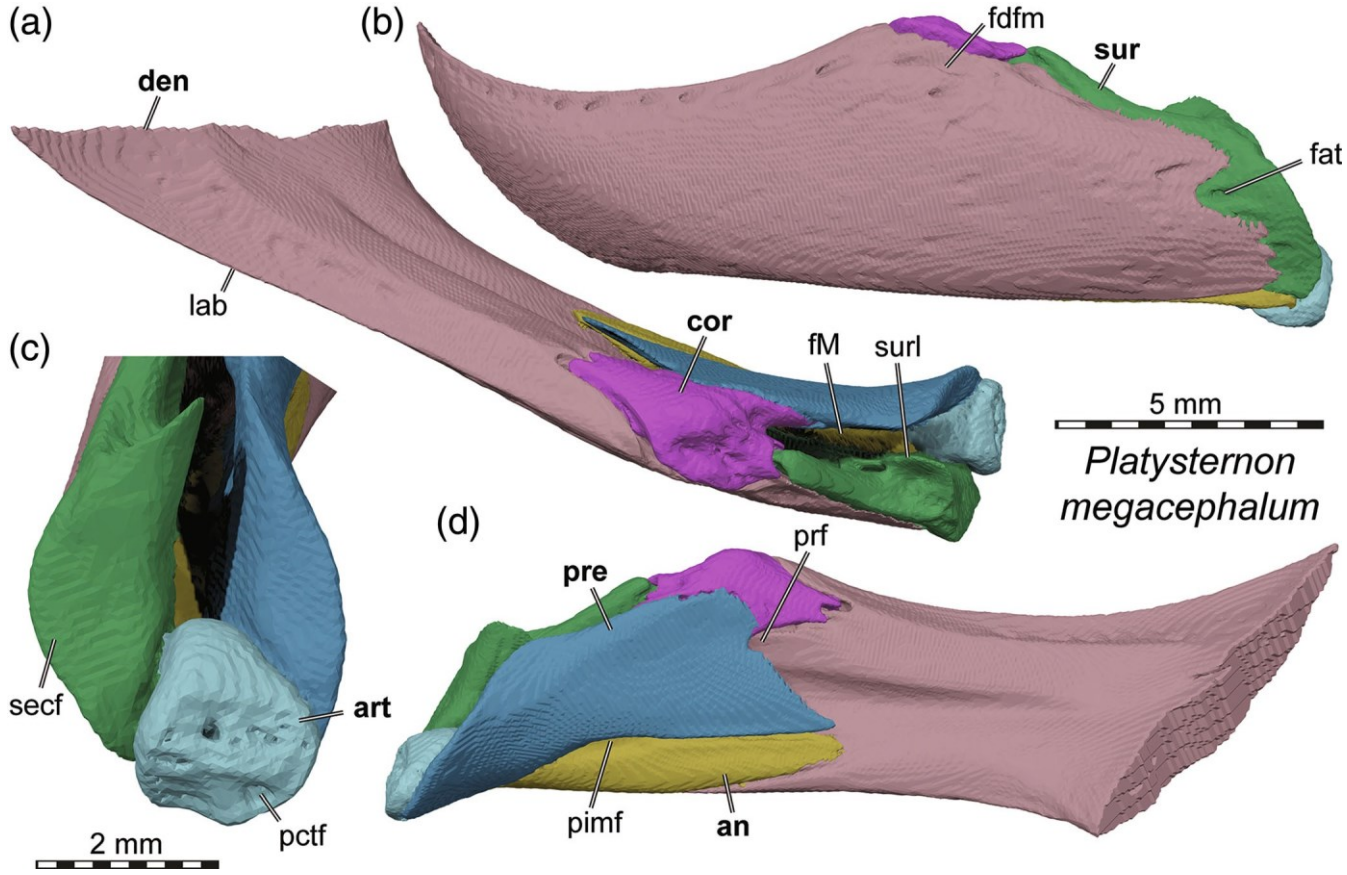

FIGURE 12 3D renderings of mandibles of the platysternid *Platysternon megacephalum* (NCSM herps 76497). (a) Dorsal view. (b) Left lateral view. (c) Close-up of articular surface. (d) Medial view onto left mandibular ramus. Note that bones are labeled in bold, and other features in normal font. Also note that the specimen is juvenile (ontogenetically variable features discussed in the text). an, angular; art, articular; cor, coronoid; den, dentary; fat, foramen auriculotemporalis; fdfm, foramen dentofaciale majus; fM, fossa Meckelii; lab, labial ridge; pctf, posterior chorda tympani foramen; pimf, posterior intermandibular foramen; pre, prearticular; prf, prearticular foramen; sur, surangular; secf, ectocondyle flange of the surangular; surl, surangular lamina

the adult (FMNH 51627). Posteriorly, the coronoid bridges the prearticular and surangular at the anterior margin of the dorsal opening to the fossa Meckelii. A short anteroventral process of the coronoid is present, but it does not extend into the triturating surface (Figure 12d).

The prearticular of *Platysternon megacephalum* is large, and anteriorly expanded so that it covers the foramen alveolare inferius on the medial surface of the dentary (Figure 12d). An anteriorly open, and thus only partially ossified prearticular foramen is present at the contact with the coronoid (Figure 12d). A dorsal contact with the dentary is hindered by the coronoid, and a ventral contact is prohibited by the angular. The anterior intermandibular foramen seems to be absent, but this absence does not seem to be an ossification artifact, even though our specimen is juvenile: The prearticular and angular are anteriorly well ossified, but the foramen is nevertheless not developed between the anteroventral process of the prearticular and the angular. The posterior intermandibular foramen is slightly elongated but only of moderate size, and positioned in the prearticular-angular suture (Figure 12d). Posteriorly, the prearticular forms a medially gently expanded flange with a convex margin, which expands the jaw articulation surface medially (Figure 12c). In the absence of an expanded posterior process of the angular, the prearticular is posteromedially expanded and slightly wraps around the ventral side of the articular.

The angular of *Platysternon megacephalum* is a relatively small bone, which contrasts the large size of the prearticular (Figure 12d). Only a small part of the angular is expressed on the ventral surface of the mandible, and visible from lateral view (Figure 12b). Anteriorly, the angular forms a short anterior process, which underlies the prearticular and which is limited to the medial surface of the mandible (Figure 12d), so that the dentary forms most of the ventral margin of the jaw.

The splenial is absent in *Platysternon megacephalum*.

The articular of the juvenile specimen of *Platysternon megacephalum* (NCSM herps 76497) is relatively small and limited to a block of bone in the posteroventral gap between prearticular and surangular (Figure 12c). A gentle coronoid notch is present, and a foramen chorda tympani is prominent within the notch (Figure 12c) and can be traced to connect anteriorly to the fossa Meckelii. In the adult specimen (FMNH 51627), the articular is dorsally more extensive, and fills the entire space between prearticular and surangular, supporting previous observations from other turtle species that the articular increasingly fills the gap posterior to the dorsal opening into the fossa Meckelii between prearticular and surangular during postnatal growth (e.g., *Pseudemys texana*: Bever, 2008). The surface of the articular bears a dorsoventral ridge, which forms clear medial and lateral subfacets.

3.5.6 | Emydidae

Emydids are a relatively speciose clade of turtles, and two primary subclades, the Deirochelyinae and the Emydinae can be distinguished (Joyce, Anquetin, et al., 2021). Our descriptions here are based on five deirochelyines (*Deirochelys reticularia* FMNH 98754; *Chrysemys picta* NHMUK 76.1.31.19; *Graptemys geographica* NHMUK 55.12.6.11; *Malaclemys terrapin* SMF 36419 and ZMB 16196; *Trachemys terrapen* ZMB 6572) and six emydines (*Terrapene carolina* OUMNH 8795; *Terrapene coahuila* FMNH 47372; *Terrapene ornata* FMNH 23014; *Emys orbicularis* ZMB 39445; *Glyptemys insculpta* FMNH 22240; *Clemmys guttata* FMNH 22114).

Deirochelyines show higher morphological disparity in their mandibles than emydines with regard to our sample, although the group is less speciose. The closely related *Malaclemys terrapin* and *Graptemys geographica* have expanded triturating surfaces and somewhat elongated symphyseal areas. The triturating expansion is primarily achieved by a medially protruding lamina at the lingual mandibular margin, forming a lingual shelf. This lamina has a convex medial margin, so that the triturating surfaces of *Malaclemys terrapin* and *Graptemys geographica* are broader posteriorly than near the symphysis (Figure 13a), which is generally unusual among turtles with expanded triturating surfaces. The medial margin of the triturating surface is not raised, so that a true lingual ridge is absent, although it may be argued that the expansion itself is formed by a horizontally inclined, medially protruding lingual ridge. In *Malaclemys terrapin*, the medial margin of the jaw is continuously curved along the symphyseal area, whereas the margin extends anteriorly into the symphyseal area in *Graptemys geographica*, giving the impression of a strong right–left delimitation of the triturating surfaces (Figure 13a). The medial area in between is gently anteroposteriorly grooved in *Graptemys geographica* (Figure 13a), similar to the cranial "tongue grooves" observed in many turtles. The triturating surface morphology of other deirochelyines is quite distinct from the condition described above. In *Chrysemys picta*, the triturating surface is comparatively narrow and forms a deep groove between the clearly developed labial and lingual ridges of the dentary. These ridges are not sharp-edged, but form low and robust ridges. Despite their robustness, the lingual and labial ridges of *Chrysemys picta* are serrated along their margins. As in *Graptemys geographica* and *Malaclemys terrapin*, the symphyseal area of *Chrysemys picta* is less broad than more posterior parts of the triturating surface. A symphyseal ridge is absent, as in all emydids, but a pointed symphyseal hook is present in *Chrysemys picta*. A symphyseal hook is also present in *Deirochelys reticularia*, but otherwise, this species has yet again a strongly divergent dentary morphology. In *Deirochelys reticularia*, the triturating surfaces are reduced and narrow, and the surface slopes strongly medially. A lingual ridge is absent, and the labial ridge is narrow and sharp along its dorsal edge. All deirochelyines share a far anteriorly positioned foramen dentofaciale majus of considerable size (Figure 13b; see also Bever, 2009). The foramen is positioned anteriorly to the extent of the adductor fossa, which is generally weakly demarcated in deirochelyines with the exception of *Chrysemys picta*, in which the ventral side of the fossa is bound by a ridge on the lateral dentary surface. Posteriorly the dentary of deirochelyines extends comparatively far, covering most of the surangular. The posterior end of the dentary is forked around the foramen auriculotemporalis, a feature that is absent in emydines but also seen in species of the genus *Kinosternon* (see below).

The dentaries of emydines are remarkably consistent among different species. In all emydines, the dentary is relatively low, and the triturating surfaces are narrow, weakly medially inclined surfaces without lingual ridges (Figure 13e,f,h). Labial ridges are inconspicuous too, forming a low but sharp-edged dorsal margin of the dentary. The symphyseal area is short, without symphyseal ridge, and right and left mandibular rami meet in an acute symphyseal tip that is gently curved dorsally without forming a true hooked process (Figure 13e,f). Adductor fossae are universally present among emydines (Figure 13f) and much better developed and demarked than in deirochelyines (with the exception of *Chrysemys picta*; see above). The foramen dentofaciale majus is positioned within the anterior border ridge of the adductor fossa, and thus more posteriorly positioned than in deirochelyines (Figure 13f).

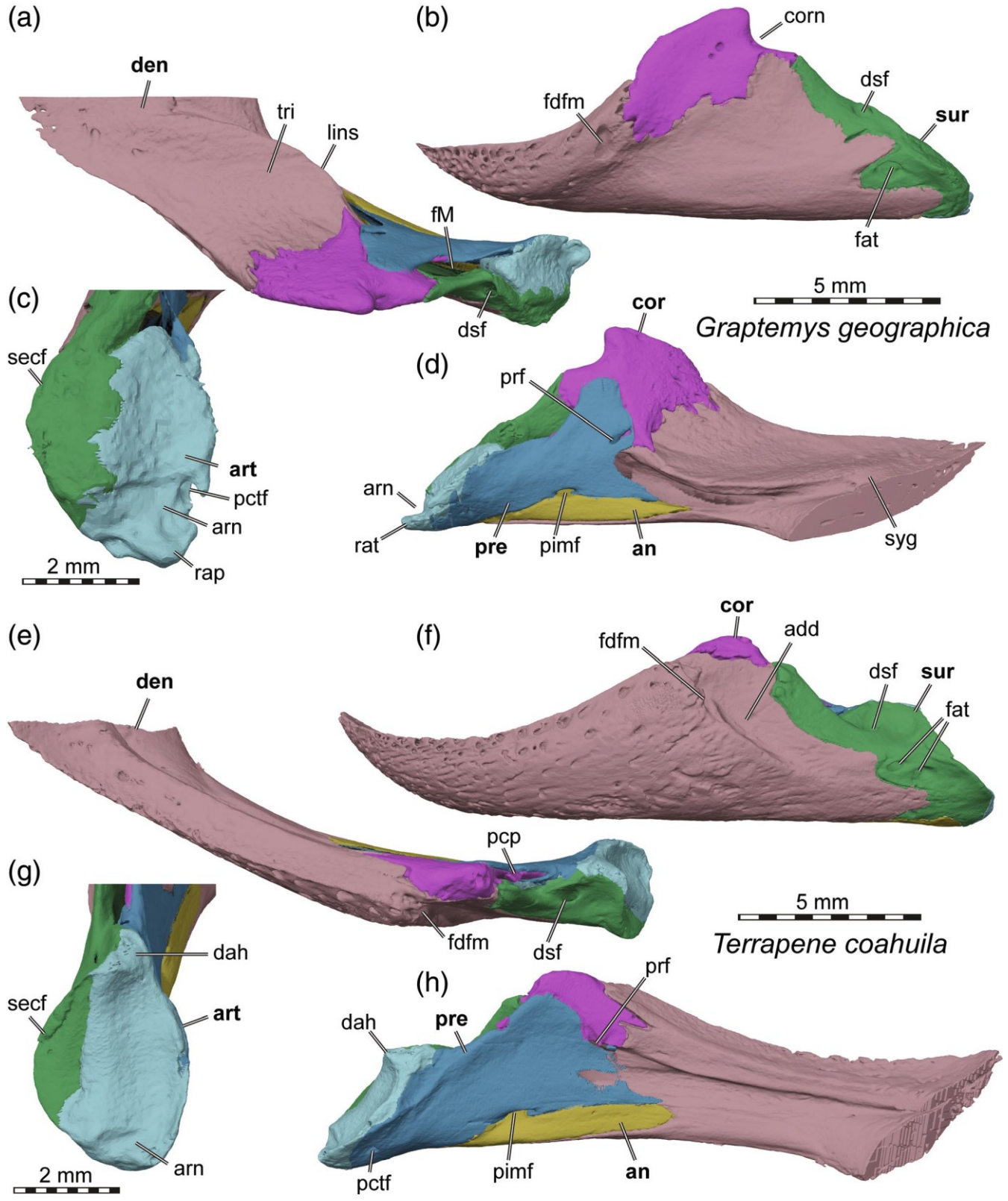

FIGURE 13 Legend on next page.

The surangular is a relatively inconspicuous bone in all emydids. Most of its lateral surface is covered by the dentary, except for a small area posteriorly to the coronoid process and another area around the articular process for the quadrate. In this latter area, the surangular forms a comparatively small ectocondyle flange, which roughly forms one-fourth of the articular surface (Figure 13c,g). Ventrally below the flange, all emydids have a large foramen auriculotemporalis, which usually is undivided (see also Bever, 2009). As in kinosternids, the foramen connects internally not only to an anteromedially directed canal that leads into the fossa Meckelii, but also connects to a prominent vertical canal, which exits as the dorsal surangular foramen just anteriorly to the margin of the jaw articulation surface (Figure 13e,f). An anteromedially recurved surangular lamina within the fossa Meckelii is absent in deirochelyines and *Glyptemys insculpta*, but present in *Emys orbicularis*, *Clemmys guttata*, and *Terrapene* spp.

The coronoid is uniformly low in emydines (Figure 13f,h), but variation in the height and dorsal shape of the coronoid exists among deirochelyines. In *Malaclemys terrapin*, *Graptemys geographica* and *Chrysemys picta*, the coronoid is tall (Figure 13b,d). It becomes posterodorsally gently recurved with its tip in the former two species, forming a weak coronoid notch (sensu Evers & Benson, 2019; Figure 13b). In *Deirochelys reticularia*, the coronoid is much lower and less robust, fitting the more gracile mandibular shape of that species. In all emydids, the coronoid forms the dorsal margin and majority of the coronoid process, which is also the case in species with overall low coronoid processes, including *Deirochelys reticularia* and emydines. The presence of an anteroventral process of the coronoid extending on the medial mandibular surface between the prearticular and the dentary is variable among emydids: many deirochelyines lack the process entirely (i.e., *Deirochelys reticularia*, *Malaclemys terrapin*, *Graptemys geographica*; Figure 13a), but it is present in *Chrysemys picta*, *Trachemys dorbigni* (Rockenback Portella et al., 2020), and *Pseudemys texana* (Bever, 2009). Among emydids, it is absent in *Terrapene ornata*, *Glyptemys insculpta* and *Clemmys guttata*, short in *Terrapene carolina*, but present and long in *Terrapene coahuila* (Figure 13e) and *Emys orbicularis*. An elongated posteromedial process of the coronoid that participates in the medial wall of the fossa Meckelii is present in emydines (Figure 13e), but less common in deirochelyines (e.g., *Chrysemys picta*; *Pseudemys texana*: Bever, 2009).

The prearticular is relatively consistent in its shape among emydids. In all species examined, there is only a single, anteroposteriorly slightly elongated intermandibular foramen (see also Bojanus, 1819–1821; Rockenback Portella et al., 2020). Due to the position of the foramen along the posterior part of the prearticular-angular contact, we identify the foramen as the posterior intermandibular foramen. Although the anterior prearticular parts are well ossified, the anterior intermandibular foramen is absent, suggesting it is fully reduced in emydids. It is possible that this feature is somewhat variable though, as Bever (2009) reported the foramen to be present in most specimens of *Pseudemys texana*, which we did not sample here. The prearticular forms the medial wall of the fossa Meckelii, as is generally the case in turtles. In nearly all emydids, the prearticular forms a small prearticular foramen near or at the suture with the coronoid, which traverses the bone mediolaterally (Figure 13d,h). In some emydines (e.g., *Terrapene coahuila*; *Clemmys guttata*; *Emys orbicularis*), the prearticular may be very closely associated with the articular, so that external and internal sutures can be partially obliterated. Our CT scans nevertheless show that the articular and prearticular remain unfused in all emydids examined, as the sutures could at least be partially traced in all specimens. The prearticular of emydids is only expressed at the very margin of the articular surface, and does not form a medial expansion of the mandibular articulation surface (Figure 13c,g), contrary to the condition in many other turtles, including *Platysternon megacephalum*. In emydids, the prearticular forms the entire posterior buttress to the articular.

The angular of emydids is strongly reduced (Figure 13d,h). Anteriorly, the bone becomes a thin and dorsoventrally low splint that is excluded from the margin of the Meckelian groove (e.g., Gaffney & Meylan, 1988; Joyce & Bell, 2004; McDowell, 1964). Posteriorly, the angular remains unexpanded in emydids, and does not expand to form a buttressing surface for the articular. This differs from the condition in most other turtles, in which the angular forms a dorsally concave, mediolaterally broadened floor of the posterior end of the mandible.

The splenial is absent in emydids.

FIGURE 13 3D renderings of mandibles of selected emydids. (a–d) The deirochelyine *Graptemys geographica* (NHMUK 55.12.6.11). (e–h) The emydine *Terrapene coahuila* (FMNH 47372). (a and e) Dorsal view. (b and f) Left lateral view. (c and g) Close-up of articular surface. (d and h) Medial view onto left mandibular ramus. Note that bones are labeled in bold, and other features in normal font. add, adductor fossa; an, angular; arn, articular notch; art, articular; cor, coronoid; corn, coronoid notch; dah, dorsal articular hook; den, dentary; dsf, dorsal surangular foramen; fat, foramen auriculotemporalis; fdfm, foramen dentofaciale majus; fM, fossa Meckelii; lins, lingual shelf; pcp, posteroventral process of the coronoid; pctf, chorda tympani foramen; pimf, posterior intermandibular foramen; pre, prearticular; prf, prearticular foramen; rap, retroarticular process; secf, ectocondyle flange of the surangular; sur, surangular; syg, symphyseal groove; tri, triturating surface

The articular forms the majority of the mandibular articulation facet in emydids (Figure 13c,g). The jaw articulation surface of the articular faces posterodorsally and is centrally depressed. Toward the lateral side, the articular bears a longitudinal ridge that separates two ento- and ectocondyle subfacets. In emydines, the articular forms a small dorsal mount-like protrusion, together with the prearticular and surangular (Figure 13g,h). This protrusion is positioned anterior to the jaw articulation surface, and gives the central part of the mandible a strong constriction or dorsal notch between the protrusion and the coronoid process, which can best be appreciated in lateral or medial view. In deirochelyines, this protrusion is much less conspicuous (Figure 13c,d), and the dorsal mandibular margin posterior to the coronoid process more or less slopes continuously posteroventrally in lateral or medial view of deirochelyine mandibles. Deirochelyines additionally have a small but clearly developed retroarticular process, which is separated from the jaw articulation surface but a transverse articular notch. Within the notch, deirochelyines have a chorda tympani foramen, which traverses the articular anteriorly and joins the fossa Meckelii (Figure 13c; Bever, 2009; Rockenback Portella et al., 2020). In emydines, a retroarticular process is absent, although a small articular notch is also present at the posteromedial edge of the articular (Figure 13g). In all emydines, the chorda tympani foramen is not positioned within the articular, but in a more anterior and medial position, on the prearticular (Figure 13g,h).

3.5.7 | Cheloniidae

Despite the small clade size of only six living species, there is considerable morphological variation among the jaws of cheloniids. Thus, we segmented three species in detail, that is, bone by bone (*Caretta caretta* ZMB 25470; *Chelonia mydas* NHMUK 1969.776; *Lepidochelys olivacea* SMNS 11070). In addition, we have simple mandibular 3D models of the remaining three species (*Eretmochelys imbricata* FMNH 22242; *Natator depressus* WAM R112123; *Lepidochelys kempii* CSIP M009-08). Variation broadly follows the phylogenetic interrelationships within cheloniids. In general, the mandibles of the sister species *Natator depressus* and *Chelonia mydas* are relatively similar, while the jaws of the subclade Carettini (*Lepidochelys* spp. and *Caretta caretta*) also show many similarities. *Eretmochelys imbricata* has similarities to both these groups of sea turtles, but is closer related to the Carettini than to the *Natator* + *Chelonia* clade. Our comparisons here are largely based on observations from our own models, but we note that Chatterji et al. (2022) and Jones et al. (2012) have additional images of cheloniid jaws of different species, which we used for comparisons.

The dentaries of cheloniids are comparatively deep and have a short lateral surface that exposes much of the surangular (Figure 14, Figure 15). Nonetheless, the dentary extends posteroventrally to about mid-length of the jaw articulation. The dentaries are robust and form a thick ridge ventrally, which marks a large adductor fossa on the lateral jaw surface between the dentary and surangular (Figure 14b,f, Figure 15b). The foramen dentofaciale majus is universally large in cheloniids, and positioned at the anterior margin of the adductor fossa (Figure 14b,f, Figure 15b). Among cheloniids, two general types of morphology can be observed regarding the triturating surfaces. *Caretta caretta* and the species of *Lepidochelys* form expanded triturating surfaces, which are notably expanded especially along the symphysis (Figure 14a,e). A posterior symphyseal mount is developed in *Lepidochelys*, but a symphyseal ridge is absent (Figure 14e). *Caretta caretta*, on the other hand, lacks any dorsally projecting symphyseal structures (Figure 14a). The triturating surfaces of carettines become narrower as they approach the coronoid process, and are formed only by the dentary. Labial ridges are absent in these taxa, and the lingual ridge is low and outwardly directed (Figure 14a,e). At the symphysis, the lingual ridge forms a low dorsal hook. This morphology is in contrast to that seen in *Eretmochelys imbricata*, *Chelonia mydas*, and *Natator depressus*. These taxa share a gently ventrally sloping anterior end of the dentary, which form low but sharp symphyseal hooks in *Natator depressus* and *Chelonia mydas* (Figure 15a,b), but a rounded symphysis in *Eretmochelys imbricata*. Although somewhat anteroposteriorly expanded at the symphysis, the triturating surfaces of non-carettine cheloniids are relatively narrow, but characterized by the presence of a medial ridge. In *Eretmochelys imbricata* and *Natator depressus*, this medial ridge is a true lingual ridge in that it is positioned at the lingual margin of the dentary (Chatterji et al., 2022). In *Chelonia mydas*, the medial ridge, although very prominent and sharp-edged, is removed from the lingual margin laterally and is thus comparable to the accessory ridges seen in some testudinids (Figure 15a). All three taxa have a symphyseal ridge, but this structure is most pronounced in *Chelonia mydas*, in which the ridge also defines deep collateral pits on the triturating surface to either side of the symphyseal ridge. Where the symphyseal ridge meets the lingual/accessory ridge, *Chelonia mydas*, *Eretmochelys imbricata* and *Natator depressus* have a sharp lingual symphyseal mount, which forms a spike-like dorsal projection that projects dorsally beyond the level of the lingual ridge and is thus

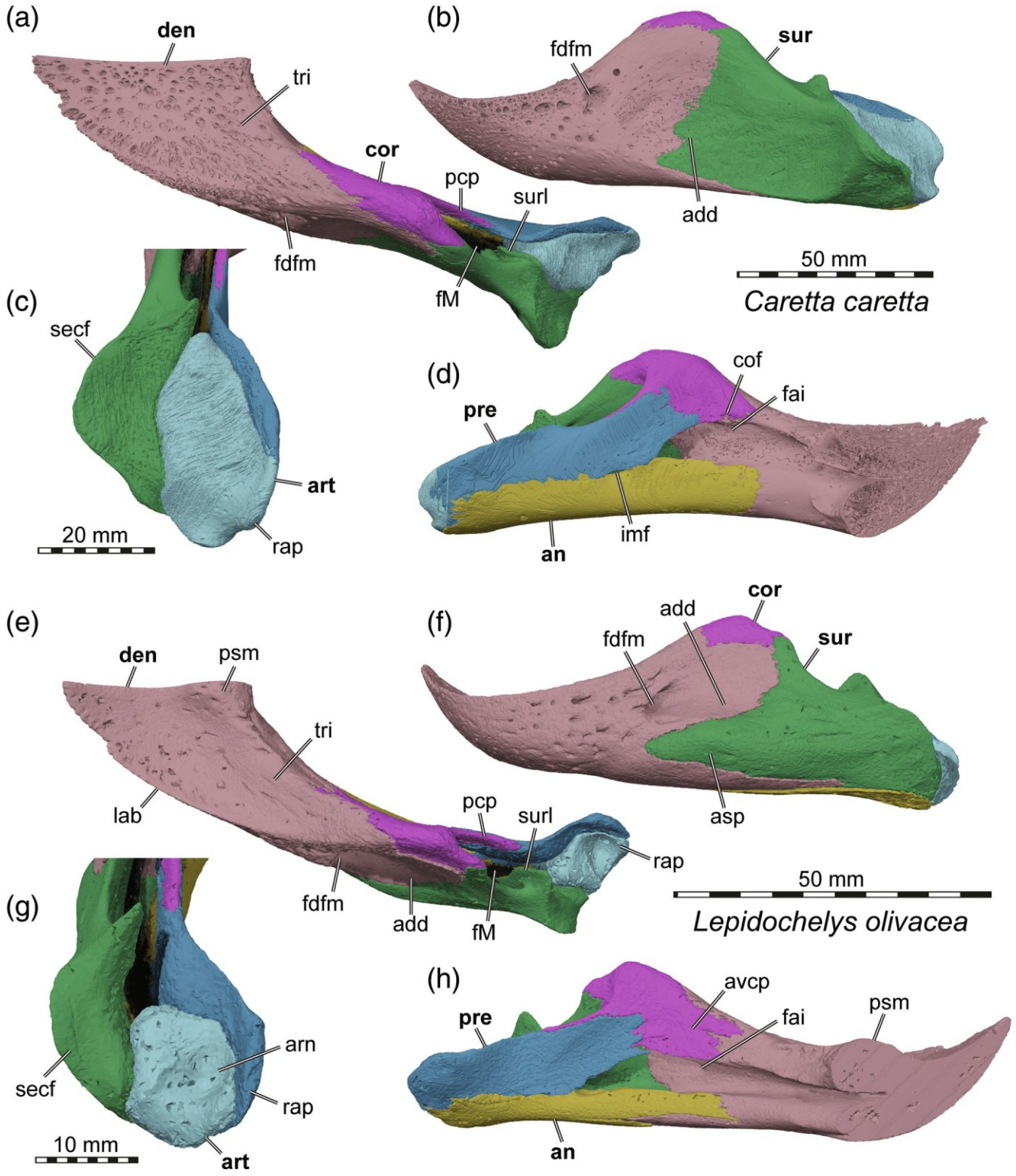

FIGURE 14 3D renderings of mandibles of carettine cheloniids. (a–d) *Caretta caretta* (ZMB 25470). (e–h) *Lepidochelys olivacea* (SMNS 11070). (a dand e) Dorsal view. (b and f) Left lateral view. (c and g) Close-up of articular surface. (d and h) Medial view onto left mandibular ramus. Note that bones are labeled in bold, and other features in normal font. add, adductor fossa; an, angular; arn, articul ar notch; art, articular; asp, anterior surangular process; avcp, anteroventral process of the coronoid; cof, coronoid foramen; cor, coronoid; den, dentary; fai, foramen alveolare inferius; fdfm, foramen dentofaciale majus; fM, fossa Meckelii; imf, intermandibular foramen; lab, lab ial ridge; pcp, posteroventral process of the coronoid; pre, prearticular; psm, posterior symphyseal mount; rap, retroarticular process; secf, ectocondyle flange of the surangular; sur, surangular; surl, surangular lamina; tri, triturating surface

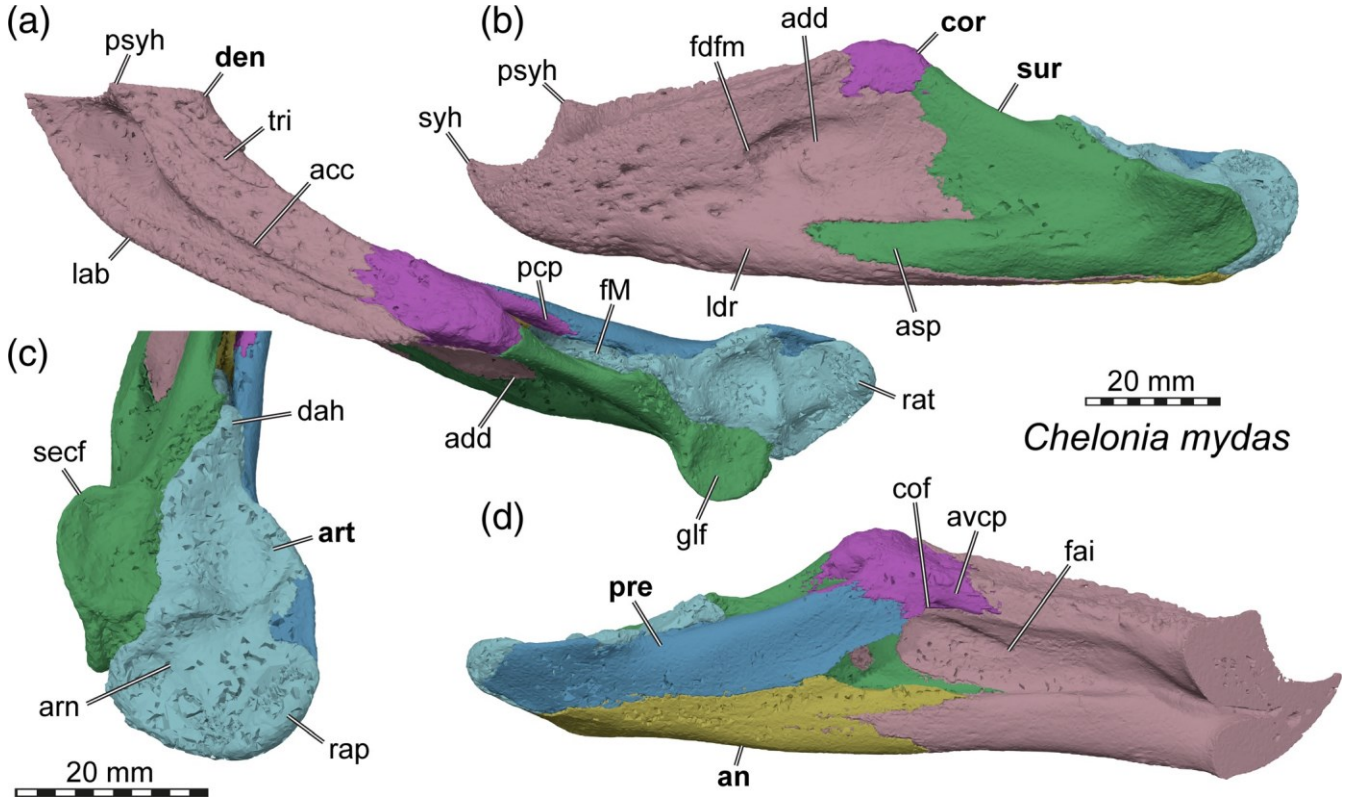

FIGURE 15 3D renderings of mandible of the cheloniid *Chelonia mydas* (NHMUK 1969.776). (a) Dorsal view. (b) Left lateral view. (c) Close-up of articular surface. (d) Medial view onto left mandibular ramus. Note that bones are labeled in bold, and other features in normal font. acc, accessory ridge; add, adductor fossa; an, angular; arn, articular notch; art, articular; asp, anterior surangular process; avcp, anteroventral process of the coronoid; cof, coronoid foramen; cor, coronoid; dah, dorsal articular hook; den, dentary; fai, foramen alveolare inferius; fdfm, foramen dentofaciale majus; fM, fossa Meckelii; lab, labial ridge; pcp, posteroventral process of the coronoid; pre, prearticular; psyh, posterior symphyseal hook; rap, retroarticular process; secf, ectocondyle flange of the surangular; sur, surangular; surl, surangular lamina; syh, symphyseal hook; tri, triturating surface

well visible in lateral view (Figure 15a,b). The medial surface of the dentary is dominated by a prominent and large Meckelian groove, which becomes anteriorly strongly constricted in the symphyseal segment of the jaws. The foramen alveolare inferius is exposed on the medial mandibular surface (Figure 14d,h, Figure 15d). Right and left dentaries are fully fused in cheloniids.

The surangular of cheloniids has a long anterior process that articulates with a respective groove on the dentary in the ventral perimeter of the adductor fossa (Figure 14f, Figure 15b). The only exception is *Caretta caretta*, in which this process is extremely short and inconspicuous (Figure 14b). The lateral surface of the surangular is devoid of any foramina in cheloniids, and no foramen auriculotemporalis could be identified in any cheloniid (Figure 14b,f, Figure 15b). Anterodorsally, the surangular has a process that reaches the coronoid and which forms the lateral wall to the fossa Meckelii. The dorsal opening into the fossa Meckelii is said to be relatively broad in cheloniids (Gaffney, 1979), but can be quite narrow in specimens of *Chelonia mydas*, *Eretmochelys imbricata*, and *Caretta caretta* (Figure 15a). At the posterior end of the fossa Meckelii, the surangular forms an anteromedially recurved, vertical lamina (see also Evers & Benson, 2019) in *Caretta caretta*, *Eretmochelys imbricata*, and *Lepidochelys* spp. (Figure 14a,e), but not in *Natator depressus* or *Chelonia mydas* (Figure 15a). The posterior end of the surangular is laterally strongly expanded to a laterally rounded ectocondyle flange in all cheloniids, which forms the lateral part of the articulation facet with its dorsal surface (Figure 14c,g, Figure 15c). The articulation surface is strongly posterodorsally inclined in *Caretta caretta*, but faces dorsally in all other cheloniids. The surface itself is slightly concave between its lateral margin and its contact with the medially adjacent articular, the contact to which is raised to a subtle ridge subdividing the jaw articulation into two facets.

The coronoid of cheloniids is robust but low, forming an arch between the surangular and prearticular at the anterior end of the foramen into the fossa Meckelii (Figure 14, Figure 15). Medially, the coronoid has a long

posteroventral process that lies against the prearticular. Anteroventrally, it has another process (= anteromedial coronoid process of Evers & Benson, 2019) that extends shortly along the dentary, but without properly contributing to the triturating surface. This anterior process has a mediolateral foramen, herein called coronoid foramen, that is usually relatively small (*Caretta caretta*, *Lepidochelys olivacea*, *Natator depressus*; Chatterji et al., 2022; Figure 14d), and which may only be partially ossified (e.g., *Lepidochelys kempii*, *Chelonia mydas*).

The prearticular of cheloniids is comparatively low dorsoventrally and retains a constant depth for most of its length (Figure 14d,h, Figure 15d). Posteriorly, it lies medially against the articular, and its dorsal margin may be interpreted as contributing to the articular surface. Centrally, the prearticular forms the medial wall of the fossa Meckelii, before anteriorly contacting the medial surface of a posteroventrally directed process of the coronoid. Intermandibular foramina are reduced in cheloniids (Siebenrock, 1897), although a singular foramen is sometimes developed along the prearticular-angular suture (e.g., our specimen of *Caretta caretta*; Figure 14d). It is difficult to homologize the foramen with either the anterior or posterior intermandibular foramen, as its position in *Caretta caretta* is much further anteriorly than expected for a posterior intermandibular foramen, which is usually the foramen retained in turtles in which one of the intermandibular foramina is reduced. A prearticular foramen at the suture with the coronoid is not developed in cheloniids.

The angular of cheloniids is comparatively large, occupying roughly half the dorsoventral depth of the posterior part of the mandibular ramus in medial view (Figure 14d,h, Figure 15d). Morphologically, it is a relatively simple, mediolaterally thin rod, which posteroventrally caps the articular and otherwise contacts all mandibular bones but the coronoid.

The splenial is absent in cheloniids.

The articular is large and complex in cheloniids. Wedged between the surangular laterally, the prearticular medially, and the angular ventrally, it forms the medial half of the articular surface of the jaw joint and borders the fossa Meckelii posteriorly (Figure 14c,g, Figure 15c). The articular surface is largely concave between the slightly raised suture with the surangular, and the dorsally projecting medial margin that is at least in part formed by the prearticular in cheloniids. Anteriorly, the articular surface forms a small knob-like, convex surface. In this part, the anterior end of the articular surface is notably upturned, resulting in a clear anterior delimitation that can be appreciated as an upturned lip in lateral view. Posteriorly, the articular surface is delimited by a less pronounced ridge, which traverses the bone mediolaterally and separates the articulation surface of the articular from a posteriorly well-developed retroarticular process. This process is formed in all cheloniids (Figure 14c,g, Figure 15c), but its development is strongest in *Chelonia mydas*, where the process is concave anteroposteriorly, producing a dorsally upcurved process along its posterior end (Figure 15c). The retroarticular process *of Caretta caretta* is much shorter than that of *Chelonia mydas*, and its posterior margin is posteriorly notched instead of forming an upturned lip (Figure 14c). We did not find any chorda tympani foramina in cheloniids, which is consistent with the remarks made by Fuchs (1931), that the chorda tympani nerve is absent in *Eretmochelys imbricata* and *Chelonia mydas*.

3.5.8 | Dermochelyidae

The leatherback sea turtle *Dermochelys coriacea* is the only living species of the Dermochelyidae. The mandible of the species has been described by Nick (1913). Although this description is quite detailed, the use of the German language and old anatomical terminology (e.g., "Goniale" instead of "prearticular") makes the paper less accessible than ideally the case. The following description largely agrees with Nick (1913) in terms of osteological observations, but uses modern nomenclature and bone homology.

The mandible of *Dermochelys coriacea* is strongly derived in many features, notably the absence of a coronoid bone, the unossified articular, and the reduction of triturating surfaces (see also Nick, 1913). The following description is based on a fully segmented specimen (UMZC R3031).

The dentary of *Dermochelys coriacea* is elongate but mediolaterally narrow (Figure 16a,b). A sharp labial ridge defines the dorsal margin of the bone (Nick, 1913), but the triturating surface is extremely reduced (Figure 16a). At the symphysis, the fused dentaries form a dorsal spike-like hook (Figure 16b; Nick, 1913). According to Nick (1913), fusion of the dentary rami is apparent even in late-stage embryos. Posteriorly, the dentary forms an extremely low coronoid process (Nick, 1913), which is slightly roughened in texture indicating the insertion site for the coronar aponeurosis (Figure 16b). The posterior part of the dentary is bifurcated into a dorsal and ventral ramus, which allows for a triangular process of the surangular to be wedged in between (Figure 16b). This is also seen in cheloniids. The foramen dentofaciale majus is completely absent in *Dermochelys coriacea*, as is any larger internal dentofacial or alveolar canal. An anteroposteriorly stretched groove on the lateral surface along the dorsal dentary margin indicates that rhamphotheca blood supply may have extended along the exterior bone

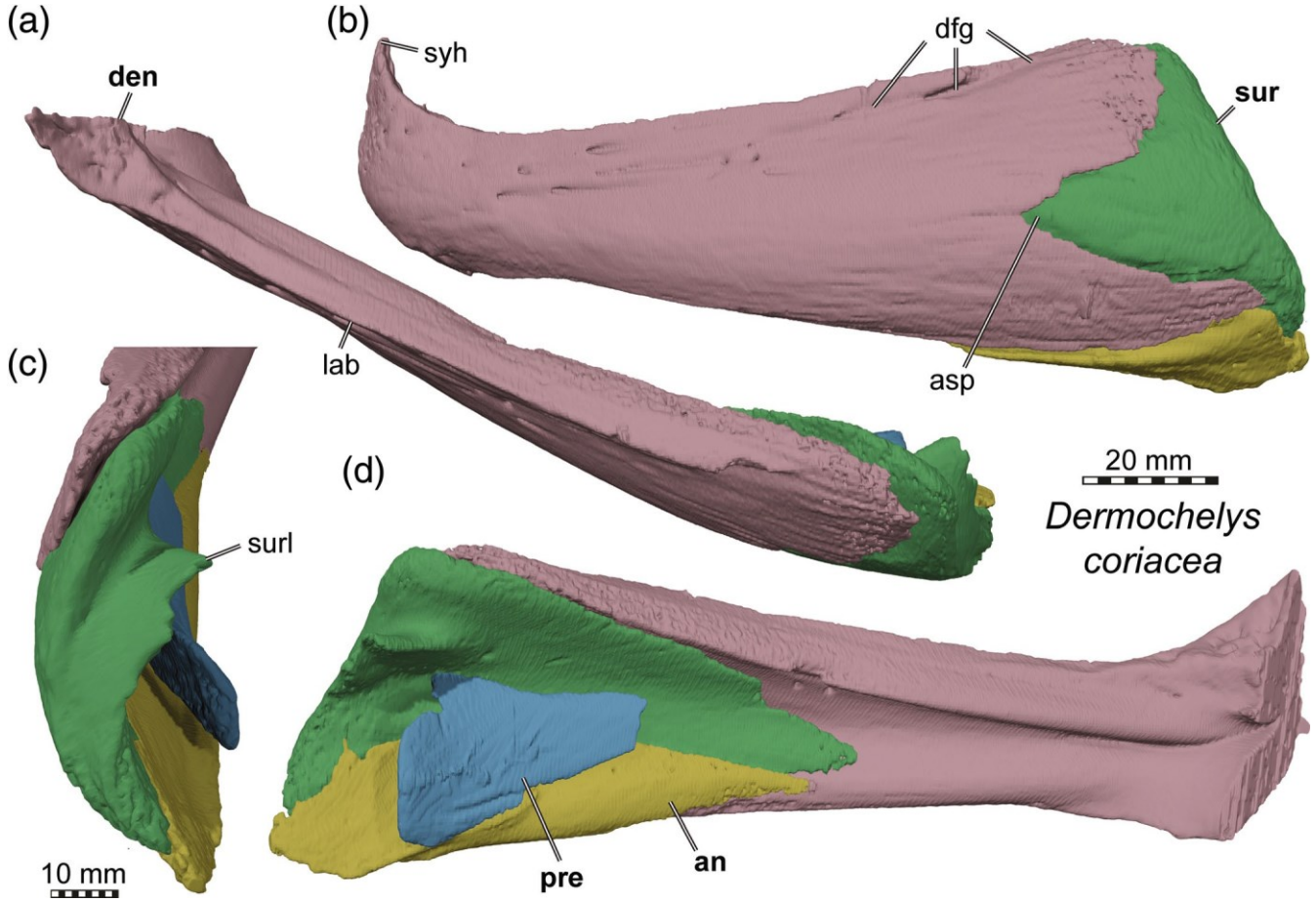

FIGURE 16 3D renderings of mandible of the dermochelyid *Dermochelys coriacea* (UMZC R3031). (a) Dorsal view. (b) Left lateral view. (c) Close-up of articular surface. (d) Medial view onto left mandibular ramus. Note that bones are labeled in bold, and other features in normal font. an, angular; asp, anterior surangular process; den, dentary; dfg, dentofacial groove; lab, labial ridge; pre, prearticular; sur, surangular; surl, surangular lamina; syh, symphyseal hook

surface (Figure 16b). Small foramina on the medial surface, nearly halfway along the dentary length, have been proposed to be the foramen alveolare inferius by Nick (1913). Given that these minute foramina lead only into short canals, the alveolar canal and foramen alveolare inferius can be interpreted as nearly fully reduced. An adductor fossa is absent, as the lateral surface of the mandibular ramus in the dentary-surangular contact area is laterally convexly bulged.

The surangular of *Dermochelys coriacea* has a well-developed, broadly triangular anterior process that articulates between the dorsal and ventral posterior dentary rami (Figure 16b; Nick, 1913), as is also the case in cheloniids. Together with the dentary, the surangular forms the low coronoid process in the absence of a coronoid bone (Nick, 1913). The foramen auriculotemporalis is absent in *Dermochelys coriacea*. A fossa Meckelii is also not formed, as the prearticular is reduced in size. However, the surangular has a recurved lamina as in cheloniids, which defines a dorsomedially open, broad groove along the dorsal surangular surface, which may be the equivalent of the fossa Meckelii (Figure 16c,d). According to Nick (1913), the surangular forms the lateral part of the mandibular articulation in *Dermochelys coriacea* (the medial part being cartilaginous). In our segmented specimen, this is not the case, and the articulation area was entirely cartilaginous, despite the adult size of the specimen.

The prearticular of *Dermochelys coriacea* is a roughly triangular plate that lies medially against the angular and surangular (Figure 16d; Nick, 1913). It is posteriorly slightly bulged medially to make room for the articular cartilages that fill the space between the posterior portions of the surangular, angular, and prearticular. Intermandibular foramina are completely reduced in *Dermochelys coriacea*.

The angular has a relatively large posteroventral exposure in lateral view of the mandible of *Dermochelys coriacea* (Figure 16b; Nick, 1913). Its ventral margin is relatively sharp-edged and does not form a mediolaterally expanded surface to hold the articular, as is the case in most other turtles. However, on the medial surface, there

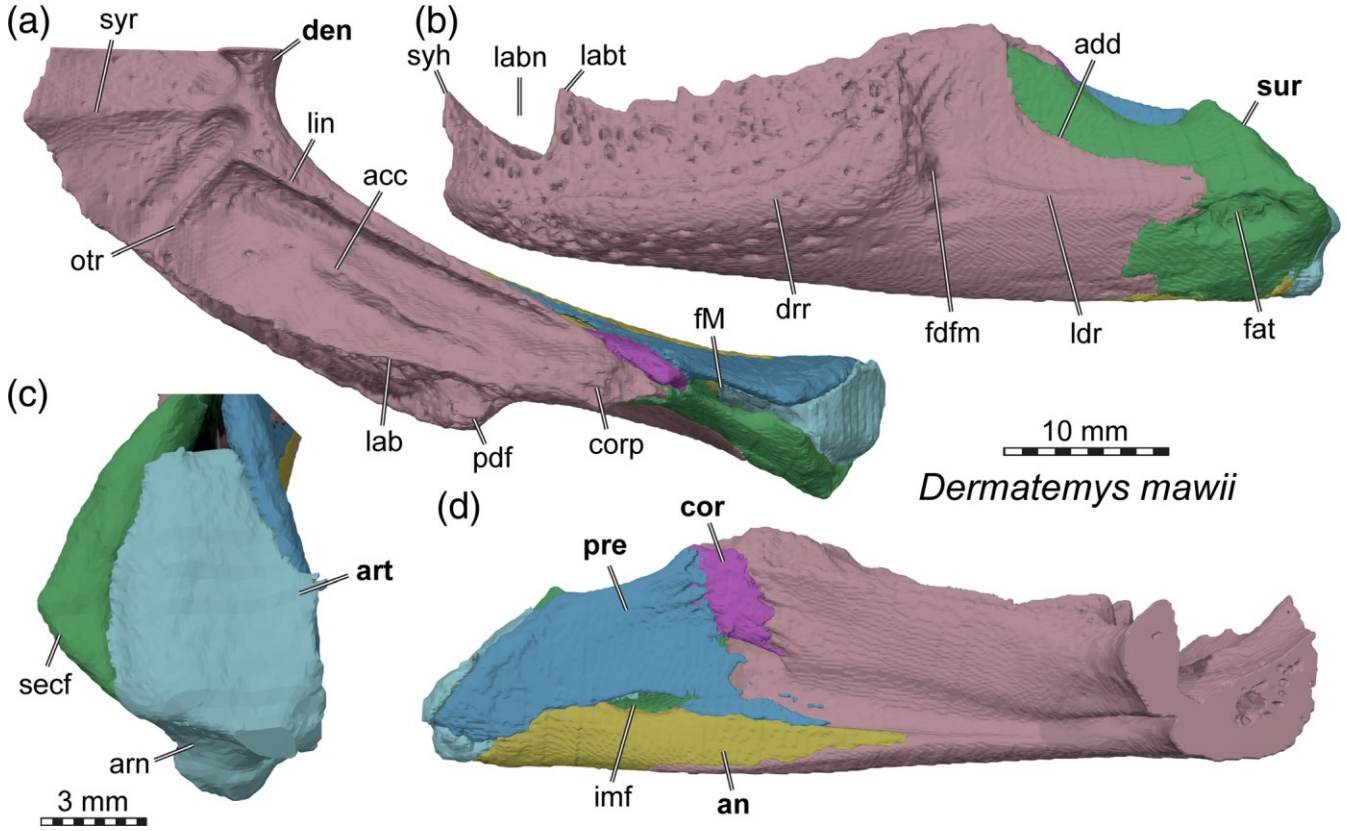

FIGURE 17 3D renderings of mandible of the dermatemydid *Dermatemys mawii* (CH-herps-117802). (a) Dorsal view. (b) Left lateral view. (c) Close-up of articular surface. (d) Medial view onto left mandibular ramus. Note that bones are labeled in bold, and other features in normal font. acc, accessory ridge; add, adductor fossa; an, angular; arn, articular notch; art, articular; cor, coronoid; corp, coronoid process; den, dentary; drr, dentary rhamphotheca ridge; fat, foramen auriculotemporalis; fdfm, foramen dentofaciale majus; fM, fossa Meckelii; imf, intermandibular foramen; lab, labial ridge; labn, labial notch; labt, labial tooth; ldr, lateral dentary ridge; lin, lingual ridge; otr, oblique triturating ridge; pdf, processus dentofaciale; pre, prearticular; secf, ectocondyle flange of the surangular; sur, surangular; syh, symphyseal hook, syr, symphyseal ridge

is a weakly protruding ridge near the ventral margin of the bone, which serves as the contact facet for the medially adjacent prearticular (Figure 16d).

The articular remains unossified in *Dermochelys coriacea*, and splenial and coronoid are entirely absent (Nick, 1913).

3.5.9 | Dermatemydidae

Our observations on Dermatemydidae are primarily based on a completely segmented mandible of the only living species of this clade, *Dermatemys mawii* (CM-herps-117802). The osteology of this specimen largely agrees with the second scan that we segmented (UF herp 04770), and which we used for the soft tissue descriptions. *Dermatemys mawii* has a very distinct mandibular anatomy and can be easily recognized and distinguished from closely related taxa, such as kinosternids.

The dentary of *Dermatemys mawii* is very robust (Figure 17). Both dentaries are fully fused, and the triturating surface increases in width from its posterior end toward the symphysis (Figure 17a). A low but distinct symphyseal ridge is present in *Dermatemys mawii*. The lingual and labial ridges are very pronounced and form sharp edges (Figure 17a). The labial ridge is serrated along its entire course, and additionally notched toward its anterior end (Figure 17b; Meylan & Gaffney, 1989). The labial ridge anterior to the notch rises to a distinct symphyseal hook. Posterior to the notch, the labial ridge forms a prominent, tooth-like spike (Figure 17b; Meylan & Gaffney, 1989). This spike is medially connected to the lingual ridge by an unusual oblique ridge, which crosses the triturating surface (Figure 17a). The intersection of the oblique ridge with the lingual ridge also forms a small dorsal protrusion, but this spike is lower than its labial pendant. The lingual ridge continues between the left and right lingual spikes as a low, dorsally concave crest from which the symphyseal ridge extends anteriorly. In addition, *Dermatemys mawii* has an accessory ridge that extends from the base of the coronoid process anteriorly

along the central area of the triturating surface (Figure 17a; Meylan & Gaffney, 1989). However, this accessory ridge is lower than the labial or lingual ridges, and does not continue anteriorly to meet the oblique ridge. The entire dentary surface area lateral and ventral to the labial ridge is deeply recessed to a facet for the articulation of the keratinous rhamphotheca, which circumscribes the dentary from one ramus to the other, including the symphyseal area (Figure 17b). This area is also densely covered in neurovascular foramina. The rhamphotheca surface is posteroventrally defined by a broad rhamphotheca ridge, the posterior surface of which also forms the entry area for a large foramen dentofaciale majus. Dorsally, the rhamphotheca ridge forms a prominent processus dentofacialis (Figure 17a), which is otherwise also prominent in chelydrids (see below). The foramen dentofaciale majus of *Dermatemys mawii* lies in the anteroventral margin of a relatively well-developed adductor fossa, which covers large parts of the posterior ramus of the dentary and continues on the surangular (Figure 17b). Ventrally, the adductor fossa is delimited by an anteroposterior ridge on the lateral dentary surface. Along this ridge, the dentary forms a posterior process that inserts into the lateral surangular surface, and which terminates just anteriorly to the foramen auriculotemporalis. Dorsally to the adductor fossa, and posterior with respect to the triturating surface, the dentary forms the coronoid process in *Dermatemys mawii* (Figure 17a,b). The process is low and well rounded. The Meckelian groove is shallow and narrow on the medial surface of the dentary. The foramen alveolare inferius is not visible in medial view, as it is covered by the coronoid-dentary contact.

The surangular of *Dermatemys mawii* is laterally largely covered by the posterior dentary process. However, the surangular has an anteroventral process that extends below the level of the adductor fossa anteriorly, similar to the condition seen in cheloniids or most testudinids, albeit far less extreme (Figure 17b). Anterodorsally, the surangular of *Dermatemys mawii* forms an ascending process toward the coronoid process, which forms the lateral wall of the opening into the fossa Meckelii. The lateral surface of this process takes part in the formation of the adductor fossa. Posteriorly, the surangular forms a small ectocondyle flange, which is only weakly concave but nonetheless contributes to the jaw articulation facet (Figure 17c). Anterolaterally and ventrally to the articulation facet is a large, oval fossa, from which the auriculotemporal canal extends anteromedially. The foramen auriculotemporalis is smaller than the fossa that surrounds the foramen itself. A dorsally projecting surangular foramen is absent, distinguishing *Dermatemys mawii* from the closely related kinosternids.

The coronoid of *Dermatemys mawii* is extremely small, and limited to the medial surface of the mandibular ramus (Figure 17a,d). It is wedged between the surangular and dentary laterally, and the prearticular medially, and contributes to the anterior margin of the fossa Meckelii. However, the dorsal extent of the bone is low (Meylan & Gaffney, 1989), and the coronoid does not contribute to the coronoid process.

The prearticular of *Dermatemys mawii* forms the medial wall of the fossa Meckelii. Along the suture with the angular, the specimen UF herp 04770 has relatively closely spaced but separate anterior and posterior intermandibular foramina. In the specimen CH-herps-117802, instead there is a single, large intermandibular foramen, suggesting that the anterior and posterior foramina are merged in this specimen (Figure 17d). Anteriorly, the prearticular forms a long, splint-like process that lies against the dorsal margin of the angular. Posteriorly, the prearticular frames the lateral surface of the articular, but without being included into the jaw articulation facet (Figure 17c).

The angular has a long and dorsoventrally narrow shape in *Dermatemys mawii* (Figure 17d). Anteriorly, it tapers to form a pointed process that lies against the ventromedial ridge of the dentary that frames the Meckelian groove.

The splenial is absent in *Dermatemys mawii*.

The articular is relatively large in *Dermatemys mawii* and forms the majority of the jaw articulation surface (Figure 17c). The articulation surface is strongly posterodorsally oriented in *Dermatemys mawii*, a condition shared with kinosternids. Along the articulation surface, there is an anteroposterior ridge trending along the lateral third of the articular, which subdivides the articulation area into a medial and lateral subfacet. Ventrally to the posterior margin of the articulation facet, there is a mediolateral groove in the articular, which forms an articular notch. The retroarticular process is strongly reduced to small knob on the ventral surface of the articular (Meylan & Gaffney, 1989). Whereas in kinosternids there is a foramen posterius chorda tympani located within this articular notch, this foramen is absent in *Dermatemys mawii*.

3.5.10 | Kinosternidae

Kinosternids can be divided into two major subclades, the staurotypines and the kinosternines. For Staurotypinae, we fully segmented *Staurotypus salvinii* (NHMUK 1879.1.7.5), and additionally have mandibular models for *Claudius angustatus* (SMNS 14380). For Kinosterninae, we produced bone-by-bone segmentations for *Sternotherus minor* (FMNH 211696), and additionally have models of *Kinosternon baurii* (FMNH 211705), *Kinosternon subrubrum* (FMNH 211711), and *Kinosternon scorpioides* (SMF 71893).

Kinosternids have relatively short and robust mandibles (Figure 18; Figure 19). The articulation surface for the quadrate is strongly posteriorly inclined in

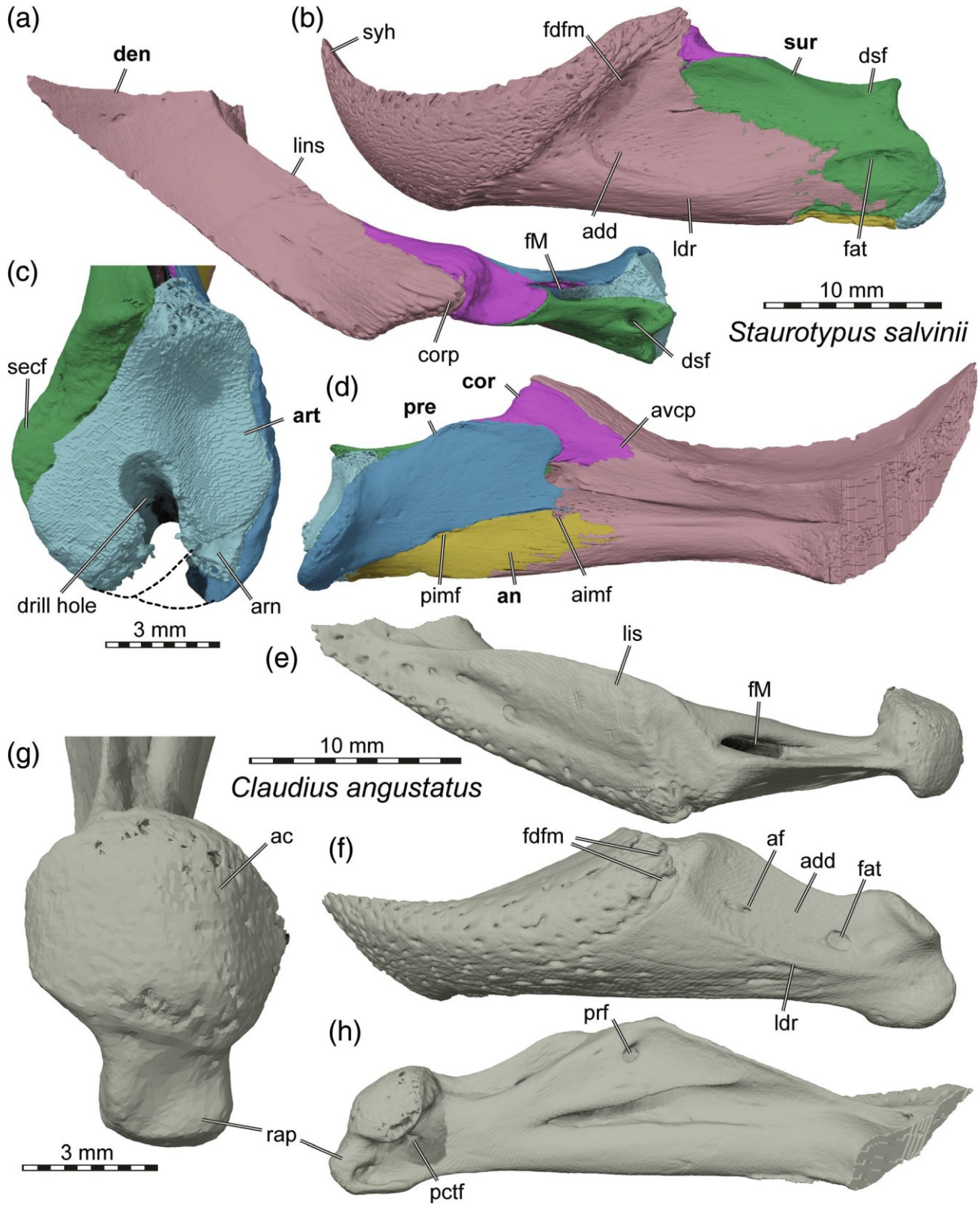

FIGURE 18 Legend on next page.

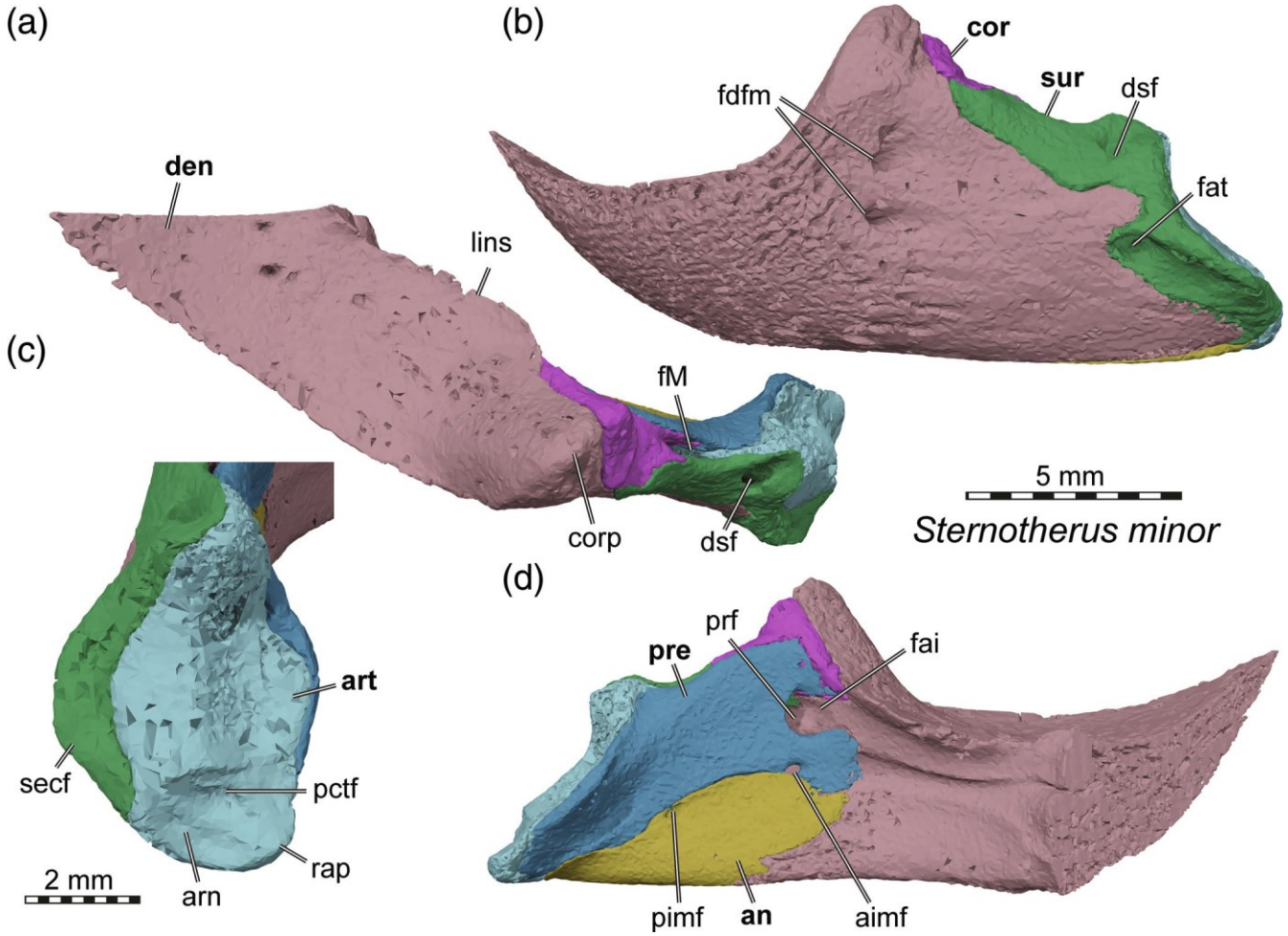

FIGURE 19 3D renderings of mandible of the kinosternine kinosternid *Sternotherus minor* (FMNH 211696). (a) Dorsal view. (b) Left lateral view. (c) Close-up of articular surface. (d) Medial view onto left mandibular ramus. Note that bones are labeled in bold, and other features in normal font. aimf, anterior intermandibular foramen; an, angular; arn, articular notch; art, articular; cor, coronoid; corp, coronoid process; den, dentary; dsf, dorsal surangular foramen; fai, foramen alveolare inferius; fat, foramen auriculotemporalis; fdfm, foramen dentofaciale majus; fM, fossa Meckelii; lins, lingual shelf; pctf, posterior chorda tympani foramen; prf, prearticular foramen; pimf, posterior intermandibular foramen; pre, prearticular; rap, retroarticular process; secf, ectocondyle flange of the surangular; sur, surangular

kinosternids, which contributes to the shortness of the mandibles. Besides their stout appearances, particular features of kinosternid mandibles are the subordinate role of the coronoid within the coronoid process, the presence of a vertical surangular canal in most species, and the surface texture around the rhamphotheca part of the mandible. There are relatively few distinct differences in morphology between kinosternines and staurotypines (Figure 18a–d; Figure 19a–d), but the staurotypine *Claudius angustatus* has a peculiar mandibular morphology that deviates from most other kinosternids in various aspects that are outlined below (Figure 18e–h).

FIGURE 18 3D renderings of mandibles of selected staurotypine kinosternids. (a–d) *Staurotypus salvinii* (NHMUK 1879.1.7.5). (e–h) *Claudius angustatus* (SMNS 14380). (a and e) Dorsal view. (b and f) Left lateral view. (c and g) Close-up of articular surface. (d and h) Medial view onto left mandibular ramus. Note that bones are labeled in bold, and other features in normal font. Note that the sutures between elements are difficult to discern in our CT scan of *Claudius angustatus*, and that we segmented the left mandibular ramus as a single model. ac, articular condyle; add, adductor fossa; aimf, anterior intermandibular foramen; af, accessory foramen; an, angular; arn, articular notch; art, articular; avcp, anteroventral process of the coronoid; cor, coronoid; corp, coronoid process; den, dentary; dsf, dorsal surangular foramen; fat, foramen auriculotemporalis; fdfm, foramen dentofaciale majus; fM, fossa Meckelii; ldr, lateral dentary ridge; lins, lingual shelf; lis, lingual surface; pctf, posterior chorda tympani foramen; prf, prearticular foramen; pimf, posterior intermandibular foramen; pre, prearticular; secf, ectocondyle flange of the surangular; Sur, surangular; syh, symphyseal hook

The dentaries of kinosternids are fully fused along the symphysis, and symphyseal ridges are absent. The tip of the beak is usually pointed and curves slightly upwards in all examined species (Figure 18; Figure 19). True labial and lingual ridges are absent (but see *Claudius angustatus*): Although the labial and lingual margins of the dentary are well defined and sharped edged, the triturating surface between both margins forms a flat or slightly concave platform (Figure 18a,d; Figure 19a,d). In *Claudius angustatus*, the lingual margin of the triturating surface is greatly expanded both laterally and dorsally, protruding far dorsally to the level of the labial margin of the mandible (Figure 18e,f). This strongly inflated lingual ridge forms a dorsolaterally exposed surface, and is separated from the lingual margin by a shallow and narrow trough (Figure 18e). In all kinosternids, the extend of the keratinous rhamphotheca is very clearly indicated by a rough surface that is densely populated by neurovascular foramina (Figure 18b,f; Figure 19b). Posterodorsally, the dentary forms most of the coronoid process, in which the coronoid is only integrated as a medially supporting bone (Figure 18b,f; Figure 19b). Posteroventrally to the rhamphotheca extent, the lateral dentary surface is dominated by an adductor fossa which can be shallow (e.g., *Claudius angustatus*; *Kinosternon scorpioides*, *Sternotherus minor*; Figure 18f; Figure 19b) or deep and well defined anteriorly and ventrally by strong margins (e.g., *Kinosternon baurii*, *Kinosternon subrubrum*; *Staurotypus salvinii*; Figure 18b). The foramen dentofaciale majus is relatively small in comparison to some other turtles, but generally present. Indeed, in most species, there seem to be two or sometimes three major opening from the anterodorsal margin of the adductor fossa leading anterolaterally into the fossa Meckelii (Figure 18f; Figure 19b). The dentary covers most of the surangular laterally, but the extent of this coverage seems stronger in Kinosterninae than in Staurotypinae: all our sampled kinosternines (*Kinosternon baurii*, *Kinosternon scorpioides*, *Kinosternon subrubrum*, *Sternotherus minor*; Figure 19b) show that the dentary is posteriorly bifurcated around the dorsal and ventral margin of the auriculotemporal foramen. In Staurotypines (e.g., *Staurotypus salvinii*), the dentary only shows the ventral posterior process, and the foramen remains dorsally unbounded by the dentary (Figure 18b).

The surangular exposure is relatively small in kinosternids, due to the large posterior extent of the dentary. The surangular is laterally expanded to an ectocondyle flange, which is smaller than in many other turtles (e.g., trionychids), and nearly vertically oriented, contributing to the posterior orientation of the jaw articulation (Figure 18c; Figure 19c). However, the surangular participation in the articulation facet is restricted to a semi-lunate area at the lateral surface margin, and most of the surface is formed by the articular (see below). All kinosternids have a vertical surangular canal, that is, a short vertical canal that traverses the bone vertically from the foramen auriculotemporalis and ends in a dorsal surangular foramen that is positioned anterior to the jaw articulation surface (Figure 18a; Figure 19a). The dorsal surangular foramen is quite large (larger than the foramen dentofaciale majus) and was specifically mentioned by Gaffney (1979) for *Staurotypus*, although the foramen was left unnamed. Meylan (1987) mentioned the foramen as present in all kinosternids. We herein generally confirm this observation but find the foramen and short vertical canal to be present in all kinosternids but *Claudius angustatus* (Figure 18e). *Claudius angustatus* only has the anteromedial auricolotemporal canal that communicates from the auriculotemporal foramen with the fossa Meckelii. Together with the prearticular, the surangular of kinosternids forms a narrow, slit-like opening into the fossa Meckelii. A recurved surangular lamina is absent (Figure 18a,e; Figure 19a).

The coronoid of kinosternids is an inconspicuous and small element, which does not form the tip of the coronoid process. Instead, the coronoid lies posteromedially against the process, which is largely formed by the dentary (Figure 18d; Figure 19d). In most species, the coronoid does not contribute to the triturating surface, although it may form a tiny part of this area in *Sternotherus minor* and *Staurotypus salvinii* (Figure 18a; Figure 19a). An expanded anteromedial process is lacking in all kinosternids. Posteriorly, the coronoid borders the fossa Meckelii.

The prearticular of kinosternids forms the medial wall of the fossa Meckelii, as in all turtles, and is a relatively simply vertical sheeted bone. Posteriorly, the prearticular expands medially around the mediolaterally broad articular, which it frames medially. This medial margin of the prearticular forms the edge of the jaw articulation, but does not contribute to its surface (Figure 18c; Figure 19c). In all kinosternids but *Claudius angustatus*, the prearticular forms two (anterior and posterior) intermandibular foramina along the sutural contact to the ventrally adjacent angular (Figure 18d; Figure 19d). The anterior intermandibular foramen may not be fully ossified in many specimens, but its outline is usually at least partially ossified. In our specimen of *Sternotherus minor*, the posterior intermandibular foramen lies fully within the angular just below the prearticular suture, but it is unclear if this is systematic or individual variation from the more generalized inter-sutural position of the foramen (Figure 19d). In *Sternotherus minor*, the anterior end of the prearticular, which in other species tapers to a pointed process along the posterior part of the Meckelian groove, forms a dorsoventrally expanded plate which comes into contact with the dentary. As a consequence, *Sternotherus minor* has a prearticular foramen as also seen in many testudinids (Figure 19d).

The angular forms a posteroventral buttressing surface for the articular, but twists to a more vertical orientation and laminar shape with its anterior parts, which are integrated into the medial surface of the mandibular ramus (Figure 18d; Figure 19d). This anterior angular part is usually dorsoventrally low and retains equal height for most of its length. This morphology is seen in staurotypines (e.g., *Staurotypus salvinii*) as well as most kinosternines (e.g., all examined species of *Kinosternon*). In *Sternotherus minor*, the angular instead becomes dorsoventrally deeper with its anterior end, so that it can be easily distinguished from *Kinosternon* spp. (Figure 19d).

The splenial is absent in kinosternids.

The articular forms most of the jaw articulation surface in kinosternids. With the exception of *Claudius angustatus*, the articular bears a low but distinct anteroposterior ridge that separates the surface into medial and lateral subfacets (Figure 18c; Figure 19c). The articulation surface is strongly posteriorly inclined, and the anterodorsal end of the bone narrows mediolaterally and forms a gently posterodorsally recurved process, to which the surangular usually contributes as well (Figure 18b,c; Figure 19b,c). The posteroventral end of the articulation area usually bears a small mediolateral groove, the articular notch, in which there is an anteriorly invading foramen posterius chorda tympani (Figure 19c). A short retroarticular process is present (Figure 19c). The articular of *Claudius angustatus* shows a completely different morphology. Although the surrounding bone contacts are not entirely clear in the CT scans of our examined specimen, it is clear that the articular forms the majority of the jaw articulation surface (Figure 18g). Rather than being a biconcave facet, the articular forms a hemispherical articular condyle, which is medially and laterally expanded with regard to the mediolateral extend of the mandibular ramus (Figure 18g). Posteroventrally, the jaw articulation surface is contacted by a tubercle-like retroarticular process that is smaller in size than the articular condyle itself, but which also forms a convexly rounded and smooth surface, which appears to have been part of the jaw joint (Figure 18c). This surface extends along the posterior end the articular and continues ventrally on the underside of the jaw. The tubercle may have allowed for hyperextension of the mandible or at least some propalineal jaw movement, or may otherwise serve as a "regular" attachment for the *m. depressor mandibulae*.

3.5.11 | Chelydridae

Chlydrids only include two living species, both of which we have CT scans of. For *Macrochelys temminckii* (FMNH 22111), we provide a bone-by-bone segmentation, whereas for *Chelydra serpentina* (UF-herp-22159), we segmented the mandible as a single unit.

The dentaries of chelydrids are well fused across the midline. Both species have an upturned symphyseal hook (Figure 20b), although the structure is lower *Chelydra serpentina* (Gaffney, 1975b). Symphyseal ridges are absent. The triturating surfaces of both chelydrids are relatively narrow, but show differences. Whereas *Chelydra serpentina* has a clearly developed, raised lingual ridge, *Macrochelys temminckii* instead has a lingual shelf that is medially expanded (Figure 20a; Gaffney, 1975b). Both species have sharp-edged labial cutting surfaces. In *Chelydra serpentina*, there is a concentration of roughly anteroposteriorly aligned neurovascular foramina just below the labial margin. In *Macrochelys temminckii*, such an aligned series of foramina is absent, and instead the entire lateral surface around the area of attachment for the rhamphotheca is roughened and lined with small foramina and grooves (Figure 20b), similar to the condition seen in kinosternids (see above). Chelydrids have a prominent processus dentofacialis at the posterolateral end of the triturating surface (Figure 20b). The foramen dentofaciale majus is relatively small in chelydrids, and enters the dentary posteromedially to the processus dentofacialis, which shields the opening in lateral view (Figure 20a). Posterior to the processus dentofacialis, the dentary contributes to the coronoid process, which is overall low and dorsally rounded (Figure 20b). The dentary and coronoid surfaces are lined with striations around the coronoid process, indicating the attachment of the coronar aponeurosis (Figure 20a). Ventrally below the coronoid process, the lateral dentary surface is smooth. An adductor fossa is absent in our specimen of *Macrochelys temminckii* (Figure 20b), but appears as a comparatively weak depression in very large adult specimens (e.g., FMNH 215473). In *Chelydra serpentina*, the adductor fossa is more clearly defined even in small specimens, but limited to the dorsal third of the mandibular height at the coronoid process level. The dentary laterally overlaps the surangular in its posterior part in chelydrids, but much of this bone remains exposed above a posteroventral dentary process that extends toward the posterior jaw end.

The surangular is prominently exposed in lateral view of chelydrid mandibles (Figure 20b). The surangular lamina on the side of the fossa Meckelii is very well developed (Figure 20a). The ectocondyle flange of the surangular is also prominent, but angled strongly dorsally in *Macrochelys temminckii* (Figure 20c). The dorsomedial surface of the flange broadly contributes to the surface for the jaw articulation. *Chelydra serpentina* has a single mid-sized foramen auriculotemporalis on the lateral

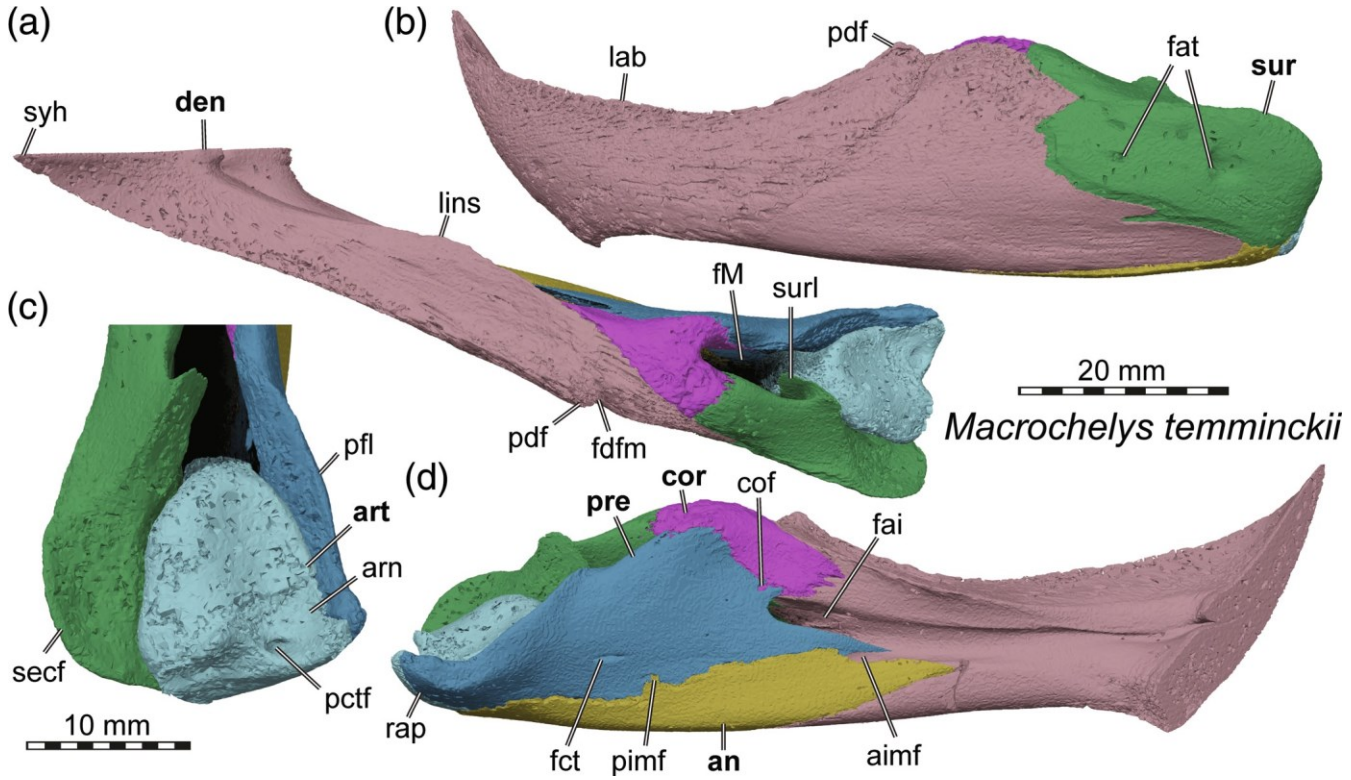

FIGURE 20 3D renderings of mandible of the chelydrid *Macrochelys temminckii* (FMNH 22111). (a) Dorsal view. (b) Left lateral view. (c) Close-up of articular surface. (d) Medial view onto left mandibular ramus. Note that bones are labeled in bold, and other features in normal font. aimf, anterior intermandibular foramen; an, angular; arn, articular notch; art, articular; cof, coronoid foramen; cor, coronoid; den, dentary; fai, foramen alveolare inferius; fat, foramen auriculotemporalis; fdfm, foramen dentofaciale majus; fM, fossa Meckelii; lab, labial ridge; lins, lingual shelf; pctf, posterior chorda tympani foramen; pdf, processus dentofaciale; pfl, prearticular flange; pimf, posterior intermandibular foramen; pre, prearticular; prf, prearticular foramen; rat, retroarticular foramen; secf, ectocondyle flange of the surangular; sur, surangular; surl, surangular lamina; syh, symphyseal hook

surangular surface, whereas there are two or three foramina in *Macrochelys temminckii* (Figure 20b). However, a vertical surangular canal and associated dorsal surangular foramen are absent in both species. Consequentially, the foramina auriculotemporalis leads to only a single, anteriorly directed canal, which connects to the fossa Meckelii.

The coronoid is relatively low and broad in chelydrids (Figure 20a,b,d). The dorsal surface of the bone forms the coronoid process, but the dentary also seems to contribute to the coronar aponeurosis attachment site (see above). The posteroventral processes of the coronoid around the anterior margin of the dorsal opening of the fossa Meckelii are strongly angled away from one another. This contributes to the opening into the fossa Meckelii being exceptionally broad in chelydrids (Figure 20a). The coronoid has an anteroventral process on the medial mandibular surface, which prohibits a dorsal contact between dentary and prearticular (Figure 20d). A small coronoid foramen is present between the prearticular and coronoid of *Macrochelys temminckii* (Figure 20d), but we could not confirm the foramen in our specimen of *Chelydra serpentina*.

The prearticular is a prominent bone in chelydrids, which reaches far anteriorly (Figure 20d). In both chelydrid species, anterior intermandibular foramina are formed in addition to the more commonly found posterior intermandibular foramina. However, in *Macrochelys temminckii*, the anterior intermandibular foramen is only partially closed, and remains anteriorly open (Figure 20d), whereas it is fully enclosed between the prearticular and angular in *Chelydra serpentina*. The posterior intermandibular foramen lies in the prearticular-angular suture in both chelydrids. Our specimen of *Macrochelys temminckii* also shows a medial small opening into a canal that traverses the prearticular anteroposteriorly (Figure 20d). The respective canal can be associated with the chorda tympani nerve, as the canal continues posteriorly in the articular and opens in the chorda tympani foramen. Anteriorly the canal opens midway along the prearticular length, on the inside of the fossa Meckelii. Posteriorly, the prearticular

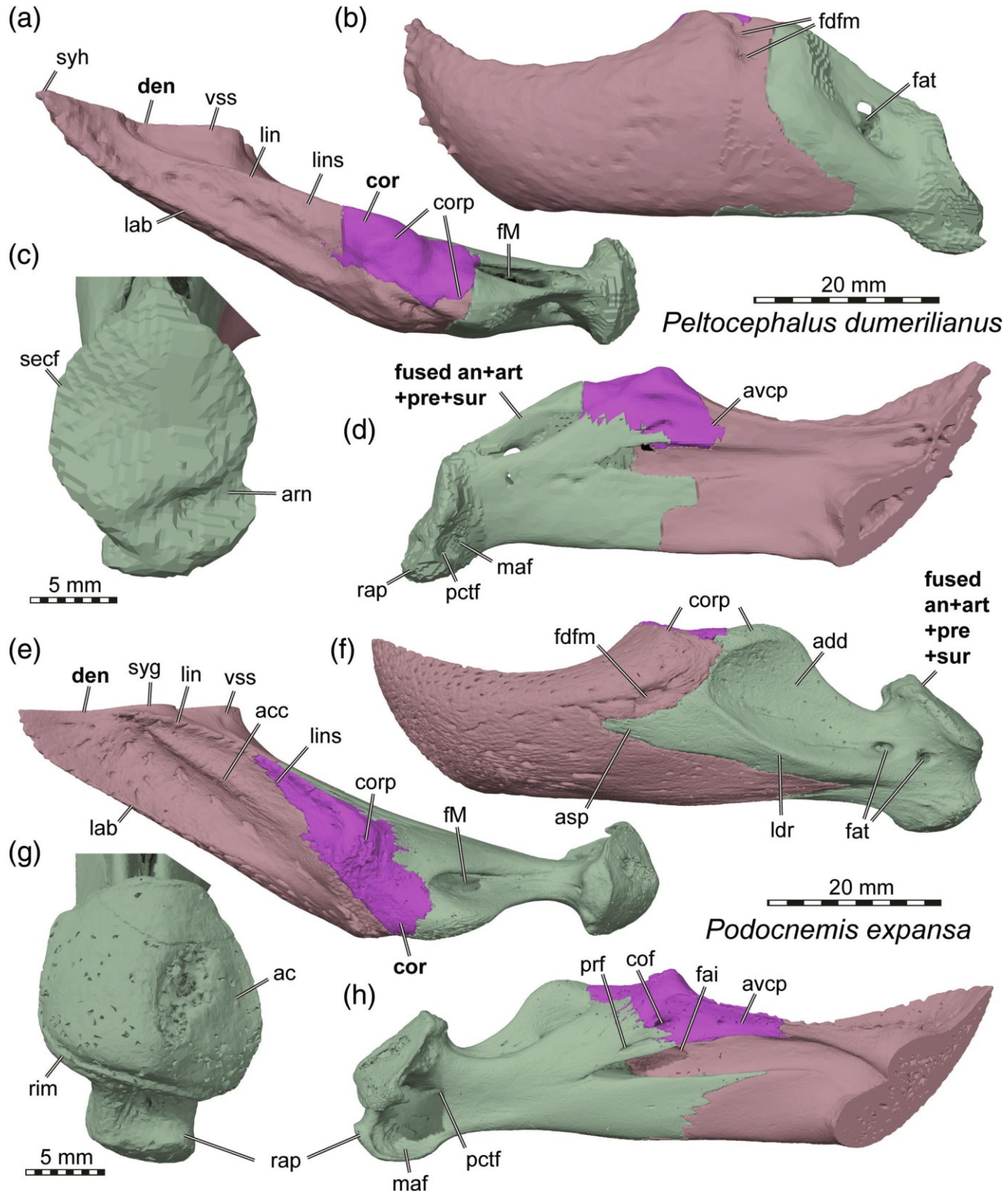

FIGURE 21 Legend on next page.

contributes to the jaw articulation in chelydrids, and even forms a medial flange in *Macrochelys temminckii* (Figure 20c).

The angular of chelydrids shows the typical morphology of most turtles, with a posterior part that is restricted to the ventral margin of the jaw, and a medially placed, laminar anterior part that tapers to a thin process (Figure 20d).

The splenial is absent in chelydrids.

The articular of chelydrids is a relatively broad but short block of bone. Laterally, the bone bears an anteroposteriorly trending, vertical ridge that separates the articular surface into clear medial and lateral subfacets (Figure 20a,c). An articular notch is present in both chelydrid species, but positioned on the posterior surface of the articular, so that it is hard to see in dorsal view (Figure 20c). The retroarticular process of chelydrids is small, and formed as a dorsally upturned lip between the articular and prearticular (Figure 20c,d). At the base of the retroarticular process, and toward the jaw articulation, the articular of both chelydrid species bears a relatively large posterior chorda tympani foramen (Figure 20c). The associated anteriorly directed canal traverses the articular and continues in the prearticular (see above). The chorda tympani canal ultimately enters the fossa Meckelii from the medial surface of the prearticular.

3.5.12 | Podocnemididae

Podocnemidids are a relatively species-poor clade today, although their fossil diversity is quite large, especially when stem-taxa such as bothremydids are considered (e.g., Ferreira et al., 2018; Gaffney et al., 2006, 2011). Our sample of 3D models includes a fully segmented mandible of *Peltocephalus dumerilianus* (MCT RR 354; Figure 21a–d), which we downloaded from MorphoSource (Hermanson, 2021). Additionally, we segmented several specimens of *Podocnemis* ourselves. We fully segmented a specimen of *Podocnemis expansa* (ZMB 90084; Figure 21e–h) and provide singular mandibular models of *Podocnemis expansa* (LIRP herp 001), *Podocnemis unifilis* (FMNH 45657), as well as an indeterminate *Podocnemis* sp. (NHMUK 60.4.16.9). The mandibular anatomy of *Podocnemis expansa* is much better known than that of most other turtles. This is primarily due to the detailed osteological and soft tissue description of Fuchs (1931), and the genus being used as a reference comparison for many extinct podocnemidid mandibles (e.g., Gaffney et al., 1998; Gaffney et al., 2011). The description of Fuchs (1931) is slightly less accessible than ideally would be the case, as the text is written in (quite antiquated) German, and as several anatomical descriptors, including the terms used for specific bones, have fallen out of favor since the early 20th century.

The most distinct feature of podocnemidid mandibular anatomy is a fusion (i.e., complete suture obliteration externally and internally) affecting the posterior mandibular bones, namely the articular, angular, prearticular and surangular (Figure 21). Right and left dentaries of podocnemidids are also fused. The dentaries of podocnemidids are relatively robust, particularly as the symphysis is posteriorly expanded along the ventral portion of the fused dentaries. This ventral symphyseal expansion, although observed in several turtle lineages (e.g., emydids; chelydrids), is strongest in podocnemidids among extant turtles. The expansion does not affect the triturating surface, which remains narrow around the symphysis so that the expansion forms a shelf of bone below the level of the triturating surfaces (Figure 21a,e). In *Peltocephalus dumerilianus*, the triturating surface remains relatively narrow posterior to the symphyseal area, although it becomes slightly medially expanded by a weak lingual shelf (Figure 21a). In *Podocnemis* spp., the triturating surfaces are much broader mediolaterally, which is caused by a more prominent medial overhang of the medial shelf (Figure 21e). The tip of the mandible forms an acute edge in *Peltocephalus dumerilianus*, which is notably upturned to a symphyseal hook (Figure 21a). In *Podocnemis* spp., the symphyseal outline is not acutely angled, but concavely curved, and the symphyseal margin is less strongly upcurved, so that a hooked symphyseal process is absent. Whereas in *Peltocephalus dumerilianus* the labial and lingual ridges are low, defining a gentle central groove trending along

FIGURE 21 3D renderings of mandibles of selected podocnemidids. (a–d) *Peltocephalus dumerilianus* (MCT RR 354). (e–h) *Podocnemis expansa* (ZMB 90084). (a and e) Dorsal view. (b and f) Left lateral view. (c and g) Close-up of articular surface. (d and h) Medial view onto left mandibular ramus. Note that bones are labeled in bold, and other features in normal font. ac, articular condyle; acc, accessory ridge; add, adductor fossa; an, angular; art, articular; asp, anterior surangular process; avcp, anteroventral coronoid process; cof, coronoid foramen; cor, coronoid; corp, coronoid process; den, dentary; fai, foramen alveolare inferius; fat, foramen auriculotemporalis; fM, fossa Meckelii; lab, labial ridge; ldr, lateral dentary ridge; lin, lingual ridge; lins, lingual shelf; maf, medial articular fossa; pctf, posterior chorda tympani foramen; pre, prearticular; prf, prearticular foramen; rim, rim circumscribing articular condyle; secf, ectocondyle flange of the surangular; sur, surangular; syg, symphyseal groove; syh, symphyseal hook; vss, ventral symphyseal shelf

the dentary ramus (Figure 21a), the respective surfaces have a more complex geometry in *Podocnemis* spp. The labial ridge is dorsally relatively high and sharp-edged. In the medial third of the triturating surface, the species of *Podocnemis* have a dorsally raised area. This area trends along the entire lingual side of the dentary, and is dorsally grooved. As a consequence, the medial and lateral margins of the raised area form prominent accessory and lingual ridges, respectively (Figure 21e). The raised areas of the left and right dentary rami do not meet anteriorly at the symphysis, but converge to one another leaving a central, anteroposterior symphyseal groove (Figure 21e). The lateral surface of the dentary is covered by a dense network of neurovascular foramina in podocnemidids. The adductor fossa is entirely limited to the surangular, and the foramen dentofaciale majus is positioned anterior to the margin of the adductor fossa (Figure 21f). Our specimen of *Peltocephalus dumerilianus* has two foramina dentofaciale majus (Figure 21b), and in *Podocnemis* spp. the number varies as we observed either a single or two foramina.

The surangular is fused with the articular, angular and prearticular in podocnemidids, but the main surangular features can still be described. The anterodorsal process of the surangular is prominent in podocnemidids. In most turtles, this process forms the lateral wall to the dorsal foramen of the fossa Meckelii and contacts the anteriorly adjacent dentary and coronoid posterior to the level of the coronoid process. In both *Peltocephalus dumerilianus* and *Podocnemis* spp., the anterodorsal end of the surangular is expanded and included into the coronoid process (Figure 21). In some specimens of *Podocnemis expansa*, the surangular even forms the dorsally highest point of the coronoid process. In addition, the surangular contacts the prearticular in the anterior margin of the dorsal foramen to the fossa Meckelii in all podocnemidids, thus excluding the coronoid from the opening (Figure 21a,e). This is unusual for turtles, but also present in pelomedusids (see below), and may thus be a pelomedusoid characteristic. The lateral surface of the dentary bears a moderately recessed adductor fossa in *Podocnemis* spp., which is ventrally bound by a marked edge (Figure 21f). Most specimens of *Podocnemis* spp. have unusual foramina along the adductor fossa surface, which internally lead into the auriculotemporal canal, although in some other specimens, these are only developed as grooves along the external surangular surface. The main auriculotemporal openings are located in their usual position anteroventrally from the jaw articulation on the lateral surangular surface (Figure 21f). In *Podocnemis* spp., usually two foramina are present, but these can be positioned within a deeper fossa. The posterior of the two auriculotemporal foramina also communicates with the chorda tympani canal system located at the medial side of the jaw (see prearticular). In *Peltocephalus dumerilianus*, the adductor fossa on the other hand is very shallow and inconspicuous (Figure 21b), and accessory auriculotemporal canals are absent. Dorsal surangular foramina are absent in all podocnemidids. *Peltocephalus dumerilianus* can be distinguished from *Podocnemis* spp. in the mode of articulation between the dentary and surangular: *Podocnemis* spp. has an anterior surangular process that inserts deeply anteriorly into the lateral surface of the dentary (Figure 21f), similar to the condition of chelonioids (see above). This anterior process is absent in *Peltocephalus dumerilianus*, and instead the surangular and dentary form a curved suture line (Figure 21b).

The coronoid of podocnemidids is a relatively large but dorsoventrally shallow bone. The coronoid process is not uniquely formed by the coronoid; instead, the dentary, surangular and coronoid all contribute to a mediolaterally broad and anteroposteriorly stretched surface to which the coronar aponeurosis attaches (Figure 21a,e). The coronoid forms a shallowly raised surface medially, but this surface is often dorsally lower than the surangular part of the coronoid process. Posteriorly, the coronoid is excluded from contributing to the foramen into the fossa Meckelii (Figure 21a,e). Anteromedially, it forms an elongated process that contributes to the triturating surface (Figure 21a,e), otherwise formed by the dentary. All examined specimens of *Podocnemis* spp. have a clearly developed coronoid foramen near the contact of the bone with the prearticular (Figure 21h; as well as a prearticular foramen, see below), but we could not confirm the presence of this foramen for *Peltocephalus dumerilianus*.

The prearticular of podocnemidids is fused with the articular, angular and surangular. Nonetheless, most prearticular features can be distinguished from those of neighboring bones. In podocnemidids, the prearticular seems to lack an anteroventral process that lies against the angular, as there is a deep bifurcation of the prearticular-angular region toward the foramen intermandibulare medius and Meckelian groove (Figure 21d, h). We interpret the dorsal ramus of this bifurcation to be the prearticular part of the fused bony element, and the ventral ramus the angular. In *Podocnemis unifilis*, a single posterior intermandibular foramen may be enclosed by the prearticular and angular rami, whereas intermandibular foramina are absent in the two specimens examined for *Podocnemis expansa* (Figure 21h). Near the contact with the coronoid, all examined species of *Podocnemis* also have a prearticular foramen (Figure 21h). Intermandibular and prearticular foramina seem to be absent in *Peltocephalus dumerilianus* (Figure 21b). In this species, the foramen alveolare inferius on the medial surface of the dentary is covered in medial view by the

prearticular, whereas the foramen remains exposed in *Podocnemis* spp. (Figure 21h). Posteriorly, the prearticular forms the medial margin to the foramen into the fossa Meckelii. The foramen, however, is limited to the anterior part of the mandibular region between jaw articulation and coronoid process in *Podocnemis* spp. (Figure 21e), and surangular and prearticular have an anteroposteriorly expanded contact between the posterior margin of the foramen and the jaw articulation. *Peltocephalus dumerilianus* instead has the more common morphology, in which the foramen into the fossa Meckelii stretches over nearly the entire space between the coronoid and the jaw articulation area (Figure 21a). Podocnemidids also share with other pleurodires a dorsally relatively low prearticular, which results in the surangular being visible in medial view, and the foramen into the fossa Meckelii being more medially positioned than is the case in cryptodires (Figure 21d,h). Siebenrock (1897) already made this observation for chelids, but our models clearly show that the same morphology can be seen in all pleurodires, including podocnemidids.

The angular is tightly fused to the other postcoronoid bones in podocnemidids. Its shape can nonetheless be inferred from the position of the foramen intermandibulare medius, and the Meckelian groove, as the angular usually forms the mandibular ramus below these structures. Based on this, the angular part of the postcoronoid bone complex can be said to be dorsoventrally relatively deep in all pelomedusoids, but particularly in podocnemidids.

The splenial is conceivably absent in podocnemidids, as the sulcus Meckelii is broadly exposed on the medial surface of the mandibular ramus.

The articular of podocnemidids is fused with the other postcoronoid bones. As all these elements converge together around the articular in turtles, it is more difficult to discern articular features from those usually formed by the other bones than it is for the surangular, angular, and prearticular. Thus, we describe the entire jaw articulation region of podocnemidids in this section, acknowledging that we cannot know for certainly how strongly other bones, particularly the prearticular, are integrated in this region. The articulation region of *Peltocephalus dumerilianus* varies from that of *Podocnemis* spp. in several features. In *Peltocephalus dumerilianus*, the articular surface is formed as in many cryptodires, with vaguely defined medial and lateral subfacets and an overall slightly concavely excavated contact area for the quadrate (Figure 21c). The surface is both medially and laterally expanded, so that is seems likely that at least the surangular is incorporated into the jaw articulation via an ectocondyle flange of the surangular that is fused with the articular. In *Podocnemis* spp., the articulation area forms a convexly rounded condyle (Figure 21g), which is the morphology that is commonly attributed to pleurodires more generally (Gaffney, 1979). The articular condyle is circumscribed by a rim of slightly thickened bone (Figure 21g) and is both medially and laterally expanded. The articular condyle of *Podocnemis* spp. is separated from the retroarticular process by a ventral step (Figure 21g). The retroarticular process is knob-like, and projects ventrally from the posterior end of the mandibular ramus (Figure 21g), and is not posteriorly expanded as in some other turtles (e.g., trionychids). The ventral and posteroventral surface of the retroarticular process is anteroposteriorly rounded and very smooth, and overall similar to the cartilage capped jaw articulation surface. The retroarticular process of *Peltocephalus dumerilianus* is quite different from that of *Podocnemis* spp., and simply forms a small posteromedial lip that is slightly upturned (Figure 21c). Along the medial end of the mandibular ramus of all podocnemidids, the rims of the articular condyle and retroarticular process form a shelf that defines a medial articular fossa (Figure 21d,h). Within this fossa, both *Peltocephalus dumerilianus* and *Podocnemis* spp. have large chorda tympani foramina (Figure 21d,h), the canals of which extend anteriorly through the mandibular ramus and into the fossa Meckelii, sometimes also communicating internally with the auriculotemporal canal system.

3.5.13 | Pelomedusidae

Pelomedusids include two extant genera, the monospecific *Pelomedusa subrufa*, and the relatively speciose genus *Pelusios*. We herein sampled two pelomedusids, which were both fully segmented: *Pelomedusa subrufa* (FMNH 17161; Figure 22a–d) and *Pelusios sinuatus* (USNM 42144; Figure 22e–h).

The dentaries of pelomedusids are robust but mediolaterally narrow. The dentaries are fused in *Pelusios* spp., but they remain sutured in *Pelomedusa subrufa* even in adulthood (Siebenrock, 1897). The symphysis bears a pointed hook in *Pelomedusa subrufa* (Figure 22b). In *Pelusios sinuatus*, the dentary margin is also upturned around the symphysis, but the margin is well rounded so that a hook is absent. In *Pelusios sinuatus*, the lingual side is weakly expanded by a lingual shelf (Figure 22e), as in podocnemidids (see above). The lingual margin in this turtle, although forming a well-defined edge, is not dorsally raised so that a true lingual ridge is absent. However, there is an accessory ridge that traverses the triturating surface anteroposteriorly (Figure 22e). In *Pelomedusa subrufa*, the triturating surface is very narrow and bears relatively well-developed lingual and labial

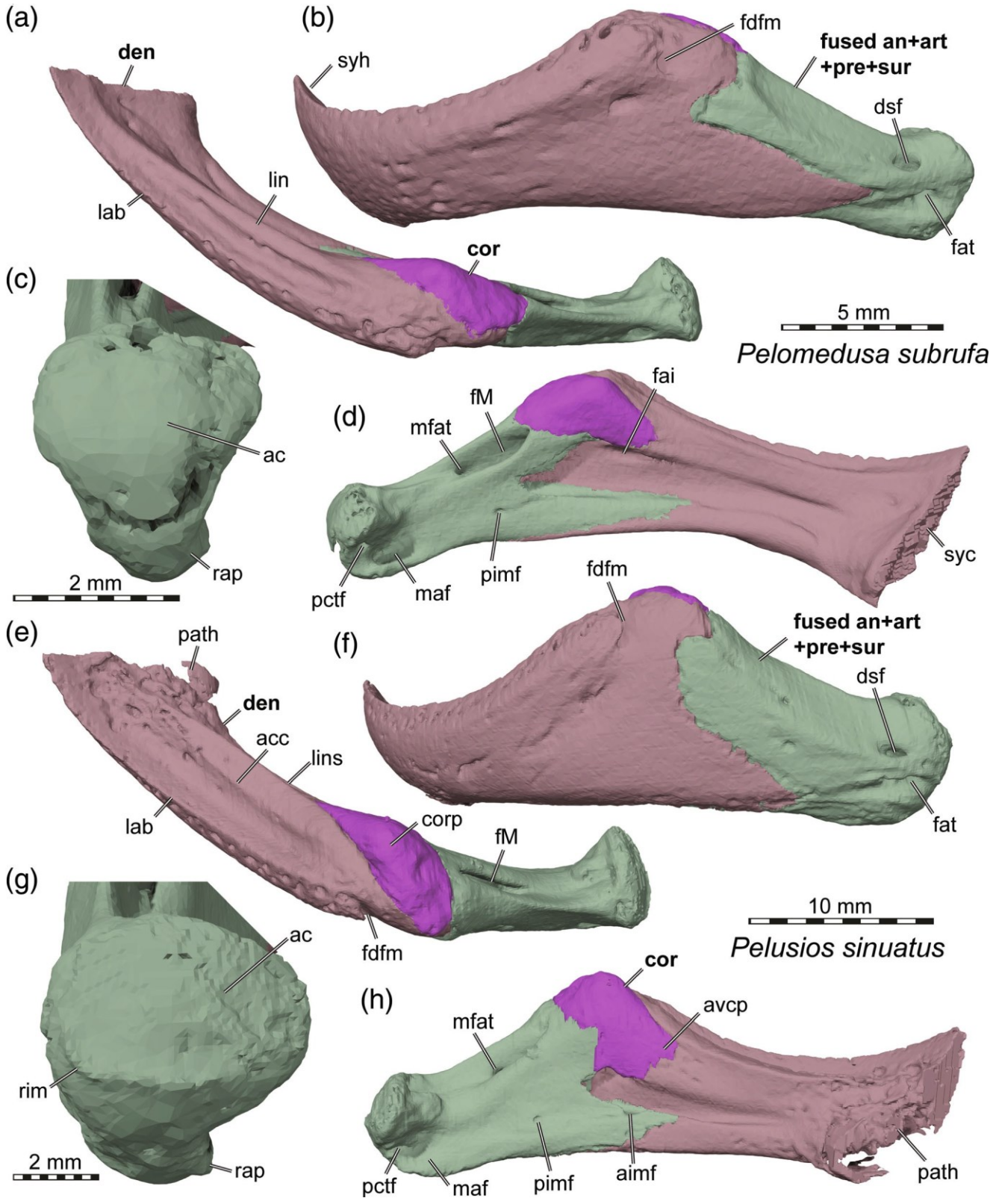

FIGURE 22 Legend on next page.

ridges (Figure 22a), the latter of which is also present in *Pelusios sinuatus*. The lateral dentary surface in the beak area has few neurovascular foramina in pelomedusids (Figure 22b,f). The foramen dentofaciale majus is formed as a single, relatively small opening in both examined pelomedusid species (Figure 22b,f). Adductor fossae are absent both on the dentary, and also the surangular. The dentary covers most of the coronoid in lateral view, but the latter bone remains the element with the highest dorsal extent. Posteroventrally, the dentary has a process that extends ventrally below the surangular.

The postcoronoid bones (surangular, angular, prearticular, articular) are fused in pelomedusids (Figure 22). Despite the fusion, many features typical of the unfused bones can be identified and compared with other species, including those that lack fusion. The surangular of pelomedusids is restricted to the region of mandible posterior to the coronoid (Figure 22b,f). This is a conspicuous difference to podocnemidids, in which the surangular extends into the coronoid process. As in all turtles, the surangular of pelomedusids forms the lateral wall of the foramen into the fossa Meckelii. The foramen that opens into this fossa is located more on the medial side of the mandible, as in other pleurodires (Figure 22d,h). A shared feature with podocnemidids is that the surangular and prearticular have a contact in the anterior margin of the foramen, thereby excluding the coronoid from contributing to the foramen (Figure 22a,e). The foramen into the fossa Meckelii is restricted to the anterior half of the mandibular ramus between the coronoid process and quadrate articulation. This is also the case in *Podocnemis* spp., but not in *Peltocephalus dumerilianus*, so that this feature may be a synapomorphy of pelomedusoids that was reversed in the *Peltocephalus* lineage. The lateral surface of the surangular of pelomedusids bears a very subtle ridge that defines an equally subtle adductor fossa (Figure 22b,f). Pelomedusids have a single foramen auriculotemporalis, which is anteriorly connected to the fossa Meckelii, and dorsally to a dorsal surangular foramen via a very short vertical surangular canal (Figure 22b,f). This is another difference to podocnemidids (and most chelids), in which a dorsal surangular foramen was not found.

The coronoid of pelomedusids is barely visible in lateral view, but prominent in medial view (Figure 22d,h). It forms a rounded coronoid process, which is slightly angled medially (Figure 22a,e). An anteroventral process is present in both examined species but more prominent in *Pelusios sinuatus* than in *Pelomedusa subrufa* (Figure 22d,h). Coronoid foramina are absent in pelomedusids.

In most turtles, the prearticular and angular form an elongate, anteroposteriorly trending suture, in which the intermandibular foramina are formed, when they are present. As these foramina are present in pelomedusids (Figure 22d,h), we use the position of the foramina to roughly distinguish the prearticular and angular parts of the fused postcoronoid bone complex. The angular and prearticular form a plate in the medial surface of the mandible of pelomedusids, and diverge anteriorly with a dorsal process that is formed by the prearticular, and a ventral process that is largely formed by the angular, but may incorporate an anteroventral process of the prearticular. In *Pelomedusa subrufa*, a posterior intermandibular foramen is encased just posterior to diverging processes, and an anterior intermandibular foramen is not formed (Figure 22d). Thus, we interpret that the ventral process of *Pelomedusa subrufa* corresponds entirely to a structure formed by the angular. In *Pelusios sinuatus*, the posterior intermandibular foramen is also present, but the angular and prearticular are expanded anteriorly. The anterior intermandibular foramen is formed as a dorsally open notch along the ventral process (Figure 22h), which we identify to be jointly formed by the angular and an anteroventral process of the prearticular in this species. Otherwise, it is noteworthy that the prearticular of pelomedusids contacts the surangular in the anterior margin of the foramen into the fossa Meckelii (Figure 22a,e).

The splenial is conceivably absent in pelomedusids, as the sulcus Meckelii is broadly exposed on the medial surface of the mandibular ramus.

The articular region of pelomedusids is very similar to that of *Podocnemis* spp.: The articulation surface toward the quadrate forms a hemispherical articular condyle, and a weak rim surrounds the condyle edge (Figure 22c,g). Ventrally, there is a rounded retroarticular process that is mediolaterally much more constricted than the articular condyle, which itself is expanded medially and

FIGURE 22 3D renderings of mandibles of selected pelomedusids. (a–d) *Pelomedusa subrufa* (FMNH 17161). (e–h) *Pelusios sinuatus* (USNM 42144). (a and e) Dorsal view. (b and f) Left lateral view. (c and g) Close-up of articular surface. (d and h) Medial view onto left mandibular ramus. Note that bones are labeled in bold, and other features in normal font. ac, articular condyle; acc, accessory ridge; aimf, anterior intermandibular foramen; an, angular; avcp, anteroventral process of the coronoid; cor, coronoid; corp, coronoid process; den, dentary; dsf, dorsal surangular foramen; fat, foramen auriculotemporalis; fM, fossa Meckelii; lab, labial ridge; lin, lingual ridge; lins, lingual shelf; maf, medial articular fossa; mfat, medial foramen auriculotemporalis; path, pathology; pctf, posterior chorda tympani foramen; pimf, posterior intermandibular foramen; rap, retroarticular process; rim, rim circumscribing articular condyle; syc, symphyseal contact facet; syh, symphyseal hook

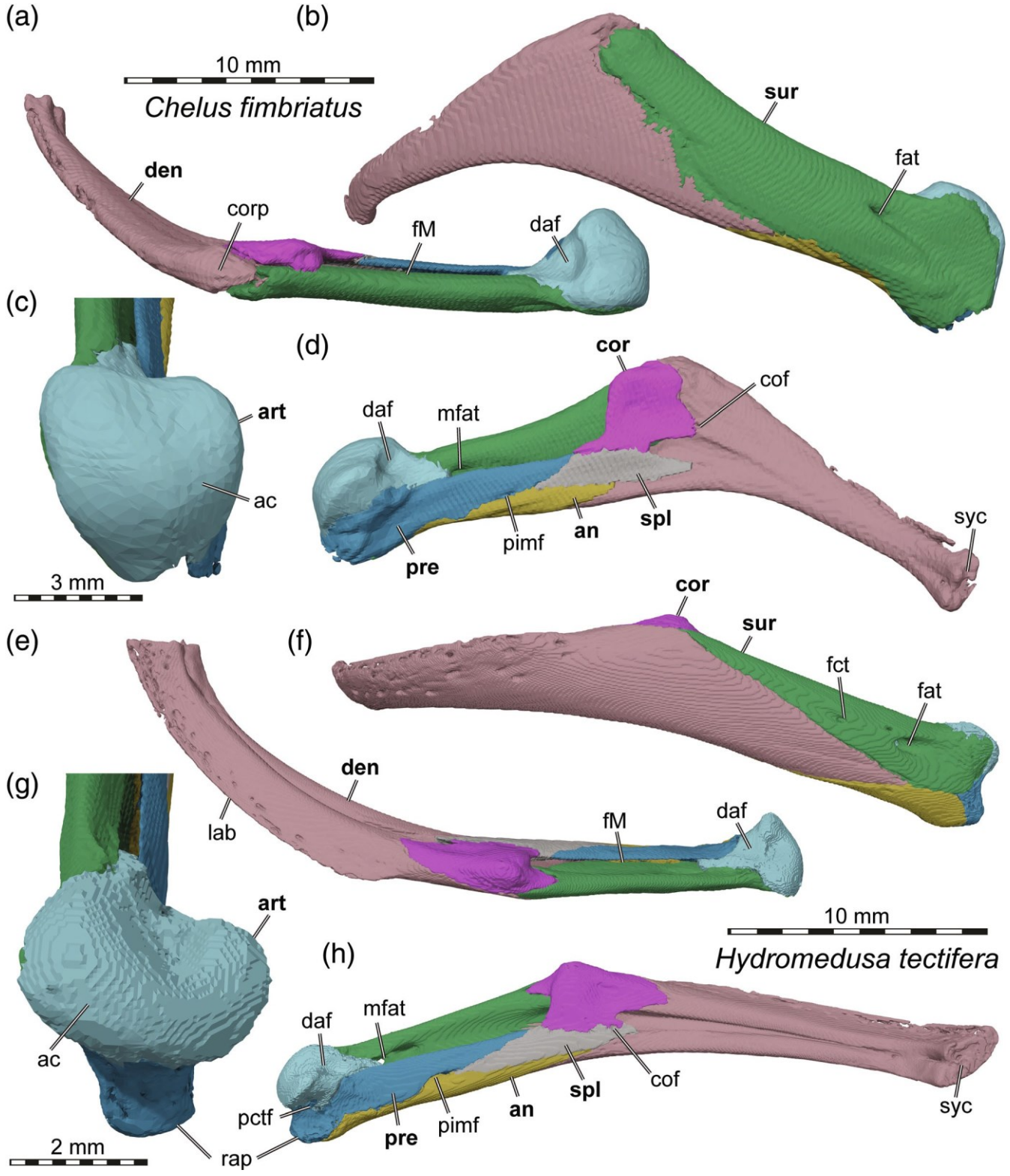

FIGURE 23 3D renderings of mandibles of selected South American chelids. (a–d) *Chelus fimbriatus* (UF herp 85199). (e–h) *Hydromedusa tectifera* (SMF 70500). (a and e) Dorsal view. (b and f) Left lateral view. (c and g) Close-up of articular surface. (d and h) Medial view onto left mandibular ramus. Note that bones are labeled in bold, and other features in normal font. ac, articular condyle; an, angular; art, articular; cof, coronoid foramen; cor, coronoid; corp, coronoid process; daf, dorsal articular fossa; den, dentary; fat, foramen auriculotemporalis; fM, fossa Meckelii; lab, labial ridge; mfat, medial foramen auriculotemporalis; pctf, posterior chorda tympani foramen; pimf, posterior intermandibular foramen; pre, prearticular; rap, retroarticular process; spl, splenial; sur, surangular; syc, symphyseal contact facet

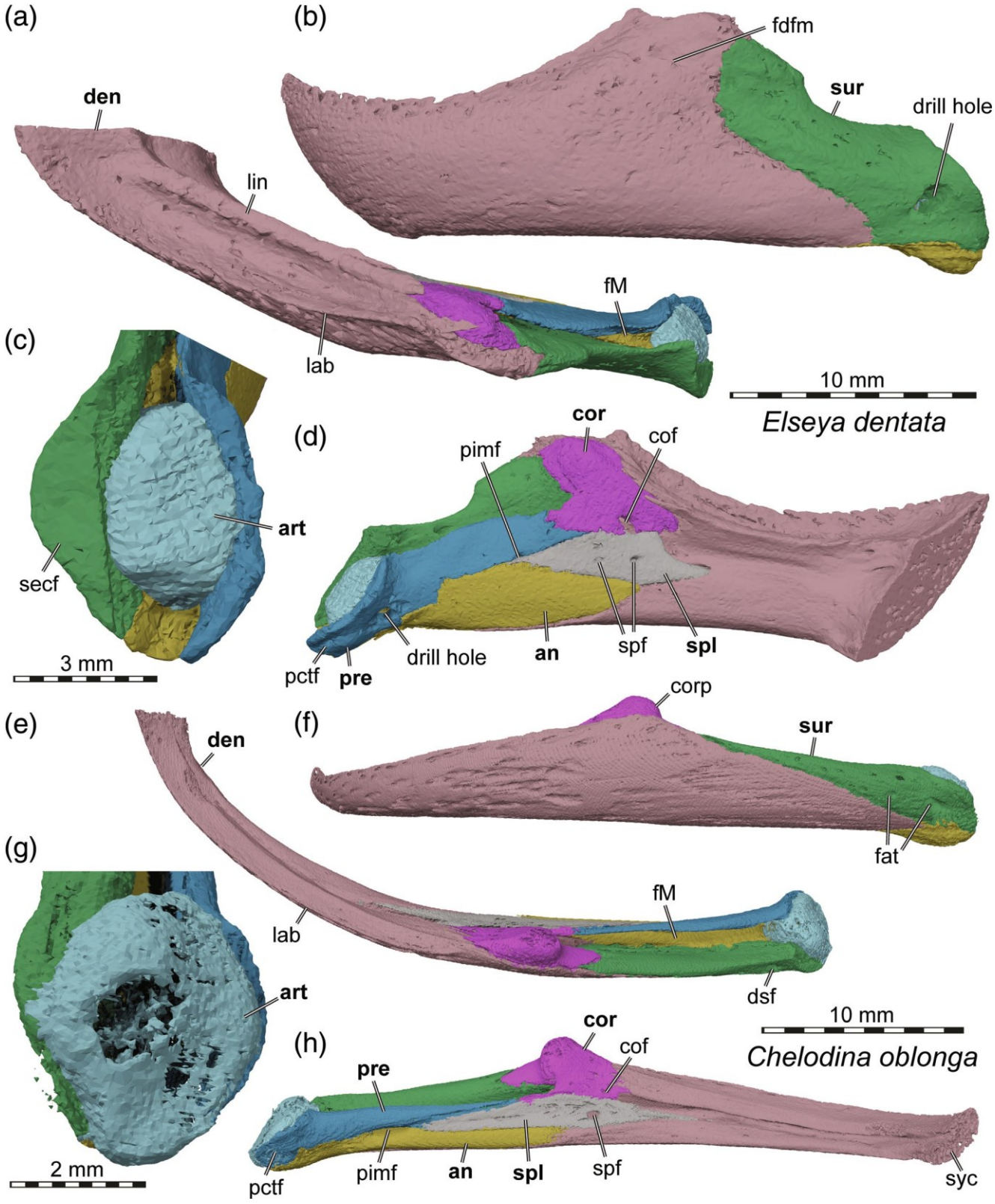

FIGURE 24 Legend on next page.

laterally (Figure 22c,g). On the medial surface of the mandible, a medial articular fossa is formed between the articular condyle and retroarticular process, which is posteriorly bound by a lamina connecting both aforementioned structures. Within the medial articular fossa, pelomedusids have a posterior chorda tympani foramen (Figure 22d,h).

3.5.14 | Chelidae

Chelids are a relative species-rich clade of pleurodires and can principally be divided into two biogeographically separated subclades, the Australasian and the South American chelids. South American chelids include the well-known, suction feeding mata mata turtle, *Chelus fimbriatus*, of which we have one specimen segmented in full (UFH 85199; Figure 23a–d). Additionally, we have a bone-by-bone segmentation of *Hydromedusa tectifera* (SMF 70500; Figure 23e–h), and a single mandibular model of *Phrynops hilarii* (NHMUK 91.3.16.1). For Australasian chelids, we sampled a snake-necked turtle, *Chelodina oblonga* (NHMUK 64.12.22; Figure 24e–h), and a specimen of *Elseya dentata* (NHMUK 76.5.19.77; Figure 24a–d), which has a more robust skull morphology.

The mandibles of chelids can easily be distinguished from other extant turtles by the presence of a splenial (e.g., Baur, 1895), and by the general presence of unfused mandibular symphyses (Baur, 1895; Siebenrock, 1897; but see *Elseya dentata* below). Unlike in pelomedusoids, the postcoronoid bones remain separate bony elements.

Dentary morphology varies relatively strongly among our sampled chelids, particularly between species with gracile mandibles and suction feeding habits (e.g., *Chelus fimbriatus*, *Chelodina oblonga*), and chelids with robust mandibles and oral food processing (e.g., *Elseya dentata*). In South American chelids and *Chelodina oblonga*, the dentaries are dorsoventrally low and mediolaterally narrow rami, which are strongly bowed medially (Figure 23). The symphyseal contact between right and left dentaries forms an unfused suture line. In *Phrynops hilarii*, the sutural contact is raised along the triturating surface, forming a symphyseal ridge that is absent in the other sampled chelids. In *Elseya dentata*, the symphysis is fused (Figure 24a,d). The triturating surfaces also vary strongly among chelid species. *Chelus fimbriatus* lacks a triturating surface and labial ridge altogether, and the dorsal surface of the dentary is simply a rounded ridge (Figure 23a). In *Hydromedusa tectifera* and *Chelodina oblonga*, the labial ridge is low but forms a sharp edge, and a narrow triturating surface slopes ventrally from the labial ridge toward the lingual side of the jaw (Figure 23e; Figure 24e). In *Phrynops hilarii*, the lingual side is expanded by a lingual shelf, so that the triturating surface is significantly broadened. *Elseya dentata*, on the other hand, has well-developed labial and lingual ridges, and a deep groove between them (Figure 24a). In South American chelids, the dentary is quite strongly ventrally angled with respect to the postcoronoid mandibular component. As a consequence, the symphyseal area lies ventrally deep below the level of the jaw articulation (Figure 23b,f). The lateral dentary surfaces of all chelids are only poorly vascularized, and the foramen dentofaciale majus is either completely reduced (i.e., *Chelus fimbriatus*, *Hydromedusa tectifera*), or only present as a very small foramen (*Phrynops hilarii*; *Elseya dentata*) or a series of small foramina (*Chelodina oblonga*) (Fig. 23a,b,f; Figure 24b,f). Adductor fossae are absent in chelids (Figure 23b,f; Figure 24b,f). The coronoid process is formed by the dentary in some chelids, particularly in *Chelus fimbriatus* (Figure 23a,b), but also at least partially in *Elseya dentata* (Figure 24a,b).

The surangular of chelids is involved in the formation of the same structures as in other turtles, but its morphology can be quite derived in gracile-jawed chelids. Chelids lack a medial surangular lamina. In contrast to the pelomedusoid condition, the foramen into the fossa Meckelii is anteroposteriorly elongate and stretches across the entire length of the jaw between the coronoid process and the mandibular articulation (Figure 23a,e; Figure 24a,e). In Australasian chelids, the surangular extends posterolaterally into the mandibular articulation surfaces (Figure 24c,g). In *Elseya dentata*, this is achieved via a laterally projecting ectocondyle flange of the surangular (Figure 24c). A true ectocondyle flange is absent in *Chelodina oblonga*, but the surangular nevertheless forms the lateral margin of the articular surface in this turtle. This contrasts with South American chelids, in all of which the surangular is clearly excluded from the articular surface margin, and limited to

FIGURE 24 3D renderings of mandibles of selected Australasian chelids. (a–d) *Elseya dentata* (NHMUK 76.5.19.77). (e–h) *Chelodina oblonga* (NHMUK 64.12.22). (a and e) Dorsal view. (b and f) Left lateral view. (c and g) Close-up of articular surface. (d and h) Medial view onto left mandibular ramus. Note that bones are labeled in bold, and other features in normal font. an, angular; art, articular; cof, coronoid foramen; cor, coronoid; corp, coronoid process; den, dentary; dsf, dorsal surangular foramen; fat, foramen auriculotemporalis; fdfm, foramen dentofaciale majus; fM, fossa Meckelii; lab, labial ridge; lin, lingual ridge; pctf, posterior chorda tympani foramen; pimf, posterior intermandibular foramen; pre, prearticular; secf, ectocondyle flange of the surangular; spf, splenial foramen; spl, splenial; sur, surangular; syc, symphyseal contact facet

mandibular parts ventrally and laterally to the articular region (Figure 23c,g). Otherwise, the surangular in chelids forms the foramen auriculotemporalis, which in most species is formed as a single foramen. A dorsal surangular foramen is absent among our sampled chelids, with the exception of *Chelodina oblonga* (Figure 24e).

The coronoid varies in shape among chelids. In the Australasian chelids, it is low and forms only the medial part of the coronoid process in *Elseya dentata* (Figure 24a,d), but forms a dorsally well-rounded tubercle in *Chelodina oblonga* (Figure 24f,h). Among South American chelids, the coronoid is lower than the dentary in the coronoid process region in *Chelus fimbriatus* (Figure 23b), but forms a rounded though only slightly dorsally projecting process in *Phrynops hilarii* and *Hydromedusa tectifera* (Figure 23f). A coronoid foramen is present in all chelids, although it is small in *Chelus fimbriatus*, *Hydromedusa tectifera* and *Chelodina oblonga* (Figure 23d,h; Figure 24h). In *Elseya dentata* (Figure 24d) and *Phrynops hilarii*, the foramen is prominent and situated in the suture with the splenial. In taxa with relatively gracile mandibles (i.e., *Chelus fimbriatus*, *Hydromedusa tectifera*, *Chelodina oblonga*, *Phrynops hilarii*), the prearticular-coronoid contact is strongly reduced to a point contact along the medial margin of the foramen into the fossa Meckelii (Figure 23d,h; Figure 24h). In *Elseya dentata* with its dorsoventrally deep mandibular ramus, the contact is of the more typical, extended type (Figure 24d).

As is generally the case in pleurodires, chelids have a dorsoventrally low prearticular (except in *Elseya dentata*; Figure 24d), which results in a medially exposed surangular and dorsomedially (rather than dorsally) directed opening into the fossa Meckelii (Figure 23d,h; Figure 24h; Siebenrock, 1897). The prearticular of chelids has an anterodorsal process that forms the dorsal part of the bifurcated plate that the prearticular and angular usually form in the medial mandibular surfaces. In chelids, the space between the prearticular and angular is filled by the splenial. All chelids have a posterior intermandibular foramen formed at the prearticular-angular contact, just posterior to the triple junction with the splenial (Figure 23d,h; Figure 24d,h). Prearticular foramina are absent in chelids. In Australasian chelids, the prearticular contributes to the margin of the articulation surfaces of the mandible, and frames the articular from medially (Figure 24c,g). At the posterior end, the prearticular of Australasian chelids bears a well-developed chorda tympani foramen (Figure 24d,h), which projects anteriorly and opens in the floor of the fossa Meckelii. Retroarticular processes are absent in Australasian chelids (Figure 24c,g). We found chorda tympani foramina in similar places in South American chelids, but their posterior end of the prearticular is otherwise quite different from those of their Australasian relatives. In South American chelids, the prearticular is excluded from the articulation surfaces of the mandible (Figure 23c,g). Posteroventrally to the articular condyle, the prearticular forms a knob-like retroarticular process that is similar in shape to the respective structure in podocnemidids (Figure 23c,g). Although not as strongly defined as in podocnemidids, South American chelids also have a medial articular fossa on the medial surface of the retroarticular process, in which the chorda tympani foramen is located (Figure 23d,h).

The angular of chelids lacks distinct features. As in most turtles, it encases the posterior intermandibular foramen with the prearticular, but an anterior intermandibular foramen is absent. The posterior end of the angular is relatively broad mediolaterally in chelids, forming a ventral buttress for the articular. Anteriorly, the bone becomes quite thin and underlays the prearticular and splenial in the medial wall of the fossa Meckelii.

The splenial is uniquely ossified in chelids among extant turtles. It is part of the medial mandibular plate that forms the medial wall to the fossa Meckelii. The bone has the same contacts in all examined species: Anterodorsally with the coronoid, posterodorsally with the prearticular, posteroventrally with the angular, and anteroventrally with the dentary (Figure 23d,h; Figure 24d,h). In Australasian chelids, we found a large and well-defined splenial foramen in the anterior half of the bone, opening between the fossa Meckelii and the intermandibular space. In *Elseya dentata*, an additional, smaller foramen is present posterior to the "main" splenial foramen (Figure 24d). Among South American chelids, we only found a splenial foramen in *Phrynops hilarii*, but not in *Chelus fimbriatus* or *Hydromedusa tectifera* (Figure 23d,h).

The articular differs in morphology between South American and Australasian chelids. In the former, the articular is the only component bone of the mandibular articulation surface, and forms a strongly convex condyle (Figure 23c,g). The exact condyle shape varies among species: In *Chelus fimbriatus*, the condyle is longer anteroposteriorly than it is mediolaterally wide (Figure 23c), whereas the opposite can be observed for *Phrynops hilarii* and *Hydromedusa tectifera* (Figure 23g). A distinct rim circumscribing the articular surface as in podocnemidids is absent. South American chelids have a small concavity, herein termed dorsal articular fossa, which is positioned anterior to the articular condyle, on a short process of the articular that contacts the surangular and prearticular (Figure 23a,e). The articular of South American chelids does not contribute to the retroarticular process, which is formed by the prearticular alone (Figure 23d,h). Australasian chelids lack the distinct condylar shape of the articular surface. Instead, the articular is wedged between the surangular and prearticular, which both minorly contribute to the formation of the articular surface (Figure 24c,g).

4 | DISCUSSION

4.1 | Osteological characters and their optimization

Our osteological descriptions above document the variation in mandibular anatomy for extant turtles. In this section, we synthesize our observations into discrete osteological characters, as described in the methods. Characters denoted by an asterisk (*) are multistate characters (for which we propose that the states form a morphocline that we treat as ordered). The characters are not figured, as all relevant variation is depicted in the clade specific figures shown in the descriptive section. Although we modeled the characters as phylogenetic characters, they could also be used for other purposes than reconstructing phylogeny, particularly to calculate rates of morphological evolution or to assess mandibular disparity.

Character 1 (Gaffney, 1977: ch. 24; Shaffer et al., 1997: ch. 50). *Dentaries*, *medial contact of right and left dentary rami*: 0 = fused; 1 = the mandibular rami are sutured to one another.

Remarks: See Figures 23 and 24e–h for examples of State 1, and other osteological figures for State 0. The dentaries of turtles are generally fused at the symphysis, even in Triassic testudinatans such as *Proganochelys quenstedtii* (Gaffney, 1990). Inter-dentary sutures fuse during the embryological development of turtles (see also Rathke, 1848), for example, during Stage 20 in *Apalone spinifera* (Sheil, 2003), during Stage 22 in *Chelydra serpentina* (Sheil & Greenbaum, 2005), and during Stage 24 in *Macrochelys temminckii* (Sheil, 2005). The images provided for *Sternotherus odoratus* by Smith Paredes et al. (2021) imply that fusion is completed during Stage 22 in that taxon. Although dentary-dentary fusion is thus the generally observed state among turtles, chelids form an exception, and the left and right dentaries are only joined along a sutured symphysis, with the exception of *Elseya dentata*, in which the dentaries are fused.

As our sample includes only one other Australasian chelid besides *Elseya dentata* (i.e., *Chelodina oblonga*), a loss of fusion at the node for Chelidae and a reversal to fused dentaries in *Elseya dentata* (ACCTRAN) is equally parsimonious as two losses of fusion (in South American chelids, and *Chelodina oblonga*; DELTRAN). As the dentaries in other, herein unsampled Australasian chelids, are also unfused (e.g., *Myuchelys latisternum*: Baur, 1895; *Emydura subglobosa*: Werneburg, 2011), we favor the ACCTRAN solution that implies that the loss of fusion is a chelid synapomorphy which becomes reversed in the lineage of *Elseya dentata*. Outside of Chelidae, unfused dentaries retained in adulthood are furthermore known in *Pelomedusa subrufa* (e.g., Siebenrock, 1897), but not in its sister taxon *Pelusios*. This results in a consistency index of CI = 0.333 for this character.

Character 2 (NEW). *Dentary*, *dorsally ascending process of the dentary along the anterior margin of the coronoid process*: 0 = absent; 1 = present.

Remarks: See Figures 4–7 for examples of state 1, and other osteological figures for state 0. This character encodes variation regarding the contact of the dentary and coronoid along their anterodorsal suture. Specifically, trionychians have an unusual dorsal process of the dentary that ascends along the anterior margin of the triturating surface, and the character state is returned as an unambiguous and unique synapomorphy of Trionychia (CI = 1).

Character 3 (modified from Hirayama, 1998: ch. 39). *Dentary*, *width of triturating surface vs. jaw length*: 0 = narrow triturating surface (measured at symphysis), less than 1/3 of jaw length; 1 = broad triturating surface at symphysis, ≥1/3 jaw length.

Remarks: See Figure 11 for examples of both states in the same clade, with *Cuora flavomarginata* (Figure 11a) illustrating State 0 and *Batagur baska* (Figure 11e) illustrating state 1. This character encodes variation that is likely related to ecology. It is not intended to measure the dorsoventral depth of the jaw at the symphysis, but the anteroposterior extension of the triturating surface at the symphysis of the mandibular rami. Although triturating surface width can vary somewhat along the mandibular ramus, the symphysis is an easy landmark along which the triturating surface width can be measured. Additionally, more posteriorly located, medial expansions of the triturating surface are encoded in a separate character here (Character 8, below). As ecological traits can evolve along phylogenies, the character may have local phylogenetic signal, despite its obvious relation to diet. According to our optimization, the character is a local synapomorphy of Carettini, for instance, and has moderate homoplasy overall (CI = 0.2).

Character 4 (modified after Meylan, 1987: ch. 95). *Dentary*, *symphyseal ridge*: 0 = absent; 1 = present.

Remarks: See Figure 11a for an example of state 0, and Figure 17a for an example of character state 1. The presence of symphyseal ridges is highly homoplastic among turtles (CI = 0.125), but may nonetheless show local phylogenetic signal. For instance, *Dermatemys mawii* has a symphyseal ridge but kinosternids as the sister clade lack them. This feature may thus be insightful regarding the identification of stem members of *Dermatemys mawii*. Within cheloniids, the presence of a symphyseal ridge distinguished the *Chelonia mydas-Natator depressus* clade from other cheloniids.

Character 5 (modified after Hirayama, 1998: ch. 42). *Dentary*, *posterior end of symphysis with dorsally raised tubercle*: 0 = absent; 1 = present.

Remarks: An example of the derived character state 1 can be seen in Figure 15a. This character encodes

morphology that we only observed among cheloniids, of which all species but *Caretta caretta* have a pointed or blunt tubercle at the posterior end of the symphysis. Consequently, the character has low homoplasy (CI = 0.5). The absence of this structure in *Caretta caretta* is autapomorphic among extant cheloniids, but may help in future to identify fossil representatives of the *Caretta* lineage.

It is not entirely clear if the variation we encoded here was previously used in character concepts. Hirayama (1998: ch. 42) included a character that encoded the relative height of a symphyseal ridge that may dorsally protrude beyond the level of the labial margin in lateral view. According to our observation, this dorsally protruding "ridge" may be the same structure we identify as the dorsally raised tubercle, and thus we tentatively list Hirayama (1998) as the original source for this character.

*Character 6 (modified after Gaffney, 1975b: ch. 16; Gaffney, 1977: ch. 25; Hirayama, 1998: ch. 40). *Dentaries*, *hook development*: 0 = absent, labial margin is curved and low at symphyseal end; 1 = the anterior labial margin is upcurved, but not pointed; 2 = the anterior labial margin is upcurved, and forms a pointed symphyseal hook. *Ordered.

Remarks: See Figure 5 for examples of state 0, Figure 17 for an example of state 1, and Figure 20 for an example of state 2. We modified previous definitions and changed this to a multistate character to acknowledge finer levels of variation than was the case in the previous version of this character. The character is ordered as its states form a morphocline. We were relatively generous in our definition of the "hook," as we score all turtles with an upward pointed symphyseal tip as a hook, regardless of whether this tip is particularly long. Our optimization reveals that the character is strongly homoplastic (CI = 0.1), but it nonetheless has phylogenetic information on a low hierarchical level. For instance, chelydrids have a symphyseal hook.

Character 7 (NEW). *Dentary*, *labial ridge*: 0 = absent; 1 = present.

Remarks: See Figure 18 for variation in this character within a clade, with *Claudius angustatus* (Figure 18e–h) illustrating state 0 and *Staurotypus salvinii* (Figure 18a–d) illustrating state 1. The presence of a labial ridge is common but not ubiquitous in turtles. Here, we define a labial ridge as a dorsally protruding cutting edge of the labial margin of the triturating surface. Thus, turtles in which the labial margin is blunt are not interpreted as having a labial ridge, even if the triturating surface always forms an edge with the lateral mandibular surface, which is sloping ventrally from this intersection of surfaces. We are not aware of any previous studies which explicitly included characters about the potential absence of the labial ridge. As *Proganochelys quenstedtii* has a clearly developed labial ridge (Gaffney, 1990), the loss of the ridge is returned as synapomorphic for some larger clades (e.g., trionychians; chelids under ACCTRAN), but this also appears homoplastically in many species of other turtle lineages (CI = 0.083), such as kinosternids (e.g., *Claudius angustatus*) or geoemydids (e.g., *Malayemys subtrijuga*).

Character 8 (NEW). *Dentary*, *expansion of lingual margin*: 0 = absent; 1 = lingual margin is medially expanded to a shelf, which often is broader along the central part of the mandibular ramus than near the coronoid and symphyseal ends.

Remarks: See Figure 11 for examples of both states in the same clade, with *Cuora flavomarginata* (Figure 11a) illustrating state 0 and *Batagur baska* (Figure 11e) illustrating state 1. An example for the broad central part of the expansion can be seen in Figure 8a (*Testudo marginata*). This and the following character are coded to capture variation of the lingual triturating surface margin, which has so far mostly been captured in relatively simple characters that ask about the presence versus absence of a lingual ridge (e.g., Hirayama, 1998: ch. 43; see next character's remarks). In this first character, we distinguish between an unexpanded versus expanded lingual margin, and the topology of the lingual margin (sloped, edged, ridged) is encoded in a second character. The observations are independent from one another, as taxa exists that have combinations of an expanded lingual shelf with or without lingual ridges, and taxa without a lingual expansion and with or without a lingual ridge.

The optimization of this first character implies that lingual shelf expansions evolved repeatedly among turtles (CI = 0.083), which may be expected as variation in this feature is likely related to dietary adaptations. Nevertheless, some clades can be locally distinguished by the presence of an expanded shelf, such as Testudona among testudinids.

*Character 9 (modified after Hirayama, 1998: ch. 43). *Dentary*, *shape of lingual margin*: 0 = blunt, surface slopes medioventrally, no sharp edge or lingual ridge is formed; 1 = lingual margin has a sharp edge, but no dorsally protruding ridge; 2 = lingual margin has a sharp edged, dorsally protruding lingual ridge. *Ordered.

Remarks: Figure 10a,d shows an example of state 0, Figure 13 illustrates examples for state 1, and Figure 9 shows two turtles that are coded as having state 2. Independent of the relative expansion of the lingual margin, the topology of the lingual edge varies among turtles. Here, we distinguish three states that encode gradational differences which we treat as an ordered morphocline. Previous characters have often only used a presence versus absence state for the lingual ridge (e.g., Hirayama, 1998), but clear variation exists when a true ridge (i.e., a dorsally protruding lingual cutting edge) is not developed. Specifically, many turtles have a lingual margin that forms a "sharp edge" that is formed by the

intersection of the medial mandibular surface and the triturating surface. In cross-section, these surfaces meet approximately at a 90⁰ angle, thus forming an edge although a dorsally protruding cutting ridge is absent. In yet other turtles, the triturating surface slopes medioventrally. The edge it may form with the medial mandibular surfaces is much blunter and results from an intersection angle that is much higher than 90⁰. Our character optimization indicates that the lingual margin shows high evolvability (CI = 0.069), which might be expected given the ecological signal that can be expected among triturating surface structures.

Character 10 (NEW). *Dentary*, *lingual ridge extension*: 0 = extends along entire lingual dentary side until very shortly before the symphysis; 1 = limited to posterior two-thirds of triturating surface, with prominent anterior hiatus in ridge. This character is scored as inapplicable when the lingual margin has no developed ridge.

Remarks: Figure 8a shows the apomorphic character state 1. This state is only seen among testudonan testudinids and is thus returned as an unambiguous synapomorphy of Testudona. To our knowledge, this variation has not been coded in previous phylogenetic characters.

Character 11 (modified after Hirayama, 1985: ch. 44). *Dentary*, *accessory longitudinal ridge*: 0 = absent; 1 = present, accessory ridge trends anteroposteriorly, near-parallel to the labial and lingual jaw margins.

Remarks: Figures 11e, 15, 17, and 21e show turtles with the apomorphic character state 1. The presence of cranial accessory ridges is commonly used as a phylogenetic character in turtle studies, even if their presence is likely related to dietary specializations. We note that the presence of cranial accessory ridges does not warrant the presence of mandibular accessory ridges; specifically, many testudinids that have cranial accessory ridges lack them in the mandible (e.g., *Gopherus polyphemus*). Thus, we recommend not encoding the presence vs. absence of cranial and mandibular accessory ridges together in a single character, as sometimes done (e.g., Joyce & Bell, 2004: ch. 30). However, all turtle species in which we detected mandibular accessory ridges also seem to have cranial pendants. Given this distribution of accessory ridges, it may be useful to have two characters in studies that include cranial and mandibular information: One that asks for the presence versus absence of accessory ridges in general, and a second one that encodes whether these, if present, are limited to the cranium, or found in the cranium and mandible. Currently, the mandibular ridges are less frequently encoded as characters that the cranial ridges, but they can be found in several studies (e.g., Hirayama, 1985; Cadena et al., 2010). In our matrix, the character is optimized as highly homoplastic (CI = 0.0167), but local phylogenetic signal is apparent among geoemydids or podocnemidids.

Character 12 (NEW). *Dentary*, *oblique accessory ridge*: 0 = absent; 1 = present, ridge expands across dentary transversely, forming 90⁰ angles to the labial and lingual jaw margins.

Remarks: Examples of the apomorphic state 1 can be seen in Figures 11e and 17a. Oblique accessory ridges are rare among turtles, and in our taxon sample only occur in *Dermatemys mawii* and *Batagur baska*. Due to the isolated appearance of these ridges, the character currently does not convey phylogenetic information, but may be helpful to distinguish *Batagur*-lineage or *Dermatemys*-lineage stem members from other kinosternoids or geoemydids, respectively. We could not find any previous mention of a similar character, and thus declare it as a new character herein.

Character 13 (modified after Hirayama, 1985: chs. 41/43/44). *Dentary*, *serrations along triturating ridges*: 0 = absent; 1 = present.

Remarks: Character state 0 can be seen in most turtles (e.g., Figure 7), and character state 1 is exemplified in Figures 8f, 9, and 11f. Previous character versions encoding variation about the presence versus absence of serrations along the triturating ridges was usually restricted to the labial ridge. We expanded the definition to the triturating ridges more generally, as the serrations are usually present on all triturating ridges. Although serrated triturating ridges occur in several distinct turtle lineages and are likely related to dietary specializations, they are useful local synapomorphies. For example, among geoemydids, member of the *Batagur* + *Morenia* group have serrated ridges, including species not sampled here (e.g., *Pangshura tecta*: NHMUK 1889.2.6.1).

Character 14 (NEW). *Dentary rhamphotheca ridge*: 0 = absent; 1 = present.

Remarks: The apomorphic state 1 is illustrated in Figures 11f and 17b. The dentary rhamphotheca ridge is herein defined as a laterally bulged ridge on the dentary, which extends anteroposteriorly and parallels the labial margin. The ridge likely defines the ventral extend of the rhamphotheca, and the dentary surface above it is usually highly vascularized, while the surface below is smooth. Among our taxon sample, the dentary rhamphotheca ridge occurs autapomorphically in *Dermatemys mawii* and is additionally returned as a synapomorphy of the *Batagur*-clade. We are not aware of previous characters encoding variation related to this structure.

Character 15 (NEW). *Dentary*, *processus dentofacialis*: 0 = absent; 1 = present, formed as lateral spike at the posterior end of the triturating surface.

Remarks: Examples for the apomorphic state 1 can, for example, be seen in Figures 17a and 20. The processus dentofacialis has been noted for chelydrid turtles before (Młynarski, 1980), but this feature has, to our knowledge,

not been coded as a phylogenetic character before. Although the process is maybe most distinct in chelydrids, the process is also present outside of this clade. Our optimization returns the presence of the process as an unambiguous synapomorphy for Emydinae, in which the process is relatively small. The process further appears in Testudona, certain kinosternids, *Dermatemys mawii*, and some pelomedusoids.

*Character 16 (modified after Hirayama, 1985: ch. 47). *Dentary*, *foramen dentofaciale majus*: 0 = absent, foramen completely reduced; 1 = small, size of a small vessel; 2 = enlarged, foramen is several mm in diameter. *Ordered.

Remarks: The absent state can for example be seen in Figure 5e, whereas Figure 5b shows state 1. An enlarged foramen (state 2) can for example be seen in Figure 7. The size of the foramen dentofaciale majus varies among turtles and includes the complete reduction of the foramen, which is plesiomorphically present but small in *Proganochelys quenstedtii* (personal observation S.W.E.). Previous characters on the foramen dentofaciale majus encoded its relative size (Hirayama, 1985), but not its absence. Given that the foramen is plesiomorphically present in Testudinata (see above), paleontological prior knowledge tells us that the absence of the foramen is the result of a secondary reduction (i.e., zero size). Thus, it is justifiable to encode the "absence" observation together with different "presence" observations as a size morphocline. Among chelonioids, cheloniids share a large-sized foramen, whereas the foramen is completely reduced in *Dermochelys coriacea*. Complete reductions of the foramen otherwise occur in taxa with mandibles that show reduced robusticity, such as the trionychids *Chitra chitra* and *Cycloderma frenatum*, or the South American chelid *Chelus fimbriatus*. Conversely, large foramina are commonly observed in robust mandibles, such as cheloniids, *Dermatemys mawii*, geoemydids of the *Batagur*-clade, or *Carettochelys insculpta*.

Character 17 (NEW). *Dentary*, *foramen dentofaciale majus position*: 0 = within the anterior margin of the adductor fossa; 1 = clearly anteriorly removed from the adductor fossa. This character is scored as inapplicable when the foramen dentofaciale majus is absent.

Remarks: Variation in this feature is maybe best exemplified by emydids (Figure 13), as different species show character state 0 (*Terrapene coahuila*: Figure 13f) and state 1 (*Graptemys geographica*: Figure 13b). In most turtles, the foramen dentofaciale majus is located at the anterior margin of the adductor fossa, but the foramen may be placed in a more anterior position. Examples for this include chelonioids (with the exception of *Lepidochelys* spp.), Deirochelyinae, and pleurodires. Hutchison (2008: ch. 11) used the relative position of the foramen dentofaciale majus with regard to the coronoid process as a character within his chelydroid analysis. However, we cannot reproduce the character scores of this study, as the foramen dentofaciale majus always is level with or anterior to the coronoid process according to our observations, and never posterior to it. Thus, although Hutchison (2008) indeed used a character about the relative position of the foramen in question, his observations seem to encode variation that differs from the basis for our character here, so that we declare it as being new.

Character 18. (NEW). *Dentary*, *small posterior ramus extending dorsally above the foramen auriculotemporalis*, *thereby framing the foramen dorsally*, *anteriorly*, *and ventrally by the dentary*: 0 = absent; 1 = present.

Remarks: The apomorphic state 1 can be seen in Figures 11b, 13b, and 18b. This feature is variably present in emydids and geoemydids, and thus highly homoplastic (CI = 0.1). However, among kinosternids, it is ubiquitously present in kinosternines, but absent in staurotypines. Thus, this character is among those that can have local phylogenetic impact, even if it is relatively strongly homoplastic over the entire turtle tree. We note that some previous characters encoded a "highly interdigitated surangular-dentary suture" (e.g., Joyce & Bell, 2004: ch. 25), but this observation is separate from ours, and originally based on Crumly's (1982) observation of an elongated, anteriorly directed surangular process (see also Joyce & Bell, 2004), which we encode in a separate character (ch. 19 below) herein. Thus, the dentary framing of the foramen auriculotemporalis qualifies as a new character observation.

Character 19 (Crumly, 1982: ch. 12). *Surangular*, *anterior surangular process*: 0 = absent; 1 = present, process deeply expands into a posterior bifurcation of the dentary along the lateral surface of the mandible.

Remarks: The more common condition of state 1 can for example be seen in Figure 5, and state 1 is for example shown in Figures 8, 14, and 21f. The variation underlying this character was previously coded into a character that additionally made statements regarding the posterior extends of the dentary ventral to the surangular. Here, we modify the character to only contain information regarding the presence of an anterior process of the surangular, as the ventral length of the dentary varies independently from the absence versus presence of this process. The process is plesiomorphically present in *Proganochelys quenstedtii*, but absent in most crown turtles, with notable exceptions. For instance, the anterior surangular process is present among all extant chelonioids, and thus unites *Dermochelys coriacea* with cheloniids, despite the highly derived mandibular anatomy of the former. In addition, the presence of the process is a synapomorphy among the genus *Podocnemis* in our sample,

distinguishing it clearly from its sister taxon *Peltocephalus dumerilianus*. The process is also variably present among testudinids, as noted by Crumly (1982: ch. 12), who is the earliest source for a phylogenetic character encoding this variation. Despite its relatively high homoplasy (CI = 0.143), the character has strong local phylogenetic signal.

Character 20 (Evers & Benson, 2019: ch. 178). *Surangular, with anteromedial process forming a vertical lamina that projects anteriorly into fossa Meckelii*: 0 = absent; 1 = present.

Remarks: Character state 0 can be seen in Figure 9, and character state 1 is shown in Figure 14, but note that Evers and Benson (2019) also figured this character. This character is highly homoplastic (CI = 0.067), but only appears among cryptodires. Within cheloniids, the presence of the lamina is shared by all members of Carettini, showing that it can have local phylogenetic signal.

Character 21 (NEW). *Surangular-prearticular contact along the anterior margin of the dorsal opening into the fossa Meckelii, excluding the coronoid from the foramen*: 0 = absent, coronoid forms anterior margin; 1 = present.

Remarks: The apomorphic state 1 can be seen in Figures 21 and 22. In most turtles, the coronoid forms the anterior margin of the dorsal opening into the fossa Meckelii. In pelomedusoids, this is prohibited by an anterior contact of the surangular and prearticular. This character state is thus found to be a unique and unambiguous synapomorphy of Pelomedusoides (CI = 1). To our knowledge, this character has not been used previously.

Character 22 (modified after Meylan, 1987: ch. 97). *Dorsal surangular foramen*: 0 = absent; 1 = present.

Remarks: State 0 can be seen, for instance, in Figures 14 and 17, and state 1 can be seen, among others, in Figures 13 and 19. The dorsal surangular foramen is an opening on the dorsal side of the surangular, usually somewhat anterior to the jaw articulation area. The foramen communicates with the foramen auriculotemporalis via a vertical canal. The foramen is not identical to a foramen on the medial surface of the surangular, which connects the foramen auriculotemporalis with the fossa Meckelii. The dorsal surangular foramen is present in all emysternids that we sampled, and nearly all geoemydids (with the exception of *Morenia ocellata*). Depending on the optimization criterion used, the presence of the foramen is either returned as a synapomorphy of Testudinoidea (ACCTRAN, then reversed within testudinids in which the foramen is absent in all examined species), or as synapomorphies of Emysternia and Geoemydidae separately (DELTRAN). Paleontological evidence favors the former, as the stem-testudinoid *Mongolemys elegans* also has a dorsal surangular foramen (see plate 9, fig. 1c in Danilov, 2001). Outside of Testudinoidea, the foramen is present among kinosternids (with the exception of the staurotypines *Claudius angustatus*), but also various pleurodires (i.e., *Chelodina oblonga*, *Pelomedusa subrufa*), resulting in relatively high homoplasy (CI = 0.143). We never found the foramen in trionychids or chelonioids. The absence of the foramen in trionychids was already noted by Meylan (1987), which is the first phylogenetic study to include a character about the dorsal surangular foramen. However, Meylan (1987) considered the foramen to be only present in kinosternids.

Character 23 (NEW). *Adductor fossa ridge on coronoid*: 0 = coronoid without strong anterodorsal ridge on lateral side, even if adductor fossa extends onto coronoid; 1 = anterodorsal surface of coronoid has a strong ridge that forms the margin of the adductor fossa.

Remarks: The apomorphic state 1 can, for instance, be seen in Figure 7. In some turtles, the adductor fossa is particularly deeply developed and this can result in the coronoid forming a strong anterodorsal ridge. This ridge is present in *Carettochelys insculpta*. As this taxon is the only living species of the Carettochelyidae, it may be a useful feature in identifying fossil carettochelyids. In addition, the character unites geoemydids of the *Batagur* group, and is present in some emydids closely related to *Trachemys scripta*. The character has moderate homoplasy (CI = 0.2).

Character 24 (Evers & Benson, 2019: ch. 179). *Coronoid, anteromedial process*: 0 = absent; 1 = present.

Remarks: Character state 0 can be seen in Figure 10, whereas Figures 6 and 7 exemplify the condition scored as 1. This character was noted by Evers and Benson (2019) as a feature that is present among Jurassic marine turtles (thalassochelydians), but absent in chelonioid sea turtles (see also their figures). Here, we confirm the process is absent in chelonioids and also absent in geoemydids and most testudinids, whereas it is usually present in other groups. Due to several reversals within most turtle clades, the character is moderately homoplastic (CI = 0.2).

Character 25 (Evers & Benson, 2019: ch. 180). *Coronoid, contribution to triturating surface*: 0 = absent; 1 = present.

Remarks: State 0 is exemplified by most turtles (e.g., Figure 11a), and very clear contributions (state 1) can for example be seen in Figures 5, 11e, and 15. This character, although moderately homoplastic across our matrix (CI = 0.25), serves as local synapomorphies. For instance, the presence of a coronoid contribution to the triturating surface is an unambiguous synapomorphy for trionychids; distinguishes the species of *Podocnemis* from *Peltocephalus dumerilianus*; unites *Malayemys subtrijuga*, *Batagur baska*, and *Morenia ocellata* among the geoemydids according to our data; and is autapomorphically present in *Chelonia mydas*, which may in the future help to identify fossils on its stem lineage.

Character 26 (Evers & Benson, 2019: ch. 182). *Coronoid foramen*: 0 = absent; 1 = present, at anterior end, leading from fossa Meckelii into space between mandibular rami.

Remarks: A good example for the apomorphic State 1 is shown in Figure 21h (*Podocnemis expansa*), as the coronoid foramen is relatively large in this taxon and co-occurs with a prearticular foramen. Overall, the coronoid foramen is a structure that is relatively rarely observed among turtles. Evers and Benson (2019) first used the variable presence of the foramen as a phylogenetic character. The foramen, if present, is usually a small opening within the anteromedial part of the coronoid, and opens from the fossa Meckelii into the open space between the mandibular rami. Our optimization recovers the presence of the foramen as an unambiguous synapomorphy of Podocnemididae, as it is universally present among our sampled podocnemidids. The foramen also is a synapomorphy of Chelinae. Our optimization recovers the presence of the foramen as a DELTRAN synapomorphy for cheloniids or ACCTRAN synapomorphy for chelonioids. However, the DELTRAN optimization should be favored here, as the ACCTRAN optimization is a result of the inapplicability of the character to *Dermochelys coriacea*, which lacks a coronoid. Besides the aforementioned cases, the foramen appears in the trionychid *Cycloderma frenatum*, and several kinosternid species, resulting in relatively high homoplasy (CI = 0.125).

Character 27 (Evers & Benson, 2019: ch. 183). *Coronoid process*, *principally formed by*: 0 = coronoid; 1 = dentary; 2 = surangular. Not ordered.

Remarks: Most of the figures provide examples for State 0 (e.g., Figure 7). Character state 1 is documented in Figure 23a,b, and state 2 can be seen in Figures 16 and 21e–h. The coronoid process for the attachment of the coronar aponeurosis is usually formed by its namesake element, the coronoid. This is also the plesiomorphic condition in turtles (*Proganochelys quenstedtii*; see Gaffney, 1990). However, in some turtles, the coronoid process (i.e., the bony process that serves as the attachment site of the coronar aponeurosis) is instead formed by other bones. These changes have evolved repeatedly (CI = 0.4), but the formation of the process by the dentary is a local unambiguous synapomorphy for kinosternids.

Character 28 (modified after Hirayama, 1985: ch. 45). *Coronoid process*: 0 = relatively low, dorsally well rounded or flat; 1 = relatively high, process is dorsally or posterodorsally pointed.

Remarks: Variation for this character within a clade is illustrated in Figure 13, in which *Terrapene coahuila* indicates state 0 (Figure 13e–h), and *Graptemys geographica* state 1 (Figure 13a–d). Other clear examples for state 1 are seen in Figures 6 and 7. The coronoid process is relatively low and well-rounded dorsally in most turtles. However, in some turtles, the process becomes elongated and almost rod-like in some taxa, particularly in *Malayemys subtrijuga*. This character also unites trionychians as an unambiguous synapomorphy. Among emydids, the relatively high process forms a synapomorphy for the clade that includes *Graptemys geographica*, *Malaclemys terrapin*, and *Trachemys scripta*. It should be noted that the shape of the process is distinct in the aforementioned emydids from the more rod-like appearance of the process in *Malayemys subtrijuga* or many trionychids. However, the process is still high and posterodorsally pointed and has thus been scored the same here. High coronoid processes also occur among some kinosternids, so that the character overall has high homoplasy (CI = 0.2).

Character 29 (Evers & Benson, 2019: ch. 181). *Coronoid*, *notch on posterior margin of coronoid*: 0 = absent; 1 = present.

Remarks: The apomorphic character state 1 is illustrated in Figure 7. This character was coded by Evers and Benson (2019) to capture variation they found in thalassochelydian turtles, but these authors already scored certain extant turtles for state 1, acknowledging that the trait has a wider distribution. Here, we find the coronoid notch to be present as a synapomorphy for the species of *Apalone*, and for the clade that includes *Graptemys geographica*, *Malaclemys terrapin*, and *Trachemys scripta*. It also appears autapomorphically in several turtles, including some kinosternids, *Malayemys subtrijuga*, and *Carettochelys insculpta*, so that it has a low consistency index (CI = 0.2).

Character 30 (NEW). *Coronoid*, *posteromedial process of coronoid*: 0 = short or virtually absent; 1 = extends along the medial margin of the dorsal opening of the fossa Meckelii, partially or fully excluding the prearticular from forming its margin.

Remarks: Character state 0 can be seen in Figure 17, and state 1 is illustrated in Figure 11. In most turtles, the coronoid forms a bridging structure above the fossa Meckelii, contacting the surangular and prearticular with ventrally directed lateral and medial processes, respectively. These processes are usually short, and the surangular and prearticular form most of the walls of the fossa Meckelii. However, the posteromedial process of the coronoid that contacts the prearticular becomes elongated homoplastically in some turtles (CI = 0.1), to the point where it forms 50% or more of the length of the margin of the dorsal opening into the fossa Meckelii. This is a synapomorphy of cheloniids (optimized as DELTRAN because the character is inapplicable in the sister taxon *Dermochelys coriacea*), of Emydinae, and of the

Manouria + *Gopherus* clade. Additionally, the elongate process is found in non-*Rhinoclemmys*-group geoemydids (with the exception of *Cuora mouhotii*) and unites the species of *Kinosternon* to the exclusion of other kinosternids. Thus, despite its low consistency index, the character is very useful to distinguish subclades of turtles.

Character 31 (NEW). *Postcoronoid bones*: 0 = unfused; 1 = fused, the articular, surangular, prearticular, and angular form a single unit.

Remarks: Character state 1 can be seen Figures 21 and 22. Bone fusion can be tricky to evaluate in turtles, as some sutures, and particularly sutures of the articular with surrounding bones, can externally be nearly obliterated in ontogenetically old turtles. However, even the sutures of the articular with surrounding bones are generally visible in CT scans. True fusion of postcoronoid bones is, however, seen in pelomedusoids. In this pleurodiran lineage, the fusion of postcoronoid bones is already evident in ontogenetically young individuals, and even CT scans show no traces of internal sutures. Although this postcoronoid bone fusion is thus returned as an unambiguous (and unique; CI = 1) synapomorphy of extant pelomedusoids, it will be interesting to explore the evolution of this character on their stem lineages, as several turtles currently hypothesized to be stem pelomedusoids or stem podocnemidids seem to have unfused postcoronoid bones (e.g., Gaffney et al., 2006; Joyce, Rollot, et al., 2021).

Character 32 (NEW). *Prearticular-surangular contact at the posterior end of the fossa Meckelii*: 0 = absent, the dorsal opening to the fossa Meckelii remains posteriorly open toward the mandibular articulation surface or the articular extends anteriorly into the margin of the fossa; 1 = present, the dorsal opening to the fossa Meckelii is posteriorly closed by a surangular-prearticular contact.

Remarks: The variation underlying the character can see seen for a single clade in Figure 13, where *Graptemys geographica* (Figure 13a) illustrates state 0, whereas *Terrapene coahuila* (Figure 13e) provides an example for state 1. Although a posterior prearticular-surangular contact at the fossa Meckelii is highly variable among turtles (CI = 0.1), the presence of this contact serves as a local synapomorphy for pelomedusoids, for the sister species *Testudo marginata* and *Testudo graeca*, and among emydids for the clade that includes *Terrapene* spp., *Emys orbicularis*, and *Clemmys guttata*. The process is variably present in trionychids, in which optimization either requires several independent gains or losses, contributing to the high homoplasy.

Character 33 (NEW). *Subdivision of dorsal opening into the fossa Meckelii*: 0 = single opening; 1 = opening subdivided anteroposteriorly by a transverse contact of the prearticular and surangular.

Remarks: The only taxon currently known with a subdivision of the dorsal opening of the fossa Meckelii is *Cycloderma frenatum* (Gaffney, 1979) and can be seen in Figure 6a. Thus, the character is currently parsimony uninformative and an autapomorphy. However, trionychid phylogeny is poorly constrained for fossil members of the lineage. For this reason, we include the character, as the presence of a subdivided fossa Meckelii could be a good character to identify fossil *Cycloderma*-lineage members.

Character 34 (NEW). *Prearticular*, *exposure of foramen alveolare inferius in medial view*: 0 = absent, the foramen is covered by expansions of the prearticular and/or coronoid; 1 = present, the foramen can be seen in medial view.

Remarks: The concealed condition can be seen, for example, in Figures 12 and 13, whereas Figures 5–7 exemplify the condition scored in state 1. The foramen alveolare inferius is positioned within the medial surface of the dentary, and opens from the fossa Meckelii or Meckelian sulcus into the dentary. Depending on how far the fossa Meckelii is anteriorly closed by the prearticular and/or coronoid, the foramen may be openly visible or concealed in medial view. This character is fairly consistently absent or present among the subclades of turtles, but its optimization depends on the state of *Proganochelys quenstedtii* as an outgroup, which is currently unknown to us. Our optimization polarizes the foramen to be plesiomorphically visible, as it is exposed in trionychids (without exceptions), and most pelomedusoids (but *Pelusios sinuatus* and *Podocnemis unifilis*). Thus, the absence state (i.e., foramen concealed) is optimized as an unambiguous synapomorphy for chelids. All geoemydids and most emydids have a medially exposed foramen alveolare inferius so that its absence is optimized as an unambiguous synapomorphy of Testudinidae, in which we otherwise find two reversals (*Chelonoidis niger*, *Homopus areolatus*). The foramen is exposed in most kinosternids, all chelydrids, but becomes covered in all chelonioids. Overall, the character has high homoplasy (CI = 0.083).

Character 35 (modified after Gaffney et al., 2006: ch. 122). *Prearticular*, *anteroventral process below the Meckelian groove/foramen intermandibulare medius*: 0 = absent; 1 = present, prearticular has anterior bifurcation into a dorsal and a ventral ramus.

Remarks: The absent state is illustrated in Figures 5–7 and 14–15, whereas the present state (1) can be seen, for instance, in Figure 11. The prearticular of turtles has two principal shapes along its anterior end: It is either bifurcated into a dorsal and ventral process, which frame the foramen intermandibulare medius of the fossa Meckelii; or only the dorsal process is present. The absence

condition is the plesiomorphic state as indicated by *Proganochelys quenstedtii*, which is retained in most pleurodires and also trionychians. Among durocryptodires, the process is only absent in chelonioids (and autapomorphically in the kinosternid *Claudius angustatus*). Depending on the optimization criterion, the presence of the process is thus a durocryptodiran synapomorphy and its absence a synapomorphy of chelonioids (ACCTRAN), or its presence are independent synapomorphies among testudinoids and chelydroids (DELTRAN). This question can likely be solved in the future by sampling fossil stem members of Testudinoidea, Chelonioidea, and Chelydroidea.

We cite Gaffney et al. (2006: ch. 122) as a study that first encoded similar variation, albeit defined in a different context. The character of Gaffney et al. (2006) was phrased in terms of a long vs. short angular–prearticular contact, which may restrict ("close") the fossa Meckelii anteriorly when the contact is elongate. Essentially, the elongate condition can only be present when the anteroventral process of the prearticular is developed, and we prefer this conceptualization of the underlying variation.

Character 36 (modified from Shaffer et al., 1997: ch. 40). *Ventral prearticular-dentary contact*: 0 = absent; 1 = present. Note this character is scored as inapplicable when an anteroventral process of the prearticular is absent.

Remarks: Figure 11 shows variation of this character: In *Batagur baska*, state 0 is realized as the angular separates the prearticular and dentary (Figure 11h), whereas *Cuora flavomarginata* has this contact (Figure 11d). The prearticular and dentary may contact one another in two distinct places, which we distinguish herein as the dorsal or ventral contact. The dorsal contact occurs dorsally to the foramen intermandibularis medius (sensu Gaffney, 1972). The dorsal contact, if present, is positioned ventral to the coronoid, and may be prohibited by an anteroventral coronoid process. As this coronoid process is encoded in a character among the ones presented here, we do not encode variation of the dorsal prearticular-dentary contact separately, to avoid character dependence. The second, ventral prearticular-dentary contact that is relevant for this character may occur ventral to the foramen intermandibulare medius, and is usually present when the angular is reduced in size anteriorly. Assessment of this character is not possible when a ventral prearticular process is absent, and thus this character is scored as inapplicable when this is the case.

Among those taxa for which the character can be assessed, the presence of a ventral prearticular-dentary contact unites Testuguria, with three reversals within the clade (*Batagur baska*, *Kinixys erosa*, *Testudo marginata*), resulting in a consistency index of CI = 0.25.

We cite Shaffer et al. (1997: ch. 40) for the character origin, although the character definitions between their and our characters are quite distinct. Shaffer et al. (1997: ch. 40) had a multistate character that linked the absence of a splenial with a small or large prearticular, whereas their "large" prearticular state is described as excluding the angular for the Meckelian groove, which implies an elongate ventral prearticular process and a contact with the dentary. We adopted separate characters for these separate observations, but acknowledge that the underlying variation for this character was used previously (Shaffer et al., 1997).

Character 37 (modified after Vlachos & Rabi, 2018: ch. 68). *Anterior intermandibular foramen*: 0 = absent; 1 = present, fully or partially formed between the angular and prearticular along their anterior processes. Note that this character is scored as inapplicable when the anteroventral process of the prearticular is absent.

Remarks: The presence of the foramen (state 1) can be seen in Figure 19, and the incomplete presence (also state 1) can be seen in Figure 20. Similar to the previous character, this character can only be assessed if a ventral prearticular process is present. Among taxa for which this is true, the foramen is generally present. However, the foramen is lost in some individual turtle species homoplastically (CI = 0.1), and its loss is returned as an unambiguous synapomorphy of Emysternia (with zero reversals within the group). To our knowledge, Vlachos and Rabi (2018) are the first authors to include variation regarding the presence versus absence of this foramen as a phylogenetic character.

Character 38 (modified after Meylan, 1987: ch. 98). *Prearticular, presence of posterior or joint single intermandibular foramen*: 0 = absent; 1 = present.

Remarks: The relatively rare absent state can be seen in Figure 5h, whereas the presence state 1 can be seen, for instance, in Figure 5d. A large posterior intermandibular foramen is usually present among turtles (Gaffney, 1972, 1979). In our character definition, we acknowledge the possibility that the large posterior intermandibular foramen of some turtles may be the result of "fusion" of separate posterior and intermandibular foramina. This character concept allows to score the character whenever an intermandibular foramen is present. Among turtles, the foramen is repeatedly lost (CI = 0.111), particularly among trionychids (four of our six scored taxa), cheloniids (two of six scored taxa), and podocnemidids (two of three scored taxa). Because of this character state distribution, the optimizations for these three clades are ambiguous, but fossils could in the future show if the presence or absence of the foramen is the symplesiomorphic condition. Whereas Meylan (1987) stated that the foramen is always absent in trionychids, we found it in several species (*Amyda cartilaginea*, *Cyclo-derma frenatum*) and thus score it here as present.

However, we acknowledge the possibility that this character may show high intraspecific variation in clades such as trionychids, which seem to show an overall trend to the reduction of the foramen.

*Character 39 (NEW). *Prearticular*, *position of the posterior or joint single intermandibular foramen*:0 = fully within the prearticular; 1 = In the angular-prearticular suture; 2 = fully in the angular. *Ordered.

Remarks: State 0 can be seen in Figure 8, state 1 is seen among most turtles (e.g., Figure 12), and state 2 is illustrated in Figure 19. The presence of a single intermandibular foramen can result from the loss or unfinished ossification of the anterior intermandibular foramen, or a conjunction of anterior and posterior intermandibular foramina. In either case, the intermandibular foramen is homologous with the posterior intermandibular foramen, so that this character can be scored in turtles with one or two intermandibular foramina. Whereas the posterior intermandibular foramen is usually positioned within the suture of the angular and prearticular, the foramen can also slightly shift in position dorsally (to lie fully within the prearticular) or ventrally (fully in angular). Both positional variations are relatively rare and only occur in a few turtle species. Specifically, the posterior intermandibular foramen is located entirely within the prearticular in all three sampled species of the genus *Testudo*, rendering this an unambiguous synapomorphy of the genus. The condition also occurs autapomorphically in the testudinid *Gopherus polyphemus*, in the geoemydid *Rhinoclemmys rubida*, and the kinosternid *Kinosternon scorpioides*. The kinosternid *Sternotherus minor* is currently the only taxon, for which we observed that the foramen is entirely within the angular. The character has a consistency index of CI = 0.4.

Character 40 (NEW). *Prearticular foramen*: 0 = absent; 1 = present.

Remarks: The apomorphic character state 1 is illustrated, for instance, with Figure 19. The prearticular foramen is formed by the contacts of the anterior process of the prearticular with the dorsally adjacent bones (either the coronoid or the dentary), forming a mediolateral opening into the fossa Meckelii. Note this is not equivalent to the foramen intermandibulare medius, or the coronoid foramen. Although the character is highly homoplastic (CI = 0.067), the presence of the foramen occurs synapomorphically in the genus *Podocnemis* and in Emysternia. Within testudinids, the character is highly variable, and occurrences of the foramen are also seen among chelonioids, kinosternids, and trionychids.

Character 41 (NEW). *Prearticular-coronoid contact*: 0 = present and extensive, along the medial wall of the fossa Meckelii; 1 = strongly reduced to a point contact or entirely absent.

Remarks: The apomorphic reduction state 1 is illustrated in Figure 23. In most turtles, the prearticular has an extensive contact with the coronoid along its dorsal process. Variation to this condition is only found among chelids, in which the contact is strongly reduced, either to a point contact or even completely reduced so that the contact is absent altogether. The Australasian chelid *Elseya dentata*, however, has an extensive prearticular-coronoid, resulting in a consistency index of CI = 0.5 for the character. Given that we only sampled two Australasian chelids, this situation results in an ambiguous optimization among chelids: Under ACCTRAN, the reduced contact is a chelid synapomorphy and the extensive contact of *Elseya dentata* is a reversal. This is likely the correct optimization: The mandible of *Emydura macquarii* (NHMUK 26.8.26.5), an Australasian chelid which we did not sample as we had no CT data of it, shows that it also has the reduced contact. This makes it more likely that the condition of *Elseya dentata* is an autapomorphic reversal of this species, as optimized under ACCTRAN.

Character 42 (NEW). *Angular*, *posterior end*: 0 = the angular is posteriorly expanded, forming a transversely and dorsally concave laminar surface that buttresses the remaining posterior mandibular elements; 1 = the angular is posteriorly markedly unexpanded, and does not form a ventral cover to the remaining mandibular elements.

Remarks: The difference between these character states is maybe best illustrated in Figure 11, in which the angular of *Batagur baska* (state 0) is relatively prominent and broad, and thus visible in medial view (Figure 11h), and the angular of *Cuora flavomarginata* (Figure 11d) is strongly reduced (State 1). However, note that the medial exposure is not always indicative of state 1, as emydids, which all have the posteriorly reduced angular still have a relatively prominent medial exposure of the element (Figure 13). In most turtles, the angular is a dorsoventrally low plate of bone that is situated along the ventromedial surface of the posterior part of the jaw. Its posterior end is usually somewhat twisted to form the ventral floor of the posterior jaw end. However, the angular is reduced in size along its posterior end in several turtle clades. For example, the unexpanded state is optimized as an unambiguous synapomorphy of Emysternia, without any reversals within the clade. However, the character is more variable in other testudinoids: The unexpanded state is returned as an unambiguous synapomorphy of non-*Rhinoclemmys* geoemydids, but two reversals are observed (*Batagur baska*, *Cyclemys dentata*). The unexpanded angular also occurs in five of the 13 testudinid species we sampled. Within kinosternines, the genus *Kinosternon* can be differentiated from *Sternotherus* by a reduced angular. Overall, the character has a consistency index of CI = 0.1.

Character 43 (Dryden, 1988: ch. 34). *Splenial*: 0 = present; 1 = absent.

Remarks: See Figures 23 and 24 for illustrations of the splenial among extant turtles. Although the splenial is plesiomorphically present in turtles as known from the mandible of *Proganochelys quenstedtii* (Gaffney, 1990), the bone is absent in all extant turtles except for chelids. This character state distribution leads to an ambiguous optimization: Either, the splenial was independently lost twice (Pelomedusoides, Cryptodira, under DELTRAN), or the loss of the splenial is a synapomorphy of Testudines and its presence in chelids a reversal (ACCTRAN). This can potentially be explored in the future by investigating mandibles of stem pleurodires, stem chelids, and stem pelomedusoids. Overall, this character has low homoplasy (CI = 0.5).

Character 44 (NEW). *Splenial foramen*: 0 = absent; 1 = present. Note that this character is scored as inapplicable when a splenial is absent.

Remarks: The absence of the foramen (state 0) can be appreciated in Figure 23, whereas its presence (state 1) is illustrated in Figure 24. A splenial foramen can only be present in species with a splenial, so that the character is scored as inapplicable for most turtles in our sample. Within chelids, the presence of the foramen was observed for all sampled Australasian species, and character state 1 is thus returned as an unambiguous synapomorphy of the clade in our optimization. However, we also observed the foramen in the South American chelid *Phrynops hilarii*, resulting in a CI = 0.5.

Character 45 (NEW). *Articular/Prearticular*, *chorda tympani canals and foramina*: 0 = present, a canal extends from the periphery of the articular into the fossa Meckelii; 1 = absent, canal completely reduced.

Remarks: The absence of the foramen (state 1) can be appreciated in Figures 14 and 15. We note that the observation of the absence of a canal for the chorda tympani nerve does not necessarily mean that the nerve is not innervating the mandible. More likely, there is an external course of the nerve that leaves no osteological trace. Our observations and scorings imply that the absence of an endosseous course of the chorda tympani nerve is an unambiguous synapomorphy of Pelomedusoides and Chelonioidea, and additionally autapomorphically present in *Chelus fimbriatus*. As such, the observation is only moderately homoplastic (CI = 0.333), and can be locally informative. When present, the chorda tympani canal of the mandible can be in distinct topological positions, and this variation is encoded in a separate character (Character 46, below).

Character 46 (modified from Meylan, 1996: ch. 21). *Posterior chorda tympani foramen*: 0 = located within the articular notch on the posterior surface of the articular; 1 = located on the posteromedial jaw surface, usually on the prearticular or prearticular-articular contact. Note that this character is scored as inapplicable when a chorda tympani canal is completely absent.

Remarks: Figure 19 provides a good example of character state 0, whereas state 1 can, for example, be found in Figure 7. This character is similar to character 21 of Meylan (1996), who coded a character about whether the chorda tympani nerve is enclosed in the retroarticular process or not. Our character concept differs slightly, as we observe a specific alternative position for the course of the nerve, on top of the observation that the nerve may not be encased by bone at all (encoded in our Character 46 above).

In pleurodires and trionychids (except for *Cycloderma frenatum*), the chorda tympani foramen is located on the posteromedial jaw surface (state 1), which is optimized as the plesiomorphic condition given that the state of this character is unknown for *Proganochelys quenstedtii*. In testudinoids, this feature is quite variable, but chelydroids generally have the foramen positioned within the articular notch (with the exception of *Claudius angustatus*). This character state distribution results in overall high homoplasy and a CI = 0.1.

Character 47 (NEW). *Articular*, *dorsal articular fossa immediately anteriorly to mandibular articulation*: 0 = absent; 1 = present.

Remarks: This character is only present in South American chelids (Figure 23d,h), and thus optimized as a unique (CI = 1) and unambiguous synapomorphy of the clade.

Character 48 (modified from Meylan, 1987: ch. 99). *Prearticular-articular*, *posteroventral end*: 0 = without any retroarticular process; 1 = retroarticular process is formed as a relatively short, dorsally slightly recured lip of bone at the posteromedial end of the mandibular ramus; 2 = retroarticular process is formed as a posteroventral boss; 3 = retroarticular process is formed as a posteriorly elongate shelf, which exceeds the anteroposterior length of the articulation facet. Not ordered.

Remarks: Character state 0 can be seen, for instance, in Figure 8. State 1 is illustrated in Figure 11. The posteroventral boss-like condition can be seen in Figure 21g, and state 2 is best appreciated in Figures 5–7. The earliest phylogenetic character on the retroarticular process that we could find is from Meylan (1987: ch. 99), but this character only encoded variation regarding the elongated retroarticular process of trionychids. More variation was later added to characters pertaining to the retroarticular process (e.g., Gaffney et al., 2006. ch. 123). Our character states are similar to those of Cadena (2010: ch. 36), but we modified the character states so to have explicit anatomical descriptions of the conditions we interpret to represent separate character states.

Character 48 has a moderate consistency index (CI = 0.333), partially due to the high number of possible

character states. Overall, the distribution of states is relatively consistent among larger turtle clades. For instance, most pleurodires, including South American chelids, pelomedusids, and podocnemidids (with the exception of *Peltocephalus dumerilianus*) have state 2. All sampled Australasian chelids have state 0. All trionychids have state 3. Testudinoids have state 1, with the exception of Testudininae (all sampled nine species) and *Platysternon megacephalum*, which have state 0. Chelydrids and chelonioids have state 1. Only kinosternoids are relatively variable, with *Dermatemys mawii* having state 2, *Sternotherus minor* having state 1, *Claudius angustatus* having state 2 (otherwise only observed in pleurodires), and all other kinosternids having State 0.

Character 49 (modified from Dryden, 1988: ch. 33). *Articular*, *articulation surface for quadrate*: 0 = flat, concave, or biconcave; 1 = convex hemispheric condyle is formed.

Remarks: State 0 can be observed in most cryptodires, for example, Figure 14. state 1 can be seen, for example, in Figure 23. The observation underlying this character was first used by Dryden (1988) in a phylogenetic context. In her character version, she defined the difference by the presence vs. absence of a longitudinal ridge on the articular surface, which results in the biconcave shape that in our character is included in state 0. Dryden (1988) already noted that pleurodires have a hemispherical articulation surface, and we use this observation as the primary difference between the two states. Our state 0 essentially contains all non-convex articular surface shapes. It may be possible to further subdivide this variation, as not all non-hemispherical shaped articular surfaces always have a clearly developed biconcavity and ridge. However, we also note that the variation of this character does not fall as clearly along the pleurodire-cryptodire division as previously thought: Among cryptodires, *Claudius angustatus* has a hemispherical articular surface, and among podocnemidids, *Peltocephalus dumerilianus* has a biconcave articular surface. Our observations also show that in chelids, the hemispherical surface is only observed in South American species, whereas our two sampled Australasian chelids (i.e., *Elseya dentata*, *Chelodina oblonga*) have a flat or ridged articular surface, respectively. Thus, the character is more strongly homoplastic than originally thought (CI = 0.25), but may help to distinguish fossils belonging to the Australasian and South American chelid lineages.

*Character 50 (modified after Meylan, 1987: ch. 94). *Articulation facet*, *contribution of surangular*: 0 = absent, surangular completely retracted from articulation facet; 1 = surangular forms lateral margin of articulation facet, but without a flange; 2 = surangular forms prominent lateral ectocondyle flange, expanding the articulation surface laterally. *Ordered.

Remarks: Character state 0 can be seen in Figure 23, whereas state 1 is apparent from Figure 11, and state 2, among others, by Figure 7. Meylan (1987) coded a character about the relative size of the contribution of the surangular to the mandibular articulation surface. We find it difficult to assess percentages to the contribution, as the contact between surangular and articular is often not regular, and we therefore chose a different characterization of the underlying variation. Although the character has very high homoplasy (CI = 0.143), there are locally consistent patterns to the character state distribution. For example, all South American chelids lack any surangular contribution to the facet (state 0), whereas all trionychians and cheloniids have a prominent lateral ectocondyle flange of the surangular (state 2). Among non-chelonioid durocryptodires, the character shows most homoplasy.

Character 51 (NEW). *Articulation facet*, *contribution of prearticular*: 0 = absent, prearticular completely retracted from articulation facet; 1 = prearticular forms small medial portion of articulation facet.

Remarks: Figure 13 illustrates state 0, whereas Figures 7 and 14 are examples of state 1. Similar to the preceding character, this one has high homoplasy (CI = 0.1) but local phylogenetic signal. For instance, all emydine taxa have state 0, whereas deirochelyine emydids have state 1 (with the exception of *Graptemys geographica*). Within geoemydids, the *Batagur*-clade has state 0, whereas all other geoemydids sampled herein have state 1. Australasian chelids can be distinguished from their South American relatives (state 0) by having state 1. All trionychids lack a prearticular contribution (state 0), whereas it is present in *Carettochelys insculpta*.

4.2 | Implications for fossil identifications and phylogenetics

The main purpose of our study is the documentation of mandibular anatomy and variation for extant turtles. As such, we provide only a short discussion beyond the character remarks provided above, and our selection of statements below could certainly be extended in the future. We also acknowledge that our findings of character optimization or statements regarding diagnostic combinations of features at different clade levels must be further scrutinized by the addition of unsampled extant taxa and the addition of fossils. Intraspecific variation is also a topic that we addressed only minimally, primarily as the systematic study of 70 turtle species already was a large task. We hope that this work can stipulate further

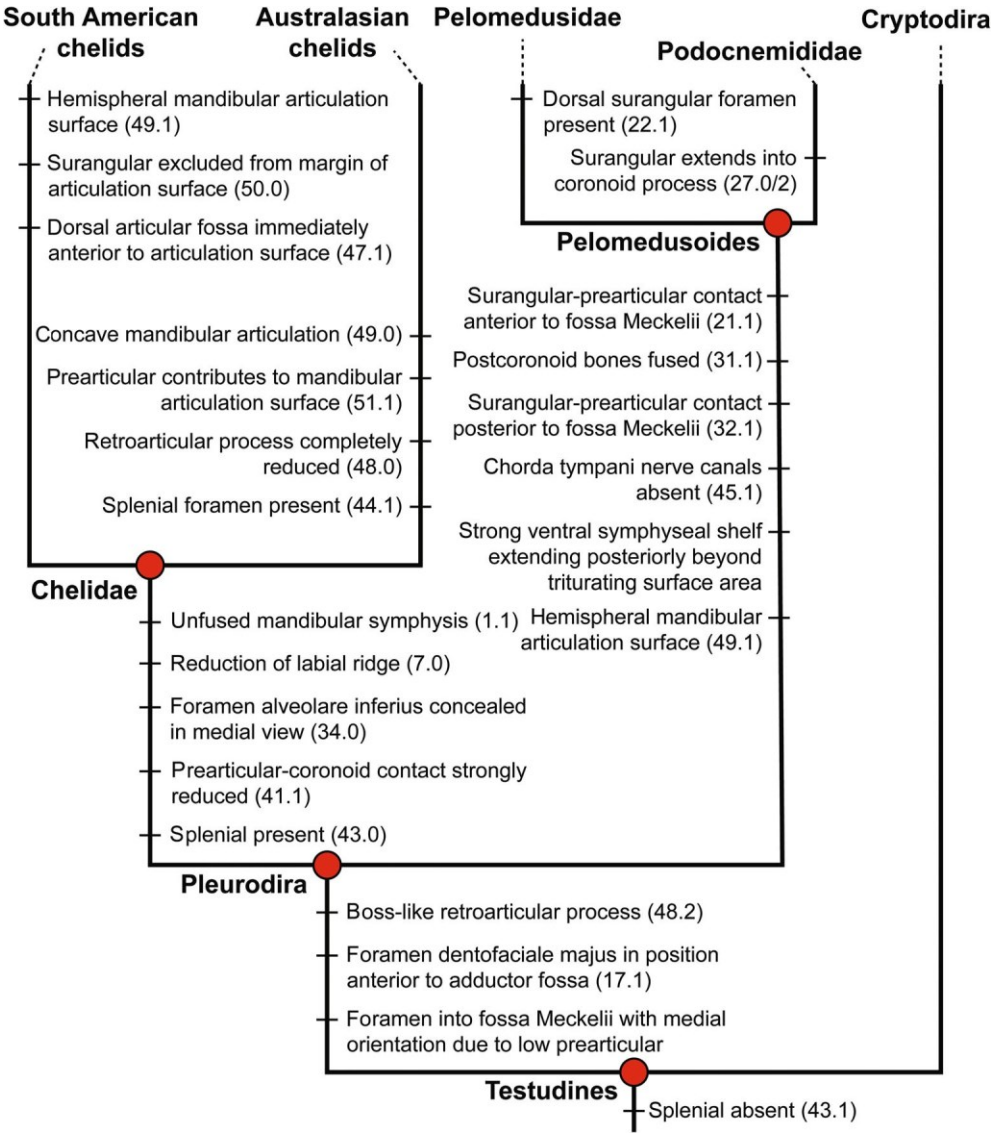

FIGURE 25 Mandibular features of pleurodires. This simplified phylogenetic tree shows the major pleurodiran lineages in context of their sister clade, Cryptodira. Tick marks on internal branches denote characteristic and/or synapomorphic features of clades, which are labeled at internal branches. Note that the branch lengths are meaningless and neither time-scaled, nor proportional to character transition rates

mandibular research, in terms of increased sampling, intraspecific variation, potential ontogenetic mandibular changes, and also application of our osteological characters in phylogenetic or disparity work.

Our examinations of the systematic anatomical variation of turtle mandibles allow the evaluation of characteristics with more nuance than before. Previously, some synapomorphic character states or diagnostic traits had in part been hypothesized based on extrapolations of a more limited sample size. Gaffney (1979), for example, states that the hemispheric, condylar shape of the mandibular articulation is diagnostic for pleurodires. While this mandibular articulation shape is herein indeed confirmed for most pleurodires and is recovered as an ACCTRAN synapomorphy of the clade, it is absent in Australasian chelids (Figure 24c,g; Figure 25), which represent one of the major pleurodiran subclades. In addition, we also find the hemispheric, condylar shape of the articulation area in the cryptodire *Claudius angustatus*, indicating the trait does not exclusively appear in pleurodires. However, our observations suggest alternative characters that are universally present in pleurodires. Specifically, members of the clade share the presence of a far anteriorly placed foramen dentofaciale majus with respect to the adductor fossa and a medial orientation of the dorsal foramen into the fossa Meckelii that is the result of a dorsally low prearticular (Figure 25).

Our character optimization and their discussions (see remarks sections for each character, above) return very few of our osteological characters as unique unambiguous synapomorphies of clades. The aforementioned anterior position of the foramen dentofaciale majus is, for instance, not only characteristic for pleurodires among our sample, but also for deirochelyine emydids and chelonioids. Indeed, many characters have low consistency indices, indicating that character states homoplastically

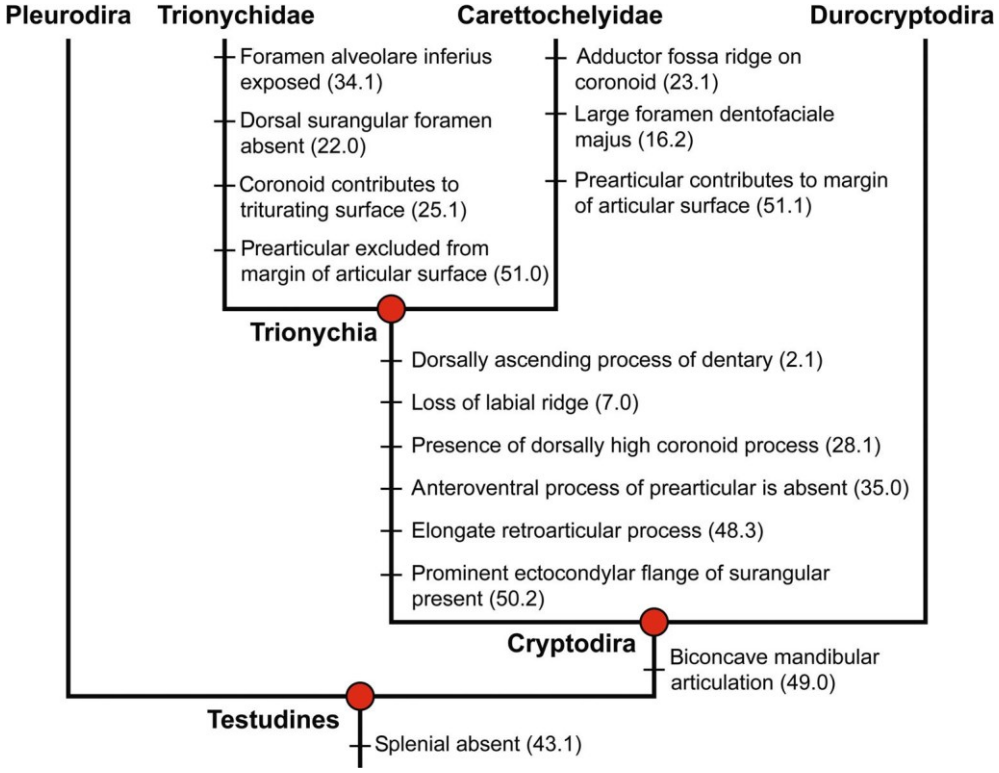

FIGURE 26 Mandibular features of Trionychia (i.e., trionychids and carettochelyids). This simplified phylogenetic tree shows the major testugurian lineages in context of their phylogenetic position. Tick marks on internal branches denote characteristic and/or synapomorphic features of clades, which are labeled at internal branches. Note that the branch lengths are meaningless and neither time-scaled, nor proportional to character transition rates

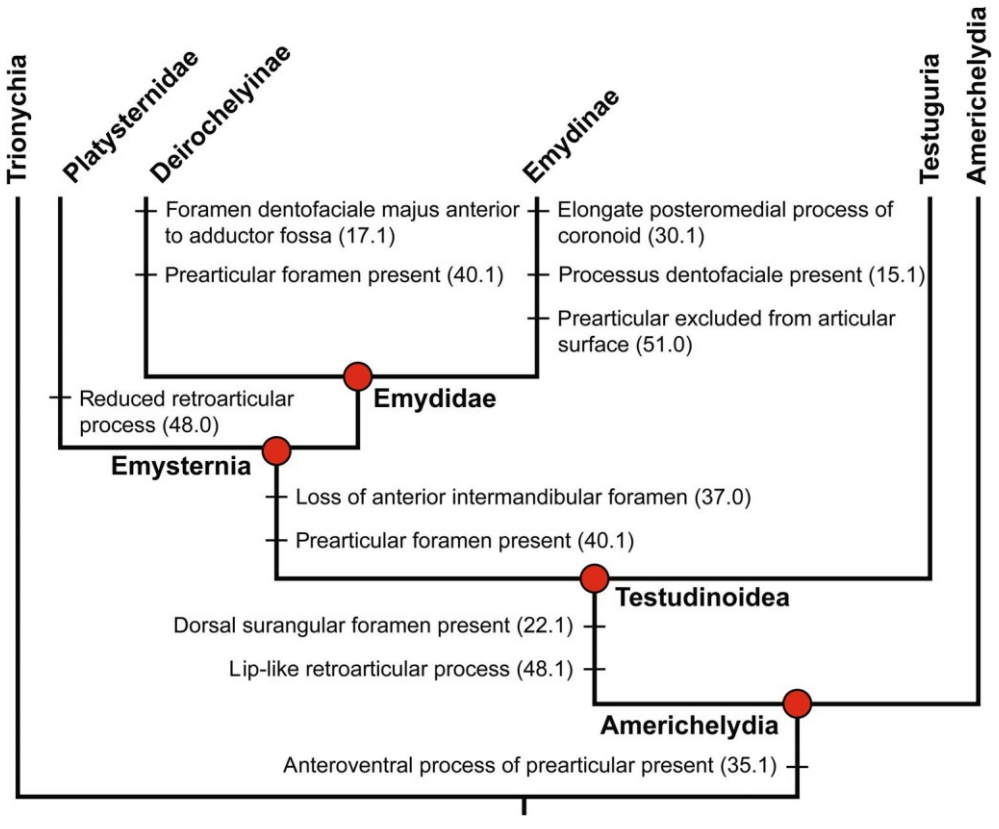

FIGURE 27 Mandibular features of Emysternia (i.e., emydids and platysternids). This simplified phylogenetic tree shows the major emysternian lineages in context of their phylogenetic position. Tick marks on internal branches denote characteristic and/or synapomorphic features of clades, which are labeled at internal branches. Note that the branch lengths are meaningless and neither time-scaled, nor proportional to character transition rates

re-appear (or disappear) across turtle phylogeny. It can be expected that homoplasy increases if fossils are additionally considered, or if the extant sample is expanded beyond the 70 extant turtles studied here. Despite the high amount of character change we observed, our optimizations also show that many character states can serve

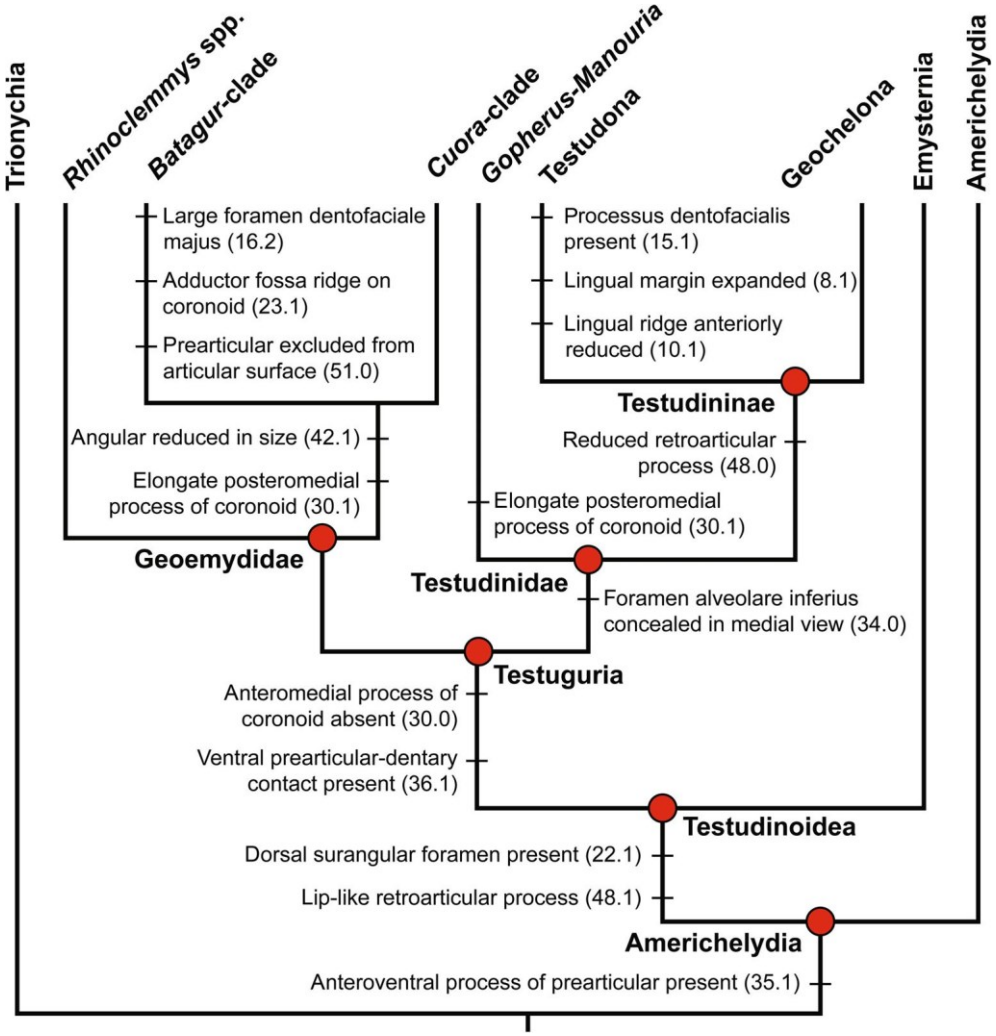

FIGURE 28 Mandibular features of Testuguria (i.e., geoemydids and testudinids). This simplified phylogenetic tree shows the major testugurian lineages in context of their phylogenetic position. Tick marks on internal branches denote characteristic and/or synapomorphic features of clades, which are labeled at internal branches. Note that the branch lengths are meaningless and neither time-scaled, nor proportional to character transition rates

as local synapomorphies for variably sized clades. Thus, even characters with high homoplasy can have a significant grouping effect that is consistent with the molecularly inferred turtle phylogeny (i.e., Pereira et al., 2017), which we herein use as a baseline upon which to judge the evolution of character states. Moreover, and regardless of the phylogenetic optimization of synapomorphies, various combinations of character states can potentially serve as taxonomically diagnostic characteristics for the different groups. We summarized this information in a series of graphs that show parts of the turtle phylogeny, with specific character state occurrences indicated at the internal branches leading to clades (Figures 25–29).

Many of our character observations may be useful especially for clade-specific, restricted phylogenetic analyses or local areas within global phylogenies. This is exemplified by the fact that many of our characters encode systematic variation below the level of clades that are traditionally regarded as "families" or "subfamilies" (see Joyce, Anquetin, et al., 2021). This information can be particularly important as a reference for identifying phylogenetic positions (or taxonomic identifications) of fossil species. For example, just as their shells or crania have many diagnostic, as well as synapomorphic features (Georgalis & Joyce, 2017; Vitek & Joyce, 2015), trionychid mandibles are easily identifiable by a unique combination of characteristics (Figure 26). However, taxonomic or phylogenetic assignments of fossil trionychids to specific sublineages are difficult: Although a wealth of fossil trionychids are known from the Cretaceous (e.g., Hay, 1908), it is unclear for most of these species if they represent members of the trionychid crown or stem lineage, or if they may be closer related to certain modern lineages than others (e.g., Georgalis & Joyce, 2017; Vitek & Joyce, 2015).

Our characters could potentially be informative for such questions. Specifically, our current matrix includes several autapomorphic character states for individual trionychid species, or synapomorphies at highly exclusive phylogenetic clade levels. *Cycloderma frenatum*, for instance, is the only known extant turtle with a subdivided fossa Meckelii (character 33 state 1; Gaffney, 1979). Potential trionychid fossils with this feature could be

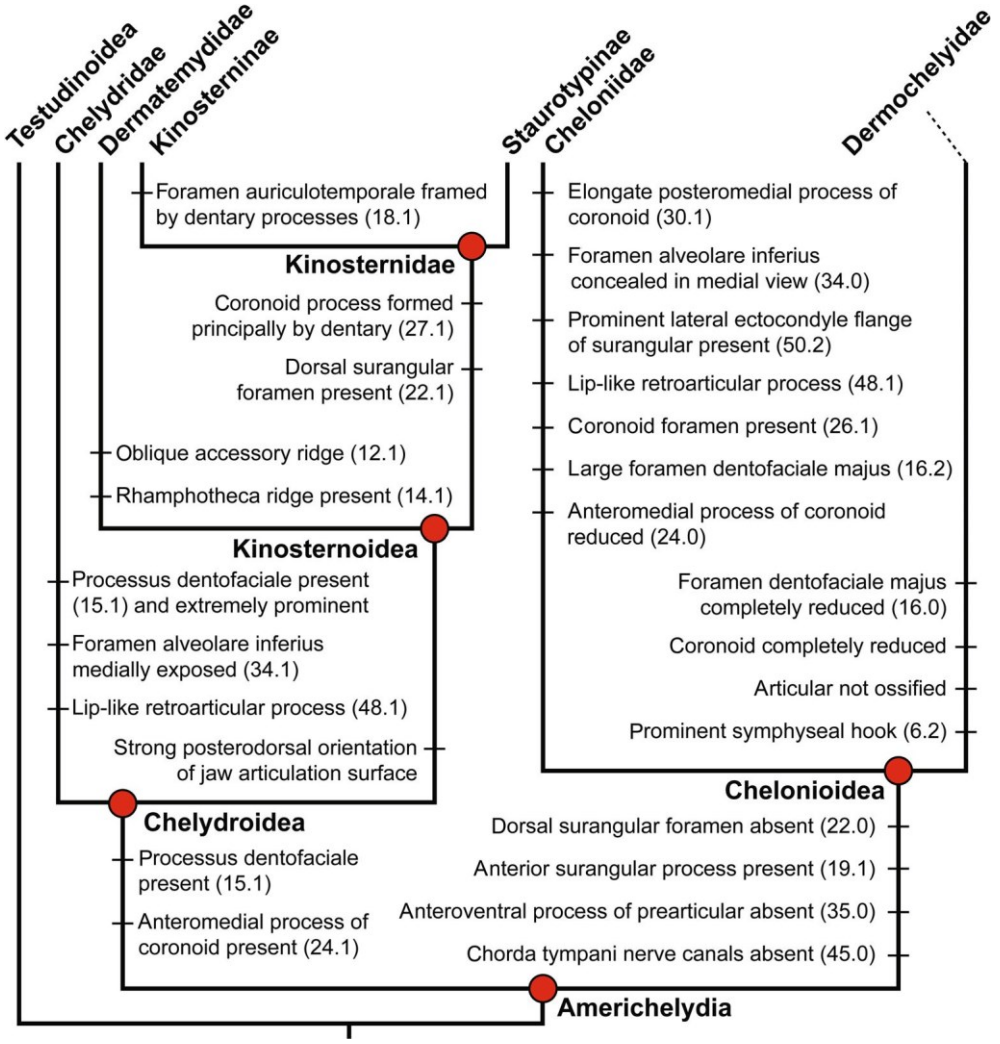

FIGURE 29 Mandibular features of Americhelydia (i.e., kinosternids, chelydrids, and chelonioids). This simplified phylogenetic tree shows the major americhelydian lineages in context of their phylogenetic position. Tick marks on internal branches denote characteristic and/or synapomorphic features of clades, which are labeled at internal branches. Note that the branch lengths are meaningless and neither time-scaled, nor proportional to character transition rates

grouped with the *Cycloderma* lineage. Similarly, the species of *Apalone* we sampled share a gentle coronoid notch (Character 29 State 1) to the exclusion of all other sampled trionychids, and this may well be a feature to identify stem members of the *Apalone*-lineage. Other aut- or synapomorphies that appear uniquely among trionychids are: the presence of a labial ridge in *Chitra chitra* (Character 7 State 1); the presence of a symphyseal ridge in *Amyda cartilaginea* (Character 4 State 1); the absence of a posterior intermandibular foramen in the *Chitra* + *Trionyx*-clade (Character 38 State 0); the presence of a coronoid foramen in *Cycloderma frenatum* (Character 26 State 1); the presence of a prearticular foramen in *Cycloderma frenatum* (Character 40 State 1); and the position of the posterior chorda tympani foramen on the posterior surface of the articular within the articular notch in *Cycloderma frenatum* (Character 46 State 0). Some of the character states of *Cycloderma frenatum* could potentially be diagnostic for the larger clade Cyclanorbinae, but we did not have access to mandibles of further cyclanorbine taxa to test this for this particular study. Although we do not provide species-by-species assessments of unique features for all turtles represented herein, our supplementary lists that include all synapomorphies (Data S2–S4) may be a guide for readers that wish to extract that information for a specific species sampled in this study.

The relevance of some of the anatomical features we describe in detail have been missed in the past. For instance, the dorsal surangular foramen, which was previously unnamed and anecdotally observed in various turtle species (e.g., Gaffney, 1979; Meylan, 1987; Siebenrock, 1897), is returned as a synapomorphy of Testudinoidea according to our optimization (Figure 27). Similarly, the anteroventral process of the prearticular is a synapomorphy of Americhelydia (although secondarily lost in chelonioids, see below).

Another insight from this study is that some features that are clearly related to feeding strategy, although homoplastic, can have strong local systematic value. For instance, triturating ridge serrations and lingual margin

expansions are repeatedly evolving features among turtles, but within the geoemydid *Batagur*-clade, itself supported by several features (Figure 28), functionally relevant character states can be used to identify successively nested clades. Specifically, the subclade (*Orlitia borneensis*, *Malayemys subtrijuga*; *Geoclemys hamiltonii*; *Morenia* spp.; *Pangshura* spp.; *Batagur* spp.; *Hardella thurjii*) (see Pereira et al., 2017; Thomson et al., 2021), all have lingually expanded triturating surfaces to the exclusion of immediate outgroups (e.g., *Geoemyda spengleri*). As this clade includes species not sampled by us in terms of 3D segmentations, we used mandibles of the specimens NHMUK 1949.2.3.29 (*Orlitia borneensis*), NHMUK 87.9.30.1 (*Geoclemys hamiltonii*), UMMZ 227976 (*Hardella thurjii*) and UF-herp-85436 (*Pangshura smithii*) to verify this statement. At a less inclusive level (*Morenia* spp., *Pangshura* spp., *Batagur* spp., *Hardella thurjii*), all have clearly developed lingual ridges, whereas the smaller clade (*Pangshura* spp., *Batagur* spp., *Hardella thurjii*) additionally has serrations along the triturating ridges. The systematic value of these features is not necessarily surprising, as ecology also evolves along phylogenetic lineages, and strongly functionally related traits can thus still convey phylogenetic signal.

The stem lineage of chelonioids is another contentious part of turtle phylogenetics, and the exact position of many fossil species as either stem chelonioids, stem cheloniids, or dermochelyids is not clear (e.g., Brinkman et al., 2006, 2009; Cadena & Parham, 2015; Gentry et al., 2019; see Evers & Benson, 2019 for a recent summary). Mandibular osteology of living chelonioids shows that the crown-group is supported by several shared features (e.g., absence of ossified mandibular chorda tympani canals, absence of the dorsal surangular foramen, absence of the anteroventral process of the prearticular, presence of an anterior process of the surangular; Figure 29), despite the strongly derived mandibular osteology of the extant leatherback sea turtle, *Dermochelys coriacea*. Additionally, both dermochelyids and cheloniids can be distinguished by a large number of characteristic features, which provides the possibility that fossils may be placed along either crown- or the stem-lineage by reference to these features. To our knowledge, these features have not been widely applied in chelonioid phylogeny before (e.g., Evers & Benson, 2019). Chelonioid mandibles are relatively commonly found in the fossil record, and specifically also in taxa with contentious phylogenetic positions such as *Euclastes*-like taxa, ctenochelyids, or protostegids (e.g., Case, 1897; Evers, Barrett, & Benson, 2019; Gentry, 2016; Hirayama & Tong, 2003; Matzke, 2007; Mulder, 2003; Parham et al., 2014; Wieland, 1900; Zangerl, 1971), so that future mandibular research on fossil chelonioids may provide a research opportunity.

5 | CONCLUSIONS

We provide summary descriptions of the mandibular osteology and assessments of within-group variation for all major clades of extant turtles. This is based on the study of CT-based digital anatomy of 70 turtle species, including the detailed bone-by-bone segmentation of 31 species. Segmentation of mandibular innervation and arterial blood supply for a specimen of *Dermatemys mawii* helps to clarify the function and identify of several mandibular openings and foramina. Our soft tissue segmentation of the mandibular musculature of *Dermatemys mawii* are the first 3D muscle reconstructions of the strongly derived turtle adductor muscle system. We use our observations to propose an updated nomenclature of foramina and other mandibular features. We summarize osteological variation in 51 discrete characters. Their phylogenetic value is assessed by a character optimization imposed on the molecular turtle topology. We report synapomorphies for all clades and optimization for each character, and find that most discrete characters have high evolvability and homoplasy, but still provide support for many clades. Combinations of discrete character observations may be useful for taxonomic identifications of fossils, and ultimately also for formal phylogenetic assessment of fossil species. Our results must in the future be further scrutinized by ontogenetic work and assessments of intraspecific variation.

5.1 | Institutional abbreviations

CM, Carnegie Museum of Natural History, Pittsburgh, USA; FHSM, Fort Hays State University, Sternberg Museum of Natural History, Hays, USA; FMNH, Field Museum of Natural History, Chicago, USA; LIRP, Laboratório de Ictiologia de Ribeirão Preto, University of São Paulo, Brazil; MCT, Museu de Ciências de Terra, Rio de Janeiro, Brazil; MVZ, Museum of Vertebrate Zoology, Berkeley, USA; NCSM; North Carolina Museum of Natural History, Raleigh, USA; NHMUK, Natural History Museum, London, UK; OUMNH, Oxford University Museum of Natural History, Oxford, UK; PCHP, Chelonian Research Institute/Peter C.H. Pritchard, Oviedo; SMF, Senckenberg Museum Frankfurt, Frankfurt, Germany; SMNS; Staatliches Museum für Naturkunde Stuttgart, Stuttgart, Germany; UF, Florida Museum of Natural History, Gainesville, USA; UMZC, University Museum of Zoology, Cambridge, UK; USNM, United States National Museum, Washington, DC, USA; ZMB, Zoologische Museum Berlin, Berlin, Germany

AUTHOR CONTRIBUTIONS

Serjoscha W. Evers: Conceptualization (lead); data curation (lead); formal analysis (lead); funding acquisition (lead); investigation (lead); methodology (lead); project administration (lead); resources (lead); software (equal); supervision (equal); validation (lead); visualization (lead); writing – original draft (lead); writing – review and editing (lead). Jasper Ponstein: Conceptualization (supporting); data curation (supporting); investigation (supporting); resources (supporting); software (equal); writing – review and editing (supporting). Maren A. Jansen: Supervision (supporting); writing – review and editing (supporting). Jaimi A. Gray: Data curation (supporting); methodology (supporting); resources (supporting); writing – review and editing (supporting). Jörg Fröbisch: Conceptualization (supporting); project administration (supporting); software (equal); supervision (equal); writing – review and editing (supporting).

ACKNOWLEDGMENTS

The authors thank all researchers and institutions who share CT scans and other digital data on repositories such as MorphoSource, without which their sampling would have been considerably smaller. Serjoscha W. Evers is also thankful for the support of the MorphoSource team, particularly to Mackenzie A. Shepard and Doug Boyer. The authors also thank Ingmar Werneburg for the permission to use the CT scan of *Carettochelys insculpta*. The authors are thankful to all curators who granted access to specimens under their care, namely: Jason Head (UMZC), Alan Resatar (FMNH); Patrick Campbell (NHMUK), Alexander Kupfer and Rainer Schoch (SMNS), and Frank Tillack (ZMB). The authors would also like to thank CT technicians and CT lab managers for allowing to scan specimens in their facilities and/or assisting or performing those CT scans that the authors gathered themselves, namely: Tom Davies (University of Bristol), Farah Ahmed (NHMUK), Zhe-Xi Luo and April Isch Neander (University of Chicago), Kristin Mahlow and Eva-Maria Bendel (ZMB). Serjoscha W. Evers thanks Walter Joyce, Yann Rollot, and Guilherme Hermanson for discussions. The authors also thank Ingmar Werneburg and Walter Joyce for helpful reviewer comments, Heather Smith, Juliana Sterli and Evangelos Vlachos for editing the Turtle Evolution Symposium special issue, and Evangelos Vlachos for editing this particular article. Serjoscha W. Evers is funded by an SNF Ambizione grant with the number SNF PZ00P2_202019/1. Jasper Ponstein is funded by an Elsa-Neumann scholarship. Open access funding provided by Universite de Fribourg.

ORCID

Serjoscha W. Evers https://orcid.org/0000-0002-2393-5621

REFERENCES

Albrecht, P. W. (1967). The cranial arteries and cranial arterial foramina of the turtle genera *Chrysemys*, *Sternotherus* and *Trionyx*: A comparative study of analysis with possible evolutionary implications. *Tulane Studies in Zoology*, *14*, 81–99.

Albrecht, P. W. (1976). The cranial arteries of turtles and their evolutionary significance. *Journal of Morphology*, *149*, 159–182.

Anquetin, J. (2012). Reassessment of the phylogenetic interrelationships of basal turtles (Testudinata). *Journal of Systematic Palaeontology*, *10*, 3–45.

Anquetin, J., Püntener, C., & Billon-Bruyat, J.-P. (2015). *Portlandemys gracilis* n. sp., a new coastal marine turtle from the Late Jurassic of Porrentruy (Switzerland) and a reconsideration of plesiochelyid cranial anatomy. *PLoS One*, *10*(6), e0129193.

Bardet, N., Jalil, N.-E., De Lapparent de Broin, F., Germain, D., Lambert, O., & Amaghzaz, M. (2013). A giant chelonioid turtle from the late cretaceous of Morocco with a suction feeding apparatus unique among tetrapods. *PLoS One*, *8*, 1–10.

Baur, G. (1895). Über die Morphologie des Unterkiefers der Reptilies. *Anatomischer Anzeiger*, *11*, 410–415.

Bever, G. S. (2008). Comparative growth in the postnatal skull of the extant north American turtle Pseudemys texana (Testudinoidea: Emydidae). *Acta Zoologica*, *89*, 107–131.

Bever, G. S. (2009). The postnatal skull of the extant North American turtles Pseudemys texana (Cryptodira: Emydidae) with comments on the study of discrete intraspecific variation. *Journal of Morphology*, *270*, 97–128.

Bojanus, L. H. (1819–1821). Anatome testudinis europaeae. Vilna: Joseph Sawadzki.

Brinkman, D., Aquillon-Martinez, M. C., de Leon D'avila, C. A., Jamniczky, H., Eberth, D. A., & Colbert, M. (2009). *Euclastes coahuilaensis* sp. nov., a basal cheloniid turtle from the late Campanian Cerro del Pueblo Formation of Coahuila State, Mexico. *PaleoBios*, *28*(3), 76–88.

Brinkman, D., Hart, M., Jamniczky, H., & Colbert, M. (2006). *Nichollsmeys baieri* gen. et sp. nov., a primitive chelonioid turtle from the late Campanian of North America. *Paludicola*, *5*(4), 111–124.

Brinkman, D., Rabi, M., & Zhao, L. (2017). Lower cretaceous fossils from China shed light on the ancestral body plan of crown softshell turtles (Trionychidae, Cryptodira). *Scientific Reports*, *7*(1), 1–11.

Cadena, E., & Parham, J. F. (2015). Oldest known marine turtle? A new protostegid from the Lower Cretaceous of Colombia. *PaleoBios*, *32*, 1–421.

Cadena, E. W., Bloch, J. I., & Jatamillo, C. A. (2010). New podocnemidid turtle (Testudines: Pleurodira) from the middle-upper Paleocene of South America. *Journal of Vertebrate Paleontology*, *30*(2), 367–382.

Case, E. C. (1897). On the osteology and relationships of *Protostega*. *Journal of Morphology*, *13*, 21–55.

Chatterji, R. M., Hipsley, C. A., Sherratt, E., Hutchinson, M. N., & Jones, M. E. H. (2022). Ontogenetic allometry underlies trophic diversity in sea turtles (Chelonioidea). *Evolutionary Ecology*, 1–30. https://doi.org/10.1007/s10682-022-10162-z

Claude, J., Pritchard, P., Tong, H., Paradis, E., & Auffray, J.-C. (2004). Ecological correlates and evolutionary divergence in the skull of turtles: A geometric morphometric assessment. *Systematic Biology*, *53*(6), 933–948.

Cleary, T. J., Benson, R. B. J., Holroyd, P. A., & Barrett, P. M. (2020). Tracing the patterns of non-marine turtle richness from the Triassic to the Palaeogene: From origin to global spread. *Palaeontology*, *5*, 753–774.

Crawford, N. G., Parham, J. F., Sellas, A. B., Faircloth, B. C., Glenn, T. C., Papenfuss, T. J., Henderson, J. B., Hansen, M. H., & Simison, W. B. (2015). A phylogenomic analysis of turtles. *Molecular Phylogenetics and Evolution*, *83*, 250–257.

Crumly, C. R. (1982). A cladistic analysis of *Geochelone* using cranial osteology. *Journal of Herpetology*, *16*, 215–234.

Danilov, I. G. (2001). *Fossil turtles of the family Lindholmemydidae and phylogenetic relationships of cryptodiran turtles*. (Unpublished Ph. D. dissertation). Zoological Institute of Russian Academy of Sciences, St. Petersburg, 318 pp. [Russian].

Danilov, I. G., & Parham, J. F. (2006). A redescription of *'Plesiochelys' tatsuensis* from the Late Jurassic of China, with comments on the antiquity of the crown clade Cryptodira. *Journal of Vertebrate Paleontology*, *26*, 573–580.

Danilov, I. G., & Parham, J. F. (2008). A reassessment of some poorly known turtles from the Middle Jurassic of China, with comments on the antiquity of extant turtles. *Journal of Vertebrate Paleontology*, *28*, 306–318.

de Pinna, M. G. G. (1991). Concepts and tests of homology in the cladistic paradigm. *Cladistics*, *7*, 367–394.

Dryden, L. S. (1988). Paraphyly of the Cryptodira and phylogenetic systematics of turtles. PhD dissertation, University of Kansas. p. 1–142.

Ernst, C. H., & Barbour, R. W. (1989). *Turtles of the world*. Smithsonian Institute Press.

Evers, S. W. (2019). CT scans of extant turtle skulls. MorphoSource. https://www.morphosource.org/Detail/ProjectDetail/Show/project_id/769.

Evers, S. W., Barrett, P. M., & Benson, R. B. J. (2019). Anatomy of *Rhinochelys pulchriceps* (Protostegidae) and marine adaptation during the early evolution of chelonioids. *PeerJ*, *7*, e6811.

Evers, S. W., & Benson, R. B. J. (2018). Project: Evers & Benson 2018, Turtle CT data and 3D models. MorphoSource. http://www.morphosource.org/Detail/ProjectDetail/Show/project_id/462.

Evers, S. W., & Benson, R. B. J. (2019). A new phylogenetic hypothesis of turtles with implications for the number of evolutionary transitions to marine lifestyles supports an early cretaceous origin and rapid diversification of Chelonioidea. *Palaeontology*, *62*(1), 93–134.

Evers, S. W., Neenan, J. M., Ferreira, G. S., Werneburg, I., Barrett, P. M., & Benson, R. B. J. (2019). Neurovascular anatomy of the protostegid turtle *Rhinochelys pulchriceps* and comparisons of membranous and endosseous labyrinth shape in an extant turtle. *Zoological Journal of the Linnean Society*, *187*, 800–828.

Evers, S. W, & Ponstein, J. (2022). Turtle mandibular anatomy and 3D models. MorphoSource. https://www.morphosource.org/projects/000408332.

Ferreira, G. S., Bronzati, M., Langer, M. C., & Sterli, J. (2018). Phylogeny, biogeography and diversification patterns of side-necked turtles (Testudines: Pleurodira). *Royal Society Open Science*, *5*, 171773.

Ferreira, G. S., Rinco'n, A. D., Sol'orzano, A., & Langer, M. C. (2015). The last marine pelomedusoids (Testudines: Pleurodira): A new species of *Bairdemys* and the paleoecology of Stereogenyina. *PeerJ*, *3*, e1063.

Fuchs, H. (1931). Ueber den Unterkiefer und die Unterkiefernerven (Ramus tertius nervi trigemini et Chorda tympani) der Arrauschildkröte (*Podocnemis expansa*), nebst Bemerkungen zur Kiefergelenksfrage. *Zeitschrift für Anatomie und Entwicklungsgeschichte*, *94*, 206–274.

Gaffney, E. S. (1972). The systematics of the North American family Baenidae (Reptilia, Cryptodira). *Bulletin of the American Museum of Natural History*, *147*, 243–319.

Gaffney, E. S. (1975a). A phylogeny and classification of the higher categories of turtles. *Bulletin of the American Museum of Natural History*, *55*(5), 387–436.

Gaffney, E. S. (1975b). Phylogeny of the chelydrid turtles: A study of shared derived characters in the skull. *Fieldiana Geology*, *33*(9), 157–178.

Gaffney, E. S. (1977). The side-necked turtle family Chelidae: A theory of relationships using shared derived characters. *American Museum Novitates*, *2620*, 1–28.

Gaffney, E. S. (1979). Comparative cranial morphology of recent and fossil turtles. *Bulletin of the American Museum of Natural History*, *164*, 69–376.

Gaffney, E. S. (1990). The comparative osteology of the Triassic turtle *Proganochelys*. *Bulletin of the American Museum of Natural History*, *194*, 1–263.

Gaffney, E. S., & Meylan, P. A. (1988). A phylogeny of turtles. In M. J. Benton (Ed.), *The phylogeny and classification of the tetrapods, volume 1: Amphibians, reptiles, birds* (pp. 157–219). Clarendon Press.

Gaffney, E. S., Meylan, P. A., & Wyss, A. R. (1991). A computer assisted analysis of the relationships of higher categoried of turtles. *Cladistics*, *7*, 313–335.

Gaffney, E. S., Tong, H., & Meylan, P. A. (2006). Evolution of the side-necked turtles: The families Bothremydidae, Euraxemydidae, and Araripemydidae. *Bulletin of the American Museum of Natural History*, *300*(700), 6–698.

Gaffney, G. S., Campbell, K. E., & Wood, R. C. (1998). Pelomedusoid side-necked turtles from late Miocene sediments of Southwestern Amazonia. *American Museum Novitates*, *3245*, 1–11.

Gaffney, G. S., Meylan, P. A., Wood, R. C., & Simons, E. (2011). The evolution of the side-necked turtles: The family Podocnemididae. *Bulletin of the American Museum of Natural History*, *350*, 1–237.

Gentry, A. D. (2016). New material of the Late Cretaceous marine turtles *Ctenochelys acris* Zangerl, 1953 and a phylogenetic reassessment of the 'toxochelyid'-grade turtles. *Journal of Systematic Palaeontology*, *15*(8), 675–696.

Gentry, A. D., Ebersole, J. A., & Kiernan, C. R. (2019). *Asmodochelys parhami*, a nw fossil marine turtle from the Campanian Demopolis Chalk and the stratigraphic congruence of competing marine turtle phylogenies. *Royal Society Open Science*, *6*, 191950.

Georgalis, G. L., & Joyce, W. G. (2017). A review of the fossil record of the Old World turtles of the clade Pan-trionychidae. *Bulletin of the Peabody Museum of Natural History*, *58*(1), 115–208.

Gill, F., Donsker, D., & Rasmussen, P. (2020). IOC World Bird List, volume 10.2. https://doi.org/10.14344/IOC.ML.10.2.

Hawkins, J., Hughes, C., & Scotland, R. (1997). Primary homology assessment, characters and character states. *Cladistics*, *283*, 275–283.

Hay, O. P. (1908). *The fossil turtles of North America*. Carnegie Institution of Washington.

Hermanson, G. (2021). Turtle CT scans and 3D models. MorphoSource. https://www.morphosource.org/projects/000376254

Hirayama, R. (1985). Cladistic analysis of batagurine turtles. Studia *Palaeocheloniologica*, *1*, 140–157.

Hirayama, R. (1998). Oldest known sea turtle. *Nature*, *392*, 705–708.

Hirayama, R., & Tong, H. (2003). *Osteopygis* (Testudines: Cheloniidae) from the Lower Tertiary of the Ouled Abdoun Phosphate Basin, Morocco. *Palaeontology*, *46*(5), 845–856.

Hutchison, J. H. (2008). History of fossil Chelydridae. In A. C. Steyermark, M. S. Finkler, & R. J. Brooks (Eds.), *Biology of the snapping turtle (Chelydra serpentina)* (pp. 14–30). John Hopkins University Press.

Jones, M. E., Werneburg, I., Curtis, N., Penrose, R., O'Higgins, P., Fagan, M. J., & Evans, S. E. (2012). The head and neck anatomy of sea turtles (Cryptodira: Chelonioidea) and skull shape in Testudines. *PLoS One*, *7*(11), e47852.

Joyce, W. G. (2007). Phylogenetic relationships of Mesozoic turtles. *Bulletin of the Peabody Museum of Natural History*, *48*, 3–102.

Joyce, W. G. (2017). A review of the fossil record of basal Mesozoic turtles. *Bulletin of the Peabody Museum of Natural History*, *58*(1), 65–113.

Joyce, W. G., Anquetin, J., Cadena, E. A., Claude, J., Danilov, I. G., Evers, S. W., Ferreira, G. S., Gentry, A. D., Georgalis, G. L., Lyson, T. R., Pérez-García, A., Rabi, M., Sterli, J., Vitek, N. S., & Parham, J. F. (2021). A nomenclature for fossil and living turtles using phylogenetically defined clade names. *Swiss Journal of Palaeontology*, *140*, 1–45. https://doi.org/10.1186/s13358-020-00211-x

Joyce, W. G., & Bell, C. J. (2004). A review of the comparative morphology of extant testudinoid turtles (Reptilia: Testudines). *Asiatic Herpetological Research*, *10*, 53–109.

Joyce, W. G., Parham, J. F., Lyson, T. R., Warnock, R. C. M., & Donoghue, P. C. J. (2013). A divergence dating analysis of turtles using fossil calibrations: An example of best practices. *Journal of Paleontology*, *87*(4), 612–634.

Joyce, W. G., Rabi, M., Clark, J. M., & Xu, X. (2016). A toothed turtle from the Late Jurassic of China and the global biogeographic history of turtles. *BMC Evolutionary Biology*, *16*(1), 1–29.

Joyce, W. G., Rollot, Y., Evers, S. W., Lyson, T. R., Rahantarisoa, L. J., & Krause, D. W. (2021). A new pelomedusoid turtle, Sahonachelys mailakavava, from the Late Cretaceous of Madagascar provides evidence for convergent evolution of specialized suction feeding among pleurodires. *Royal Society Open Science*, *8*, 210098. https://doi.org/10.1098/rsos.210098

Matzke, A. T. (2007). An almost complete juvenile specimen of the cheloniid turtle Ctenochelys stenoporus (Hay, 1905) from the Upper Cretaceous Niobrara Formation of Kansas, USA. *Palaeontology*, *50*(3), 669–691.

McDowell, S. B. (1964). Partition of the genus Clemmys and related problems in the taxonomy of the aquatic Testudinidae. *Proceedings of the Zoological Society of London*, *143*(2), 239–278.

Meylan, P. A. (1987). The phylogenetic relationships of soft-shelled turtles (family Trionychidae). *Bulletin of the American Museum of Natural History*, *186*, 1–110.

Meylan, P. A. (1996). Skeletal morphology and relationships of the Early Cretaceous Side-Necked turtle, Araripemys barretoi (Testudines: Pelomedusoides: Araripemydidae), from the Santana Formation of Brazil. *Journal of Vertebrate Paleontology*, *16*(1), 20–33.

Meylan, P. A., & Gaffney, E. S. (1989). The skeletal morphology of the cretaceous cryptodiran turtle, *Adocus*, and the relationships of the Trionychoidea. *American Museum Novitates*, *2941*, 1–60.

Młynarski, M. (1980). Die tertiären Wirbeltiere des Steinheimer Beckens. Teil II. Die Schildkröten des Steinheimer Beckens. B. Chelydridae mit einem Nachtrag zu den Testudinoidea. *Palaeontographica, Supplement*, *8*, 1–35.

Mulder, E. W. A. (2003). Comparative osteology, palaeoecology and systematics of the Late Cretaceous turtle *Allopleuron hofmani* (Gray 1931). In E. W. A. Mulder (Ed.), *On the lates Cretaceous tetrapods from the Maastrichtian type area* (Vol. 44, pp. 23–92). Publicaties van het Natuurhistorisch Genootschap in Limburg.

Nick, L. (1913). Das Kopfskelet von *Dermochelys coriacea* L. *Zoologische Jahrbücher, Abteilung für Anatomie und Ontogenie der Tiere*, *33*, 431–552.

Ogushi, K. (1913). Anatomische Studien an der japanischen dreikralligen Lippenschildkröte (*Trionyx japanicus*). II. Mitteilung: Muskel- und peripheres Nervensystem. *Morphologisches Jahrbuch*, *46*, 299–562.

Parham, J. F., Otero, R. A., & Su'arez, M. E. (2014). A sea turtle skull from the Cretaceous of Chile with comments on the taxanomy and biogeography of *Euclastes* (formerly *Osteopygis*). *Cretaceous Research*, *49*, 181–189.

Parham, J. F., & Pyenson, N. D. (2010). New Sea turtle from the Miocene of Peru and the iterative evolution of feeding ecomorphologies since the Cretaceous. *Journal of Paleontology*, *84*(2), 231–247.

Patterson, C. (1982). Morphological characters and homology. In K. A. Joysey & A. E. Friday (Eds.), *Problems of phylogenetic reconstruction* (pp. 21–74). Academic Press.

Pereira, A. G., Sterli, J., Moreira, F. R. R., & Schrago, C. S. (2017). Multilocus phylogeny and statistical biogeography clarify the evolutionary history of major lineages of turtles. *Molecular Phylogenetics and Evolution*, *113*, 59–66.

Pimental, R. A., & Riggins, R. (1987). The nature of cladistic data. *Cladistics*, *3*, 201–209.

Platnick, N. I. (1979). Philosophy and the transformation of cladistics. *Systematic Biology*, *28*, 537–546.

Poglayen-Neuwall, I. (1953). Untersuchungen der Kiefermuskulatur und deren Innervation bei Schildkröten. *Acta Zoologica*, *14*, 241–292.

Pritchard, P. H. (1984). Piscivory in turtles, and evolution of the long-necked Chelidae. *Symposia of the Zoological Society of London*, *52*, 87–110.

Rathke, H. (1848). *Ueber die Entwicklung der Schildkröten*. Friedrich Vieweg und Sohn.

Rieppel, O. (1988). *Fundamentals of comparative biology*. Birkhauser.

Rockenback Portella, P., Oliveira, R. J., Pereira Machado, F., Jaeger Drehemer, C., Schifino Valente, A. L., & Figueiredo Dornelles, J. E. (2020). Morphology and intraspecific variation in the skull and mandible of the slider turtle Trachemys dorbigni (Testudines, Emydidae). *Zoomorphology*, *139*, 373–384.

Rollot, Y., Evers, S. W., & Joyce, W. G. (2021). A review of the carotid artery and facial nerve canal systems in extant turtles. *PeerJ*, *8*, e10475. https://doi.org/10.7717/peerj.10475

Shaffer, H. B., McCartney-Melstad, E., Near, T. J., Mount, G. G., & Spinks, P. Q. (2017). Phylogeneomic analyses of 539 highly informative loci dates a fully resolved time tree for the major clades of living turtles (Testudines). *Molecular Phylogenetics and Evolution*, *115*, 7–15.

Shaffer, H. B., Meylan, P., McKnight, M. L., & Larson, A. (1997). Tests of turtle phylogeny: Molecular, morphological, and paleontological approaches. *Systematic Biology*, *46*, 235–268.

Sheil, C. A. (2003). Osteology and skeletal development of *Apalone spinifera* (Reptilia: Testudines: Trionychidae). *Journal of Morphology*, *256*, 42–78.

Sheil, C. A. (2005). Skeletal development of *Macrochelys temminckii* (Reptilia: Testudines: Chelydridae). *Journal of Morphology*, *263*, 71–106.

Sheil, C. A., & Greenbaum, E. (2005). Reconsideration of skeletal development of *Chelydra serpentina* (Reptilia: Testudinata: Chelydridae): Evidence for intraspecific variation. *Journal of Zoology*, *265*, 235–267.

Siebenrock, F. (1897). Das Kopfskelet der Schildkröten. *Sitzungsberichte der Kaiserlichen Akademie der Wissenschaften*, *106*, 245–328.

Smith Paredes, D., Lord, A., Meyer, D., & Bhullar, B.-A. S. (2021). A developmental staging system and musculoskeletal development sequence of the common musk turtle (*Sternotherus odoratus*). *Developmental Dynamics*, *250*, 111–127.

Soliman, M. A. (1964). Die Kopfnerven der Schildkröten. *Zeitschrift für Wissenschaftliche Zoologie*, *169*, 216–312.

Sterli, J. (2010). Phylogenetic relationships among extinct and extant turtles: The position of pleurodira and the effects of the fossils on rooting crown-group turtles. *Contributions to Zoology*, *79*, 93–106.

Strong, E. E., & Lipscomb, D. (1999). Character coding and inapplicable data. *Cladistics*, *15*, 363–371.

Swofford, D. L. (2002). *PAUP*. Phylogenetic analysis using parsimony (*and other methods). Version. 4.0*. Sinauer Associates.

Thomson, R. C., Spinks, P. Q., & Shaffer, H. B. (2021). A global phylogeny of turtles reveals a burst of climate-associated diversification on continental margins. *Proceedings of the National Academy of Sciences*, *118*(7), 22012215118.

Turtle Taxonomy Working Group, Rhodin, A. G. J., Iberson, J. B., Bour, R., Fritz, U., Georges, A., Shaffer, H. B., & van Dijk, P. P. (2021). Turtles of the world: Annotated checklist and atlas of taxonomy, synonymy, distribution, and conservation status. In A. G. J. Rhodin, J. B. Iverson, P. P. van Dijk, C. B. Stanford, E. V. Goode, K. A. Buhlmann, & R. A. Mittermeier (Eds.), *Conservation biology of freshwater turtles and tortoises: A compilation project of the UUCN/SSC tortoise and freshwater turtle specialist group* (Vol. 8, 9th ed., pp. 1–472). *Chelonian Research Monographs*.

Uetz, P., Freed, P., & Hošek, J. (2020). The reptile database, http://www.reptile-database.org

Vitek, N. S., & Joyce, W. G. (2015). A review of the fossil record of New World turtles of the clade Pan-Trionychidae. *Bulletin of the Peabody Museum of Natural History*, *56*(2), 185–244.

Vlachos, E., & Rabi, M. (2018). Total evidence analysis and body size evolution of extant and extinct tortoises (Testudines: Cryptodira: Pan-Testudinidae). *Cladistics*, *34*, 652–683.

Walther, W. G. (1922). Die Neu-Guinea-Schildkröte *Carettochelys insculpta* Ramsay. PhD Dissertation, Luwdigs-University Giessen: EJ Brill. p. 607–704.

Werneburg, I. (2011). The cranial musculature of turtles. *Palaeontologia Electronica*, *14*(2), 1–99.

Werneburg, I., & Joyce, W. G. (2021). Cranial Turtle CT scans. MorphoSource. https://www.morphosource.org/projects/000353832

Wieland, G. R. (1900). The skull, pelvis, and probable relationships of the huge turtles of the genus *Archelon*. *American Journal of Science*, *9*(52), 231–251.

Wilkinson, M. (1992). Ordered versus unordered characters. *Cladistics*, *8*, 375–385.

Wilkinson, M. (1995). A comparison of two methods of character construction. *Cladistics*, *11*, 297–308.

Williams, E. (1950). *Testudo cubensis* and the evolution of western hemisphere tortoises. *Bulletin of the American Museum of Natural History*, *95*(1), 1–36.

Zangerl, R. (1971). Two toxochelyid sea turtles from the Landenian sands of Erquelinnes (Hainaut) of Belgium. *Institut Royal des Sciences Naturelles de Belgique Mémoires*, *169*, 3–32.

Zhou, C.-F., & Rabi, M. (2015). A sinemydid turtle from the Jehol Biota provides insights into the basal divergence of crown turtles. *Scientific Reports*, *5*, 16299.

SUPPORTING INFORMATION

Additional supporting information can be found online in the Supporting Information section at the end of this article.

How to cite this article: Evers, S. W., Ponstein, J., Jansen, M. A., Gray, J. A., & Fröbisch, J. (2023). A systematic compendium of turtle mandibular anatomy using digital dissections of soft tissue and osteology. *The Anatomical Record*, *306*(6), 1228–1303. https://doi.org/10.1002/ar.25037